# A FINITE ELEMENTS BASED APPROACH FOR FRACTURE ANALYSIS OF WELDED JOINTS IN CONSTRUCTION MACHINERY

A THESIS SUBMITTED TO
THE GRADUATE SCHOOL OF NATURAL AND APPLIED SCIENCES
OF
MIDDLE EAST TECHNICAL UNIVERSITY

BY

TANER KARAGÖZ

IN PARTIAL FULFILLMENT OF THE REQUIREMENTS
FOR
THE DEGREE OF MASTER OF SCIENCE
IN
MECHANICAL ENGINEERING

AUGUST 2007

Approval of the Thesis

**“A FINITE ELEMENTS BASED APPROACH FOR FRACTURE ANALYSIS OF WELDED JOINTS IN CONSTRUCTION MACHINERY”**

Submitted by **TANER KARAGÖZ** in partial fulfillment of the requirements for the degree of **Master of Science in Mechanical Engineering** by,

Prof. Dr. Canan Özgen
Dean, Graduate School of **Natural and Applied Sciences** _____

Prof. Dr. Kemal İder
Head of Department, **Mechanical Engineering** _____

Asst. Prof. Dr. Serkan Dağ
Supervisor, **Mechanical Engineering, METU** _____

**Examining Committee Members:**

Prof. Dr. Eres Söylemez (*)
Mechanical Engineering, METU _____

Asst. Prof. Dr. Serkan Dağ (**)
Mechanical Engineering, METU _____

Prof. Dr. F. Suat Kadıoğlu
Mechanical Engineering, METU _____

Assoc. Prof. Dr. Bora Yıldırım
Mechanical Engineering, Hacettepe University _____

Kadir Geniş (M.S.)
Hidromek Ltd. Sti. _____

**Date:** _____

(*) Head of Examining Committee
(**) Supervisor

**I hereby declare that all information in this document has been obtained and presented in accordance with academic rules and ethical conduct. I also declare that, as required by these rules and conduct, I have fully cited and referenced all material and results that are not original to this work.**

Name, Last name: Taner KARAGÖZ

Signature :

## ABSTRACT

A FINITE ELEMENTS BASED APPROACH FOR FRACTURE ANALYSIS OF WELDED JOINTS IN CONSTRUCTION MACHINERY

Karagöz, Taner
M.S, Department of Mechanical Engineering
Supervisor: Asst. Prof. Dr. Serkan DAĞ

August 2007, 119 pages

This study aims to develop a computer program to perform finite elements based fracture mechanics analyses of three dimensional surface cracks in T-welded joints of construction machinery. The geometrical complexity of the finite elements models and the requirement of large computer resources for the analyses necessitate the use of shell elements for general stress distribution optimization. A sub-modeling technique, together with a shell to solid conversion method, enables the user to model a local region and analyze it by defining the weld and crack parameters. It is assumed that the weld material is the same with the sheet metal material and the surface cracks are considered to occur on two weld toes and weld root. The surface cracks are assumed to have a semi elliptical crack front profile. In order to simulate the square-root strain

singularity around the crack front, collapsed 20-node three dimensional brick elements are utilized. The rest of the local model is modeled by using 20-node three dimensional brick elements. The main objective of this work is to calculate the mixed mode energy release rates around the crack front for a sub-model of a global shell model by using J-integral method.

**Keywords:** Finite elements, sub-modeling, semi elliptical surface crack, fillet weld, J-integral method

# ÖZ

İŞ MAKİNALARINDAKİ KAYNAKLI BAĞLANTILARIN SONLU ELEMANLARA DAYALI BİR YAKLAŞIMLA KIRILMA ANALİZİ

Karagöz, Taner
Yüksek lisans, Makina Mühendisliği Bölümü
Tez Yöneticisi: Y. Doç. Dr. Serkan DAĞ

Ağustos 2007, 119 sayfa

Bu çalışmanın amacı, iş makinelerinin köşe kaynaklı bağlantılarında üç boyutlu yüzey çatlaklarının sonlu elemanlara dayalı kırılma mekaniği analizlerini gerçekleştirecek bir bilgisayar programı geliştirmektir. Sonlu elemanlar modellerinin karmaşık geometrisi ve analizlerin yüksek kapasiteli bilgisayar gereksinimi genel gerilme dağılımı eniyilemesinde kabuk elemanların kullanılmasını zorunlu kılar. Bir alt modelleme tekniği, kabuktan katıya dönüştürücü bir metotla birlikte, kullanıcının tanımlanan kaynak ve çatlak parametrelerine göre lokal bir bölgeyi modellemesini ve analizlerini gerçekleştirmesini sağlar. Kaynak malzemesinin sac metal malzemesiyle aynı olduğu varsayılmış ve yüzey çatlaklarının kaynağın iki kenarında ve kökünde olduğu düşünülmüştür. Yüzey çatlaklarının yarı

eliptik çatlak yüzü görüntüsüne sahip olduğu varsayılmıştır. Çatlak yüzü çevresindeki kare kök gerinim tekilliğini benzeştirebilmek için çökertilmiş 20 düğüm noktalı üç boyutlu tuğla elemanlar kullanılmıştır. Lokal modelin geri kalan kısmı 20 düğüm noktalı üç boyutlu tuğla elemanlar ile modellenmiştir. Bu çalışmanın asıl amacı, bir global kabuk modelin alt modelinin çatlak yüzü çevresindeki karışık mod enerji açığa çıkma oranlarını J-integrali metodunu kullanarak hesaplamaktır.

**Anahtar kelimeler:** Sonlu elemanlar, alt modelleme, yarı eliptik yüzey çatlağı, köşe kaynağı, J-integrali metodu

To My Family and My Love Özgül

## ACKNOWLEDGMENTS

I wish to express my special thanks to Assistant Prof. Dr. Serkan DAĞ for his continuous help and guidance throughout the duration of this study.

I would also like to express my appreciation to Kadir GENİŞ, Prof. Dr. Eres SÖYLEMEZ and Hakan IŞIKTEKİN for their important contributions and useful discussions during the study.

I would also like to thank my friends Ferhan FIÇICI, C. Can UZER, Erkal ÖZBAYRAMOĞLU, Murat IŞILDAK and Gençer GENÇOĞLU for their suggestions and support.

Special thanks to my family for all their love, patience and support during all my life.

Finally, I wish to express my gratitude to my love M. Özgül ŞAHİNKAYA who made my life more meaningful for seven years.

This study was supported by Hidromek Ltd. Sti.

## TABLE OF CONTENTS

## LIST OF TABLES

TABLES

## LIST OF FIGURES

FIGURES

## LIST OF SYMBOLS AND ABBREVIATIONS

SYMBOLS

| | |
|---|---|
| m(x,a) | : Weight Function |
| σ(x) | : Stress Distribution |
| K | : Stress Intensity Factor |
| a | : Half Crack Length |
| b | : Crack Depth |
| $K_{IC}$ | : The Critical Mode I Stress Intensity Factor |
| $K_C$ | : The Critical Mode I Stress Intensity Factor |
| B | : Specimen Thickness |
| $\sigma_X$ | : Normal Stress Component on the Crack Front in x Direction |
| $\sigma_Y$ | : Normal Stress Component on the Crack Front in y Direction |
| $\tau_{XY}$ | : Shear Stress Component on the Crack Front |
| $r$ | : Distance from the Crack Tip |
| $\theta$ | : Angle from the Crack Plane |
| $\sigma_{ij}$ | : The Components of the Stresses |
| $u, v, w$ | : Displacement Components in x, y and z Directions |
| $\mu$ | : Shear Modulus |
| $\kappa$ | : Shear Parameter |
| $\nu$ | : Poisson's Ratio |
| $E$ | : Young's Modulus |
| $K_I$, $K_{II}$, $K_{III}$ | : Mode I, II, III Stress Intensity Factors |
| $s$ | : Arc Length of the Crack Front |
| $t$ | : Tangential Direction on the Crack Front |
| $n$ | : Normal Direction on the Crack Front |
| $b$ | : Binormal Direction on the Crack Front |
| $\sigma_{bb}$ | : Normal Stress Component on the Crack Front |

$u_{bb}$ : Normal Displacement Component on the Crack Front

$G$ : Energy Release Rate

$\Pi$ : Strain Energy

$G_c$ : Fracture Toughness

$G_I$, $G_{II}$, $G_{III}$ : Mode I, II, III Energy Release Rates

$J$ : J-integral

$W$ : Strain Energy Density

$T$ : Kinetic Energy Density

$u_j$ : Displacement Vector

$\Gamma$ : Integration Path

$\bar{J}$ : Converted J-integral

$A$ : Area inside Integration Path

$q_1$ : A Function Introduced in J-integral Conversion

$F_d$ : Bucket Cylinder Force

P : Working Pressure of the Cylinder

$D_d$ : Bucket Cylinder Diameter

$F_b$ : Bucket Breakout Force

c : Perpendicular Distance Bucket Cylinder Axis - Lever Pivot

d : Perpendicular Distance Connecting Link Axis - Lever Pivot

e : Perpendicular Distance Connecting Link Axis - Bucket Pivot

f : Radius Bucket Pivot - Tooth Lip

$F_c$ : Arm Cylinder Force

$D_c$ : Arm Cylinder Diameter

$F_a$ : Arm Breakout Force

g : Perpendicular Distance Arm Cylinder Axis - Arm Pivot

h : Distance Arm Pivot - Tooth Tip

M : Hydraulic Oil Motor-Swing Unit Moment Capacity

F : Lateral Force

Leg1 : Vertical Leg Length of the Weld

Leg2 : Horizontal Leg Length of the Weld

RD : Root Depth

Leg_1 : Vertical Leg Length of the Inner Weld

Leg_2 : Horizontal Leg Length of the Inner Weld

MCD : Middle Crack Distance

MCL : Middle Crack Length

$\alpha_x, \alpha_y, \alpha_z$ : Rotation About Global x, y and z Axes

$K_I^*$ : Normalized Mode I Stress Intensity Factor

$J^*$ : Normalized J-integral Value

$\beta, \phi$ : Crack Front Position Angles

$E(\phi)$ : Elliptical Integral

$\Psi$ : Crack Inclination Angle

$J_I, J_{II}, J_{III}$ : Mode I, II, III J-integral Values

d1, d2, d3 : Cube Dimensions in y, x, z Directions

ABBREVIATIONS

FEA : Finite Element Analysis

FEM : Finite Element Method

BEM : Boundary Element Method

GMAW : Gas Metal Arc Welding

GTAW : Gas Tungsten Arc Welding

FGM : Functionally Graded Material

ASTM : American Society for Testing and Materials

APDL : ANSYS Parametric Design Language

JSSC : Japanese Society of Steel Construction

SAE : Society of Automotive Engineers

SIF : Stress Intensity Factor

CT : Compact Tension

GUI : Graphical User Interface

# CHAPTER 1

# INTRODUCTION

Earth-moving machines are heavy-duty engineering vehicles and are primarily used for the movement of large quantities of bulk materials, earth, gravel and broken rock in road building, mining, construction, quarrying, trenching, demolition, grading, lifting, river dredging and land clearing applications. The most common types of earth-moving machines are: backhoe loaders, excavators, bulldozers, loaders, cranes, and graders.

Backhoe loaders (Figure 1.1) are the most common type of earth-moving machines in the world. Due to their relatively small size and versatility, backhoe loaders are used for urban engineering applications and small construction projects (such as building a small house, fixing city roads, small demolitions, digging holes/excavating etc). The machine is self-propelled, highly mobile with a mainframe to support and accommodate both rear-mounted backhoe and front-mounted loader. Backhoe loader consists of two main mechanisms: backhoe and loader. The Backhoe digs, lifts, swings and discharges the material while machine is stationary. When used in Loader mode, the machine loads material into the bucket through forward motion of the machine and lifts, transports, and discharges the material [1].

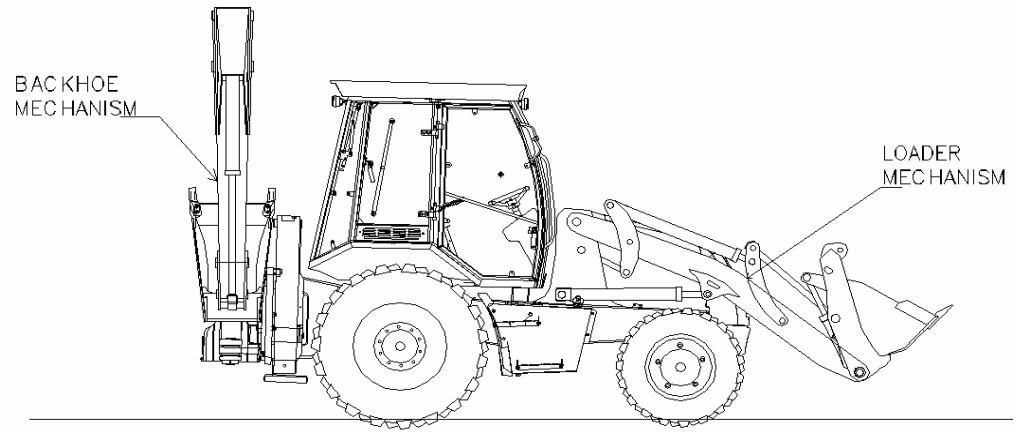


Figure 1.1 HMK 102 B Energy Series Backhoe Loader General View

Excavator (Figure 1.2), which is also called a 360-degree excavator or digger, sometimes abbreviated simply to a 360, is an engineering vehicle consisting of a backhoe and cab mounted on a pivot (a rotating platform) atop an undercarriage with tracks or wheels [2]. It is a mobile machine which has an upper structure capable of continuous rotation and which digs, elevates, swings, and dumps material by action of the boom, the arm, or telescopic boom and bucket [3]. Excavators come in a wide variety of sizes. In accordance with their sizes they are used in many roles such as digging of trenches, holes, foundations, material handling, brush cutting with hydraulic attachments, demolition, general grading/landscaping, heavy lift, mining, river dredging.

Often the bucket can be replaced with other tools like a breaker, a grapple or an auger.

Excavators are usually employed together with loaders and bulldozers.

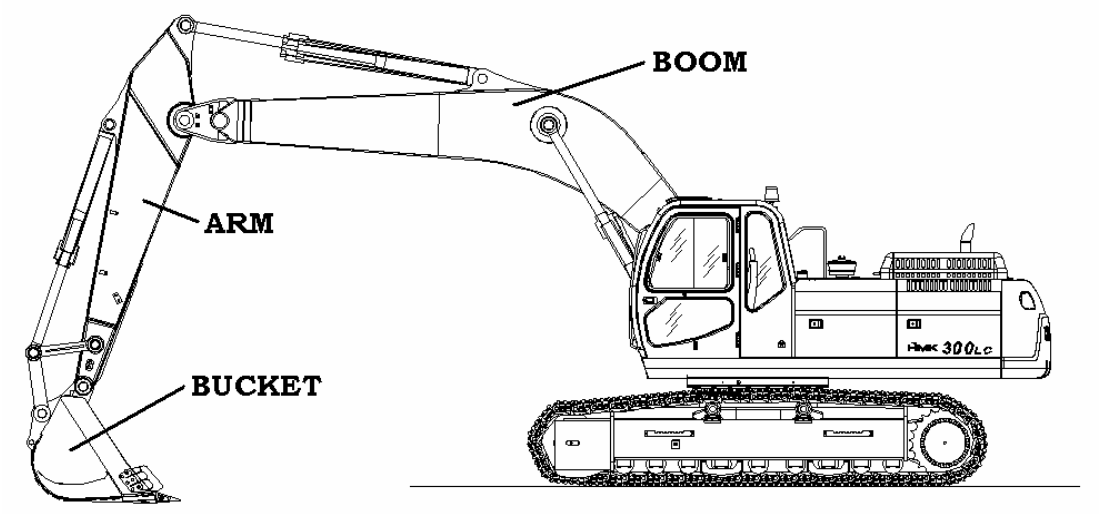


Figure 1.2 HMK 300 LC Excavator General View

Both excavators and backhoe loaders must work reliably in severe and unpredictable working conditions. While these machines are performing their required tasks some components of these machines are exposed to repeated fluctuating stresses, which cause fatigue cracks, especially on digging and loading components, to occur. Owing to these cracks, the components of the machines can malfunction, fracture or even cause danger to the life of people.

Welding is the most dominant joining method during the manufacturing process of all earth-moving machines and it is the main source of cracks occurring on the components. The assessment of the welded joints is a major industrial problem because the welds are the determining factor of expected life of earth-moving machines. Accordingly, the welded joints are the regions of weakness in a structure and must be fully understood to improve the expected life of the earth-moving machines.

The crucial problem in assessment of welded joints is the difficulty of defining weld geometry in a manner, which is sufficiently precise for analysis but sufficiently simple for industrial use. For this reason, designers have not been able to take full advantage of the advent of finite element analysis (FEA) and other numerical methods, which have revolutionized the assessment of stress concentrations in solid components. In principle a welded joint can be analyzed using FEA, but in practice a very detailed model is required to capture the local stresses around the weld bead, making the approach impractical for real components, especially if they contain many welds. Due to these reasons, in the previous studies, methods for fatigue assessment of welds mostly tend to be feature-based and empirical [4] [5] [6] [7] [8] [9] [10] [11]. In these work, fatigue life predictions were made by using the 'Paris-Erdoğan equation' according to the tests results.

In literature, numerical methods have not been investigated as extensively as their experimental counterparts. This is possibly due to the complexity in the formulation of the problems, the requirement of large computer resources for numerical calculations, and the lack of efficient methods to provide accurate results. Among the methods used for studying welded joints and calculating fracture parameters, the finite element method (FEM) together with domain integrals is commonly used to extract the results for the energy release rate [12] [13] [14] [15] [16].

In real life applications, the most dominant fatigue cracks evolve into surface cracks, which often have a semi-elliptical shape. Accordingly, different semi-elliptical surface cracks were placed into finite element models and boundary element models by using various software [17] [18] [19] [20]. In these studies, 3-D models were created either manually or parametrically; boundary conditions were defined either for full or axi-symmetric models. To calculate the stress intensity factor different techniques are used.

In the present study, three-dimensional semi-elliptic surface crack problem in T-welded joints are examined using a three-dimensional finite element technique. The crack problem is analyzed by using sub-modeling technique and the boundary conditions are directly taken from the global model. A shell to solid conversion technique creates the 3-D solid local models, according to the selected region. A prepared graphical user interface applies the desired weld and fracture parameters to automatically formed local model. Then, by applying J-integral approach to generated 3-D solid models energy release rate is evaluated for mixed mode loading type. During the study, commercial finite element analysis software MSC.Mentat-Marc is used.

# CHAPTER 2

# LITERATURE REVIEW

The main objective of this study is to model the three-dimensional semi-elliptical surface crack at toe and root of fillet welded joints and to calculate the mixed mode J-integral values around the crack front and performing structural zooming analysis by using the finite element method (FEM). The present study focuses only on T-welded joints and it can be considered as one of the first in the literature dealing with automatically generated three-dimensional surface cracks at fillet weld toe and root in a structural zooming analysis.

The accurate calculation of stress intensity factors for 3-D surface and corner cracks has long been recognized as an important computational problem in fracture mechanics. Irwin, who first obtained an approximate solution for surface crack problem in 1962, recognized this. Since the introduction of the J-integral as a fracture mechanics parameter by Cherepanov [54] and Rice [55], many numerical solutions have been developed. The application of the finite element method (FEM) and the boundary element method (BEM) to the evaluation of the J-integral is well established for two-dimensional problems. For three-dimensional problems the J-integral has been directly applied to the finite element method by various workers, however, the evaluation of surface integrals is cumbersome in FE analyses. This led to the modification of the J-integral to a domain integral by Nikishkov and Atluri, in which the J-

integral is multiplied by a simple function called an "S" function. The method is known as equivalent domain integral (EDI) and is computationally appealing as the domain integral is accurately and easily obtained in FE analysis [21].

Most studies in the literature that deal with surface and corner cracks concentrate on mode I loading where mode II and mode III stress intensity factors are zero along the crack front. In practical applications, however, surface cracks under mixed mode conditions can be encountered frequently. These flaws may experience mixed mode loading due to mainly three factors: (1) mixed remote loading, i.e., normal and shear remote loads acting on a component having perpendicular crack to the normal loading direction, (2) deflected or inclined crack under normal/uniaxial remote loading, and (3) mechanical and/or thermal loads combined with arbitrary restraint conditions [19].

Singh et al. [5] performed experiments to determine the effect of fillet geometry on fatigue properties of cruciform welded joints in structural steels. They predicted the fatigue life of AISI 304L cruciform joints failing at the weld toe using a two stage model. The local stress life method was applied to calculate the fatigue crack initiation life, whereas the fatigue crack propagation life was estimated using fracture mechanics concepts. Constant amplitude fatigue tests with stress ratio R=0 were carried out using a 100 kN servohydraulic Dartec universal testing machine at a frequency of 30 Hz. An automatic crack monitoring system based on crack propagation gauges was used to obtain the propagation data during the fatigue process. In their study they reported that there are two types of fatigue cracking in fillet welded joints, namely, (i) root cracking and (ii) toe cracking. According to the test data they obtained fatigue crack growth curves by using Paris-Erdogan equation. The results showed that crack growth rate of GMAW with convex fillets is greater than GTAW joints with concave fillets. Their results show good correlation with the BS 5400: part 10 design curve.

Lahti et al. [23] conducted three-point bending fatigue tests on stainless steel fillet welds by using two stainless steel grades: ferritic–martensitic EN 1.4003 and austenitic EN 1.4310. The test results obtained were shown to be in good agreement with suggested fatigue classes in the Eurocode 3 design standard, derived from fatigue data on structural steels. However, if the size of the weld was increased, and the failure location could be moved to the weld toe instead of the weld root, a significant increase in fatigue strength was observed. Eurocode 3 was found to describe well the fatigue characteristics of the 'worst-case' welds, i.e., welds prone to root failure.

Kainuma et al. [6] performed another experimental study to investigate the fatigue strength of load-carrying fillet welded cruciform joints with weld root failures. They used five different weld shapes: an isosceles triangle, two types of scalene triangles, a concave curvature, and a convex curvature in their study. They used JSSC average design curve to determine the crack propagation rate and stress intensity factor. In the study finite element analysis were also performed to determine the stress intensity factors by applying energy method to FEM. Based on the experimental and analytical results, the influence of weld shape, weld size, weld penetration depth, and plate thickness on fatigue strength was determined, and a numerical expression for the weld throat thickness was derived to evaluate fatigue strength.

In the paper by Statnikov et al. [22], the fatigue test was applied to T-weld joints from steel weldox 420 by means of four-point-bending test method. The work was intended to obtain the initial data to compare the efficiency of the post-weld treatment techniques in terms of increasing fatigue strength of welded joints and develop ultrasonic impact treatment technique that ensures rather high efficiency of the method. In all tests the cracks were formed at the weld toe of the specimens. Finally, the fatigue curves for welded joints in the as-welded and improved conditions were obtained.

Fricke et al. [24] studied fillet welded joints in ship hulls experimentally. The study proposes a simplified approach for the fatigue strength assessment with respect to root cracking, which is based on a local nominal stress in a defined area of the weld throat and on common fatigue classes for the assessment of cruciform joints. Fatigue tests and numerical analyses of local stresses and crack propagation from the root gap have been performed. Some tests showed unexpected results in comparison with the calculations. The study resulted that two different types of cracks are possible, starting from the weld toe and from the non-welded root gap. The most critical crack initiation site depends highly on the weld throat thickness and on the actual axial misalignment. The latter influences more the cracks starting from the weld toe, which are usually assessed on the basis of the structural hot-spot stress approach. The approach has been verified by experimental and numerical (such as BEM and FEM analysis) investigations of two typical structural configurations.

In the thesis study of Ficici [17] semi– elliptical surface cracks in a test specimen are modeled. The specimen is declared in the standard ISO/DIS 14345 [25]. The specimen is examined by considering axial and bending types of loading. All parts of the model including the semi- elliptical surface crack are generated in the finite element software MSC.MENTAT– MARC and the crack profile can be placed at the weld toe or at the weld root depending on the user's choice. The study uses displacement correlation technique for computing modes I, II and III stress intensity factors under mechanical loading. The main goal is to prepare a parametric model with user interface, which makes all of the stages– including modeling the specimen, placing the crack, loading, post-processing and computing the mixed-mode stress intensity factors– automatically.

Gray et al. [26] presented a modification to the quarter-point crack tip element and employed this element in two-dimensional boundary integral fracture analysis. They calculated the stress intensity factors with the

displacement correlation technique. The obtained results are highly accurate, and significantly more accurate than with the standard element. The improvements are especially dramatic for mixed mode problems involving curved and interacting cracks.

Inan [18] worked on modeling of semi-circular surface cracks in a ceramic (ZrO2) – titanium alloy (Ti-6Al-4V) FGM coating bonded to a homogeneous titanium alloy substrate under mode I mechanical or thermal loading conditions. A three dimensional finite element model containing a semi-circular surface crack is generated using the general purpose finite element software ANSYS. Mode I stress intensity factor was derived by three–dimensional displacement correlation technique. The stress intensity factors are calculated for FGM coating– substrate systems subjected to uniform tension, bending, fixed-grip tension, three point bending and temperature gradients. In order to examine the accuracy of the model, calculated stress intensity factors are compared with those given by Newman and Raju [56] for various crack dimensions under tension or bending loads. These results show that calculations of mode I stress intensity factor by means of displacement correlation technique using finite element analysis was sufficiently accurate.

In the thesis study of Sabuncuoglu [27], stress intensity factors at the crack tip for functionally graded materials (FGM's) were evaluated via the finite element method in conjunction with the displacement correlation technique. A parametric modeling code for test specimen given in ASTM E399 was prepared for mode I stress intensity factor calculations by using ANSYS software. All the parametric modeling stages were carried out by APDL codes. Since the cracks are symmetric one forth of the model was formed in the analysis. In the analysis, 20 nodes brick elements were used in order to satisfy the strain singularity at the crack front. It is seen that the calculated values are very close to those given in the studies Kadioglu et al. [28] and Guo et al. [29]. From these analyses, it can be said that displacement

correlation technique is a suitable way of determining the stress intensity factor for FGM structures.

Ayhan [19] reported mixed mode stress intensity factor solutions for deflected and inclined surface cracks in finite-thickness plates under uniform tensile remote loading by using three-dimensional enriched finite elements. The study demonstrates the convenience of the enriched finite element technique for these types of problems. Regardless of how a surface or corner crack is initiated or introduced in a component, accurate prediction of the fracture conditions, i.e., mixed mode stress intensity factors, is very important to assess its remaining life. Accordingly, mixed mode stress intensity factor solutions are generated for semi-circular surface cracks with various deflection and inclination angles ranging from $0^0$ to $75^0$. The mixed mode stress intensity factor solutions presented in the paper are obtained using FRAC3D, a three-dimensional fracture analysis program. It was shown, for both crack types, that mode I stress intensity factors decrease in magnitude along the whole crack front as the deflection or inclination angle increases. Mode II and mode III stress intensity factors, on the other hand, increase initially as the deflection or inclination angle increases and then decrease for higher deflection or inclination angles. It was also demonstrated that decreasing the plates thickness has a magnifying effect on the fracture parameters, especially on the mode I stress intensity factor. Finally, crack propagation angles along deflected and inclined crack fronts were shown to increase in magnitude along the whole crack front with increasing deflection or inclination angle.

Guo et al. [30] attempted to simplify the stress intensity factor calculation for integral welded integral structures, which is the current trend in commercial aircraft manufacture instead of conventional built-up riveted structures. It is well known that on the conventional T-plate welded joint, many failures are due to the fatigue cracks initiating and developing from the weld toes where large stress concentrations are present. The fracture and fatigue analysis are

usually very complex and exact solutions for stress intensity factors are not always available. Therefore, the weight function method is often used because it enables the stress intensity factors for a variety of loading conditions to be calculated by simple integration of the weight function m(x,a) and the stress distribution σ(x) expression. The stress intensity factor weight function for a single edge crack originating from the T-plate weld toe was derived from a general weight function form and two reference stress intensity factors.

The stress intensity factors (K) are obtained using the finite element method. The finite element analysis was conducted using ABAQUS standard (version 6.4). The model containing a one-dimensional edge crack originating from the weld toe was analyzed. The sub-modeling technique of the Finite Element Method was used, so that the mesh at crack tip vicinity could be refined substantially. The stress intensity factor (K) for Mode I was calculated from the J-integral which was calculated using the energy domain integral methodology.

The comparisons showed that the derived weight function can make accurate predictions for stress intensity factors. The derived weight function is valid for the relative depth $a/t \leq 0.8$. It is also shown that this weight function is suitable for the stress intensity factor calculation for the cracked laser-welded padded plate geometries under general loading conditions.

Baumjohann et al. [13] have written a computer code for parametric modeling of crack geometries. Then, they determined J-integrals of ductile growing cracks located between two comparative contours by interpolation. The automatic modeling and a mathematical program processing the finite element results evaluate the crack growth of the finite element results very effectively. In their study they used the finite element analysis software ABAQUS to determine temperature distribution, displacements, stresses and

J-integrals. Their study indicated that parametric modeling is very important for effective SIF calculations.

In their study Lin et al. [15] described a multiple degree of freedom numerical procedure applicable to the prediction of the fatigue crack growth of surface cracks in plates under a combined tension and bending load. The procedure performs a three-dimensional finite element analysis to estimate the stress intensity factors at a set of points along the crack front, and then calculates the crack growth increments at these points invoking a fatigue crack growth relationship. A new crack front is established using a cubic spline approximation. A remeshing technique developed enables the procedure to be implemented automatically, and then fatigue crack growth can, therefore, be predicted in a step-by-step way.

The study displays the sensitivity of stress intensity factor results to crack shape, the effect of mesh orthogonality and the J-integral path independence. According to the results the stress intensity factor results are sensitive to the crack front shape, that the cubic spline approximation gives more accurate results than the polygonal line approximation. The orthogonal mesh seems unnecessary for the J-integral but necessary for 1/4-point displacement method. J-integral path independence is usually maintained but is lost at the free surface if a slightly non-orthogonal intersection exists between the free surface and the crack front.

The variation of stress intensity factors along the crack front is estimated using the 1/4-point crack opening displacement method or the J-integral method. Based on the results J-integral method gives more reliable results. The present technique is sufficiently accurate if the crack front is defined by the cubic spline curve.

In the paper by Hou et al. [31], the finite element method and crack growth laws in fracture mechanics were combined. The main approach was that the

stress intensity factors for general three-dimensional cracks were calculated by means of the finite element method and the crack growth behavior was observed by using the crack growth principles in 3-D cases. The computer code ZENCRACK, which has a direct interface with FE code ABAQUS, automatically generates the 3D 20-noded crack elements and replaces them by a group of crack elements to form a desired crack front. The crack front can be either semi-circular/semi- elliptical or linear within a crack block. Based upon a cracked FE model the stress intensity factor can be determined at each node along the crack front using the J-integral method in ABAQUS.

Courtin et al. [16] aimed to present the test results of several existing numerical techniques reported in the literature. Both the crack opening displacement extrapolation method and the J-integral approach are applied in 2D and 3D ABAQUS finite element models. The results obtained by these various means on CT specimens and cracked round bars are in good agreement with those found in the literature. From the results obtained it is indicated that the J-integral method shows some advantages compared to the displacement extrapolation one. First of all, this method may be applied automatically with the ABAQUS code. Then, the knowledge of the exact displacement field in the vicinity of the crack tip is not required, and the use of singular finite elements is not essential anymore. Besides, non-orthogonal meshes are without effect on the SIF calculations. The user has just to be sure that a convergent value is obtained on the different rings. As a consequence, this approach seems to be particularly suitable to deal with the fatigue growth of general cracks.

Ranestad et al. [12] described a method for obtaining accurate descriptions of crack-tip stress-fields in surface cracked welded plates without the need of large 3D FEA models. The method simply uses the existing shell models in combination with a plane strain sub-model. The boundary conditions of the sub-model were taken from the global shell model. When the results were

compared to a 3D solid model, the shell models give good predictions of the J values for homogeneous materials and for weldments with fusion line crack. The need for the method is because of the expensiveness both in terms of modeling time and computation time.

Recent studies show that sub-modeling technique is one of the most powerful techniques when it is necessary to obtain an accurate and detailed solution in a local region of a large model. In real life conditions, updating the model for each changing fracture parameters is very time consuming and unnecessary. That's why Gerstle et al. [32] [33] performed studies on the determination of fracture solutions by using sub-modeling technique. They prepared their own programs for analyzing the fracture problems and get accurate results by using these programs.

There are various real life applications of sub-modeling technique in literature. One is performed by Giglio [34] dealing with the analysis of fatigue damage to upper and lower folding beams on the rear fuselage of a naval helicopter which may result from flight and folding loads. The study is a FEM-based analytical approach together with experimental tests. The finite element model of the helicopter part is created by means of an ABAQUS/Standard finite element program combined with advanced sub-modeling techniques. The finite elements calculations were confirmed by experimental test results. Thus, sub-modeling technique is found to be reliable for engineering fatigue analysis.

Kitamura et al. [35] applied the sub-modeling technique to ship structure analysis in which a Bulk Carrier is selected. In their study they used two types of boundary conditions, the displacement boundary condition and the stress boundary condition. Applying the displacement boundary condition to sub-modeling analysis is often used in practice and is a key study in the literature for the following reasons. First, it is easier to be implemented, and second, for a raw FEM solution, displacements are generally more accurate

than stresses. At the end of their study, they obtained accurate solutions by using sub-modeling technique.

Another industrial application of sub-modeling technique is carried out by Larson [36]. In the study a gearbox (2.3 Mdofs) and a control housing (2.9 Mdofs) are investigated. A GUI prepared for adaptive sub-modeling in an interactive fashion in real time. The study also couples the sub-modeling with local shape optimization.

As far as the studies mentioned above are considered the sub-modeling technique is a powerful tool in 3D analysis. In recent studies it is commonly used and give accurate results. Common commercial finite element analysis software such as MSC.MENTAT– MARC [37], ABAQUS [38], ANSYS [39] has sub-modeling technique in them. Therefore, it is easy and inexpensive to apply this method to large models, where a detailed solution in local region is desired to obtain.

# CHAPTER 3

# FRACTURE ANALYSIS IN THREE DIMENSIONS

## 3.1 Introduction

Standard design methods for engineering structures and components under static loading are usually based on avoiding failure by yielding/plastic collapse or buckling. The derivation of loading resistance is based on conventional solid mechanics theories of stress analysis. Conventional design procedures against fatigue failure are based on experimental results for particular geometric details and materials. None of these procedures are capable of allowing for the effects of severe stress concentrations or crack-like flaws. The presence of such flaws is more or less inevitable to some extent in practical fabrications.

The modes of failure which are most affected by the presence of crack-like flaws are fracture and fatigue. The study of the effects of cracks on local stress and strain fields in the neighborhood of the crack tip and the consequent effect on failure is the subject of fracture mechanics. The application of fracture mechanics methods allows analyses to be carried out to predict the effects of flaws on failure in a wide range of geometries to give complementary information to that obtained from experimental testing. For fatigue of welded structures the performance is significantly affected by the tiny flaws inherent to welding. Fracture mechanics analyses can be very

helpful in predicting the effects of geometrical variations on basic fatigue behavior [40].

Use of crack propagation laws based on stress intensity factor ranges is the most successful engineering application of fracture mechanics. This chapter gives a review of the basic concepts of fracture mechanics. In contrast to the traditional stress-life and strain-life approaches to fatigue, cracks are assumed to exist in materials and structures within the context of fracture mechanics. Fracture parameters such as K and J can be used to characterize the stresses and strains near the crack tips. A fundamental understanding of fracture mechanics and the limit of using the fracture parameters is needed for appropriate applications of fracture mechanics to model fatigue crack propagation.

In this chapter, the concept of Stress Intensity Factor (SIF) is first introduced. Then, different fracture modes and fracture toughness are discussed. Later, the expressions of asymptotic crack-tip fields are derived. Afterwards, linear elastic stress intensity factors and energy release rate are introduced. Finally, evaluation of J-integral is presented.

### 3.2 Stress Intensity Factor (SIF)

Irwin (1957) introduced the concept of stress intensity factor, K, as the parameter, which is providing complete description of the state of stress, strain and displacement near the tip of a crack caused by a remote load or residual stresses. It is basically used for representing the strength of the singularity under different loading conditions. The SIF is proportional to the applied stress. This relationship is a direct consequence of the linear nature of the theory of elasticity. Unlike the stress concentration factor, the stress intensity factor is size dependent, because it contains the crack length as parameter.

If a segment of crack front is considered, it is subjected to three primary loading modes and their combinations at different loading conditions. A Cartesian coordinate system is assigned such that the crack front is in the z direction and idealized planar crack problems, in which the stresses and strains near the crack tip can be expressed in terms of the in-plane coordinates x and y only, are considered. As shown in Figure 3.1, the crack is subject to Mode I, the opening or tensile mode, where the in-plane stresses and strains are symmetric with respect to the x axis. As shown in Figure 3.2, the crack is subject to Mode II, the sliding or in-plane shearing mode, where the stresses and strains are anti-symmetrical with respect to the x axis. As shown in Figure 3.3, the crack is subject to Mode III, the tearing or anti-plane shearing mode, where the out-of-plane stresses and strains are anti-symmetrical with respect to the x axis [41].

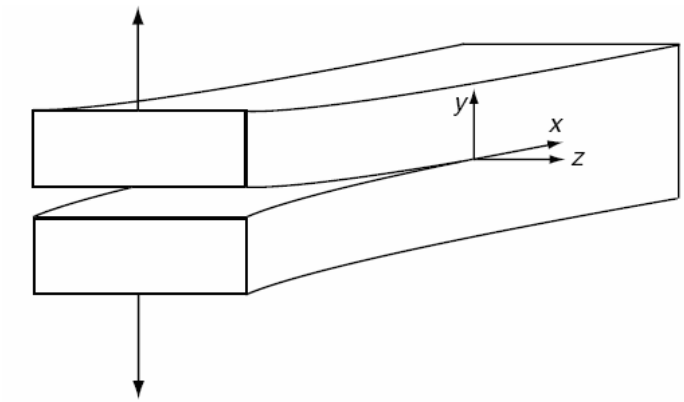


Figure 3.1 Mode I (Opening Mode)

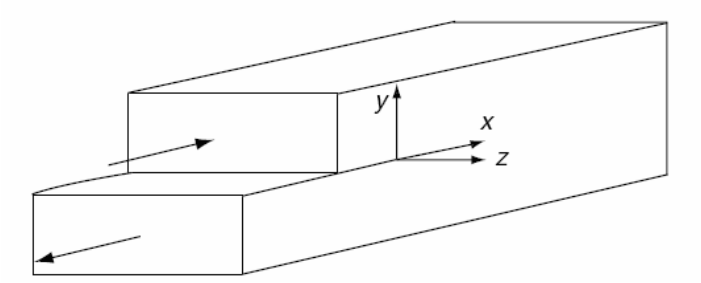


Figure 3.2 Mode II (In-plane Shearing Mode)

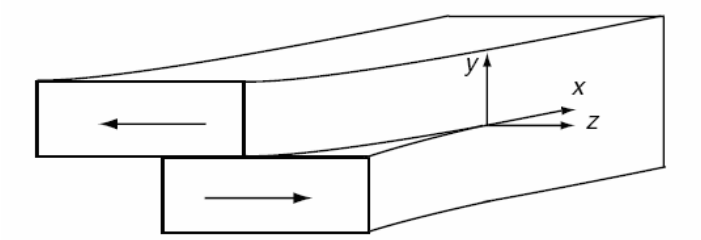


Figure 3.3 Mode III (Out-of-plane Shearing Mode)

Mode I is the most common loading type encountered in engineering design and in literature there exist many studies related to Mode I loading. Combinations of these modes are also possible and it is called mixed mode loading type. The encountered cracks, where high stresses or material imperfections existing, in industrial applications mostly have mixed mode loading. Since it is very important to assess the remaining life accurately, mixed mode loading estimations must be done precisely. This, of course, requires an accurate and physics based three-dimensional fracture solution to include all geometrical details and loading conditions in the problem. Even for surface and corner crack problems involving simple geometry, loading and boundary conditions, it is still important to apply three-dimensional

methods since the corresponding two-dimensional analyses, i.e., plane strain or plane stress, yield conservative results.

Moreover, in some problems there are truly three dimensional geometrical features to be considered. In such circumstances, three-dimensional fracture analysis is also unavoidable to account for the correct geometry and therefore the correct loading conditions near the crack region.

### 3.3 Fracture Toughness

As the stress intensity factor reaches a critical value, unstable fracture occurs.

This critical value of the stress intensity factor is known as the fracture toughness of the material. The fracture toughness can be considered as the limiting value of the stress intensity just as the yield stress might be considered as the limiting value of the applied stress. The fracture toughness depends on both temperature and the specimen thickness. Mode I plane strain fracture toughness is denoted as $K_{IC}$. $K_C$, which is the plane stress fracture toughness, is used to measure a material's fracture toughness in a sample that has a thickness that is less than some critical value, B. When the material's thickness is less than B, and stress is applied, the material is in a state called plane stress. A material's thickness is related to its fracture toughness graphically in Figure 3.4. If a stress is applied to a sample with a thickness greater than B, it is in a state called plane strain [18].

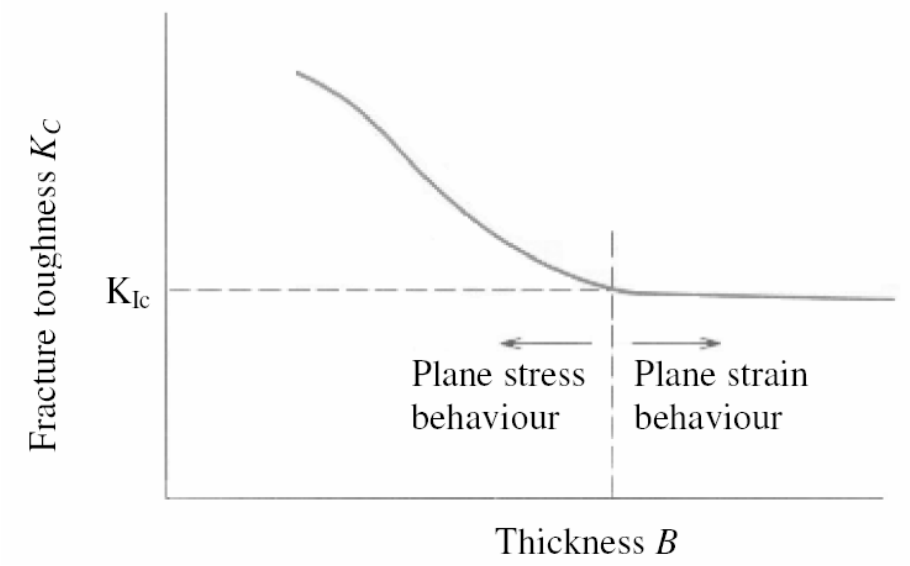


Figure 3.4 Fracture Toughness vs. Material Thickness Graph

### 3.4 Two and Three Dimensional Linear Elastic Crack Tip Fields

The stresses and strains at any point near a crack tip can be derived from the theory of elasticity. The asymptotic crack-tip stresses and strains for different modes of loading are known to satisfy a set of fundamental differential equations resulting from equilibrium, compatibility conditions and physical properties of the material which constitutes the solid body.

Figure 3.5 and 3.6 show the stress field and polar coordinate system for a two dimensional crack. Two and three dimensional linear elastic crack tip fields (stress and displacement relations) and the stress intensity factor definitions are expressed below for each loading mode.

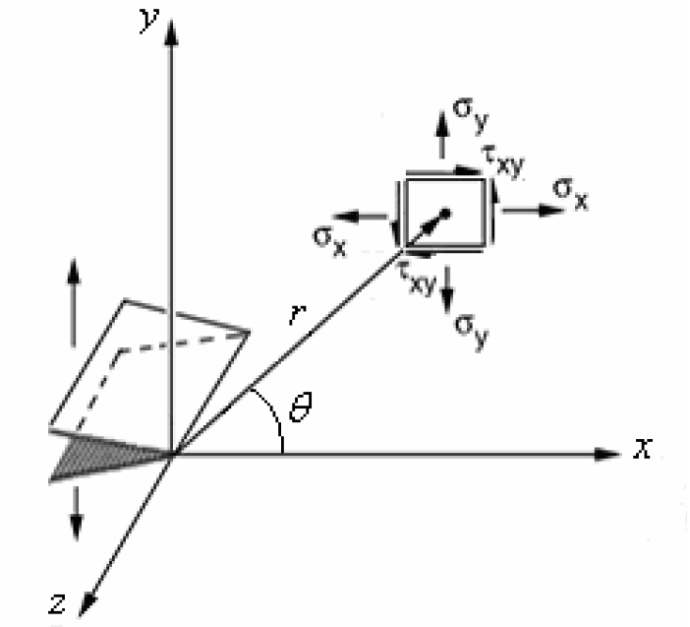


Figure 3.5 Distribution of Stresses in Vicinity of Crack Tip

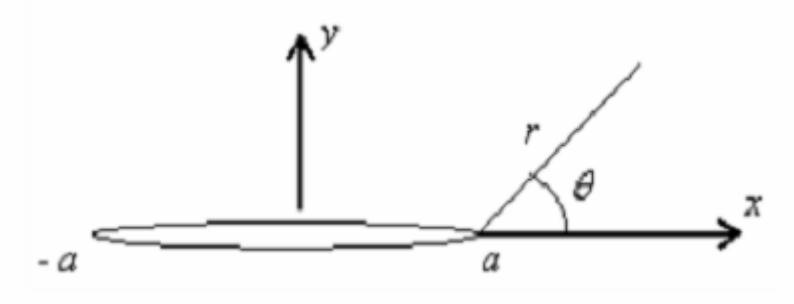


Figure 3.6 A Two-dimensional Crack Configuration

The distribution of stresses and displacements in small region around a crack tip given by asymptotic expressions are always the same for any cracked body. Although the asymptotic expressions are universal, the stress intensity factor depends on the geometry and the loading conditions. In other words,

the stress intensity factor is a function of the size and position of the crack in the geometry and the applied stress.

For each loading mode (mode I, II and III), two dimensional linear elastic crack tip fields and definitions of stress intensity factors are cited below. [42]

Mode I Crack:

$$\sigma_{yy}(r,\theta) = \frac{K_I}{\sqrt{2\pi r}}\cos\left(\frac{\theta}{2}\right)\left\{1+\sin\left(\frac{\theta}{2}\right)\sin\left(\frac{3\theta}{2}\right)\right\} \quad (3.1)$$

$$\sigma_{xx}(r,\theta) = \frac{K_I}{\sqrt{2\pi r}}\cos\left(\frac{\theta}{2}\right)\left\{1-\sin\left(\frac{\theta}{2}\right)\sin\left(\frac{3\theta}{2}\right)\right\} \quad (3.2)$$

$$\sigma_{xy}(r,\theta) = \frac{K_I}{\sqrt{2\pi r}}\cos\left(\frac{\theta}{2}\right)\sin\left(\frac{\theta}{2}\right)\sin\left(\frac{3\theta}{2}\right) \quad (3.3)$$

$$u(r,\theta) = \frac{K_I}{2\mu}\sqrt{\frac{r}{2\pi}}\cos\left(\frac{\theta}{2}\right)\left\{\kappa-1+2\sin^2\left(\frac{\theta}{2}\right)\right\} \quad (3.4)$$

$$v(r,\theta) = \frac{K_I}{2\mu}\sqrt{\frac{r}{2\pi}}\sin\left(\frac{\theta}{2}\right)\left\{\kappa+1-2\cos^2\left(\frac{\theta}{2}\right)\right\} \quad (3.5)$$

where $K_I$ is the mode I stress intensity factor and $\sigma_{xx}$, $\sigma_{yy}$ and $\sigma_{xy}$ are the stress components (Figure 3.5) at a distance $r$ from the crack tip and at an angle $\theta$ from the crack plane. In Equations 3.4 and 3.5, $u$ and $v$ are the displacements in x and y directions. $\mu$ is the shear modulus and $\kappa$ is $\left(\frac{3-\nu}{1+\nu}\right)$ for plain stress and $(3-4\nu)$ for plain strain where $\nu$ is the Poisson's ratio. The relationship between the shear modulus ($\mu$), Young's modulus ($E$) and Poisson's ratio ($\nu$) is as follows:

$$\mu = \frac{E}{2(1+\nu)} \quad (3.6)$$

Definition of the mode I stress intensity factors can be written as:

$$K_I(a) = \lim_{x \to a^+} \sqrt{2\pi(x-a)}\,\sigma_{yy}(x,0) \tag{3.7}$$

$$K_I(-a) = \lim_{x \to -a^-} \sqrt{2\pi(-x-a)}\,\sigma_{yy}(x,0) \tag{3.8}$$

where a is the half of the crack length.

Mode II Crack:

$$\sigma_{yy}(r,\theta) = \frac{K_{II}}{\sqrt{2\pi r}} \sin\left(\frac{\theta}{2}\right)\cos\left(\frac{\theta}{2}\right)\cos\left(\frac{3\theta}{2}\right) \tag{3.9}$$

$$\sigma_{xx}(r,\theta) = -\frac{K_{II}}{\sqrt{2\pi r}} \sin\left(\frac{\theta}{2}\right)\left\{2 + \cos\left(\frac{\theta}{2}\right)\cos\left(\frac{3\theta}{2}\right)\right\} \tag{3.10}$$

$$\sigma_{xy}(r,\theta) = \frac{K_{II}}{\sqrt{2\pi r}} \cos\left(\frac{\theta}{2}\right)\left\{1 - \sin\left(\frac{\theta}{2}\right)\sin\left(\frac{3\theta}{2}\right)\right\} \tag{3.11}$$

$$u(r,\theta) = \frac{K_{II}}{2\mu}\sqrt{\frac{r}{2\pi}} \sin\left(\frac{\theta}{2}\right)\left\{\kappa + 1 + 2\cos^2\left(\frac{\theta}{2}\right)\right\} \tag{3.12}$$

$$v(r,\theta) = -\frac{K_{II}}{2\mu}\sqrt{\frac{r}{2\pi}} \cos\left(\frac{\theta}{2}\right)\left\{\kappa - 1 - 2\sin^2\left(\frac{\theta}{2}\right)\right\} \tag{3.13}$$

where $K_{II}$ is the mode II stress intensity factor, which can be defined as:

$$K_{II}(a) = \lim_{x \to a^+} \sqrt{2\pi(x-a)}\,\sigma_{xy}(x,0) \tag{3.14}$$

$$K_{II}(-a) = \lim_{x \to -a^-} \sqrt{2\pi(-x-a)}\,\sigma_{xy}(x,0) \tag{3.15}$$

Mode III Crack:

$$\sigma_{xz}(r,\theta) = -\frac{K_{III}}{\sqrt{2\pi r}}\sin\left(\frac{\theta}{2}\right) \tag{3.16}$$

$$\sigma_{yz}(r,\theta) = \frac{K_{III}}{\sqrt{2\pi r}}\cos\left(\frac{\theta}{2}\right) \tag{3.17}$$

$$\sigma_{xx}(r,\theta) = \sigma_{yy}(r,\theta) = \sigma_{zz}(r,\theta) = 0 \tag{3.18}$$

$$w(r,\theta) = \frac{K_{III}}{\mu}\sqrt{\frac{r}{2\pi}}\sin\left(\frac{\theta}{2}\right) \tag{3.19}$$

$$u(r,\theta) = v(r,\theta) = 0 \tag{3.20}$$

where $w$ is the displacement in $z$ direction and $K_{III}$ is the mode III stress intensity factor, which can be defined as:

$$K_{III}(a) = \lim_{x\to a^{+}}\sqrt{2\pi(x-a)}\,\sigma_{yz}(x,0) \tag{3.21}$$

$$K_{III}(-a) = \lim_{x\to -a^{-}}\sqrt{2\pi(-x-a)}\,\sigma_{yz}(x,0) \tag{3.22}$$

In figure 3.7, a three dimensional crack front and a local coordinate system is shown. The parameter $s$ in this figure is the arc length of the crack front and $t$, $n$, $b$ is a local coordinate system located at point $P$ composed of the tangential ($t$), normal ($n$) and binormal ($b$) directions, $n$ pointing into the material side. ($r$, θ) are the polar coordinates in the normal plane ($n$, $b$) [43]. Three dimensional linear elastic crack tip fields are given below:

$$\sigma_{nn} = \frac{K_{I}(s)}{\sqrt{2\pi r}}\cos\left(\frac{\theta}{2}\right)\left[1-\sin\left(\frac{\theta}{2}\right)\sin\left(\frac{3\theta}{2}\right)\right]$$
$$-\frac{K_{II}(s)}{\sqrt{2\pi r}}\sin\left(\frac{\theta}{2}\right)\left[2+\cos\left(\frac{\theta}{2}\right)\cos\left(\frac{3\theta}{2}\right)\right] \tag{3.23}$$

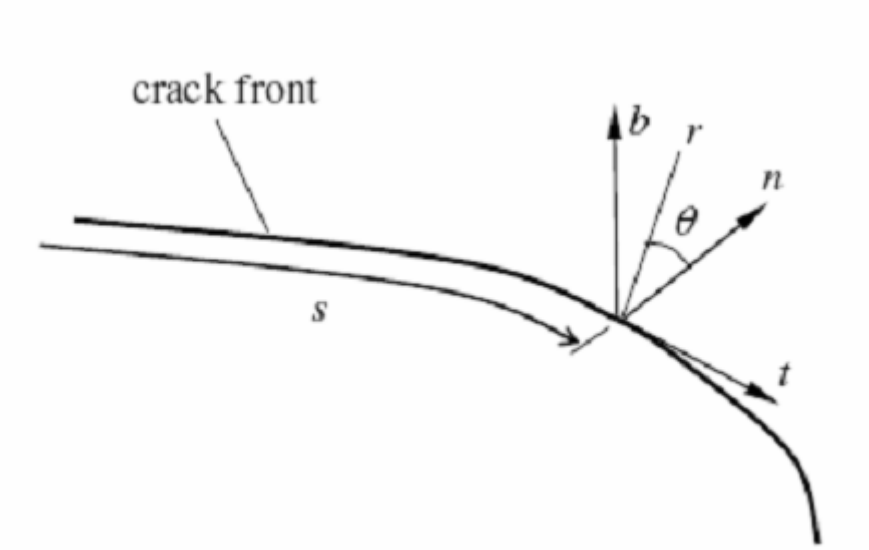


Figure 3.7 Three Dimensional Crack Front and the Local Coordinate System

$$\sigma_{bb} = \frac{K_I(s)}{\sqrt{2\pi r}}\cos\left(\frac{\theta}{2}\right)\left[1+\sin\left(\frac{\theta}{2}\right)\sin\left(\frac{3\theta}{2}\right)\right] + \frac{K_{II}(s)}{\sqrt{2\pi r}}\sin\left(\frac{\theta}{2}\right)\cos\left(\frac{\theta}{2}\right)\cos\left(\frac{3\theta}{2}\right) \tag{3.24}$$

$$\sigma_{tt} = 2\nu\left[\frac{K_I(s)}{\sqrt{2\pi r}}\cos\left(\frac{\theta}{2}\right) - \frac{K_{II}(s)}{\sqrt{2\pi r}}\sin\left(\frac{\theta}{2}\right)\right] \tag{3.25}$$

$$\sigma_{nb} = \frac{K_I(s)}{\sqrt{2\pi r}}\sin\left(\frac{\theta}{2}\right)\cos\left(\frac{\theta}{2}\right)\cos\left(\frac{3\theta}{2}\right) + \frac{K_{II}(s)}{\sqrt{2\pi r}}\cos\left(\frac{\theta}{2}\right)\left[1-\sin\left(\frac{\theta}{2}\right)\sin\left(\frac{3\theta}{2}\right)\right] \tag{3.26}$$

$$\sigma_{nt} = -\frac{K_{III}(s)}{\sqrt{2\pi r}}\sin\left(\frac{\theta}{2}\right) \tag{3.27}$$

$$\sigma_{bt} = \frac{K_{III}(s)}{\sqrt{2\pi r}}\cos\left(\frac{\theta}{2}\right) \tag{3.28}$$

$$u_n = \frac{1+\nu}{E}\sqrt{\frac{2r}{E}}\left\{K_I(s)\cos\left(\frac{\theta}{2}\right)\left[(1-2\nu)+\sin^2\left(\frac{\theta}{2}\right)\right]\right.$$
$$\left. + K_{II}(s)\sin\left(\frac{\theta}{2}\right)\left[2(1-\nu)+\cos^2\left(\frac{\theta}{2}\right)\right]\right\} \tag{3.29}$$

$$u_b = \frac{1+\nu}{E}\sqrt{\frac{2r}{\pi}}\left\{K_I(s)\sin\left(\frac{\theta}{2}\right)\left[2(1-\nu)-\cos^2\left(\frac{\theta}{2}\right)\right]\right.$$
$$\left. - K_{II}(s)\cos\left(\frac{\theta}{2}\right)\left[(1-2\nu)-\sin^2\left(\frac{\theta}{2}\right)\right]\right] \tag{3.30}$$

$$u_t = 2\frac{1+\nu}{E}\sqrt{\frac{2r}{\pi}}K_{III}(s)\sin\left(\frac{\theta}{2}\right) \tag{3.31}$$

where $K_I$, $K_{II}$ and $K_{III}$ are the stress intensity factors and these are defined as:

$$K_I = \lim_{r\to 0}\sqrt{2\pi r}\,\sigma_{bb}(r,0) \tag{3.32}$$

$$K_{II} = \lim_{r\to 0}\sqrt{2\pi r}\,\sigma_{nb}(r,0) \tag{3.33}$$

$$K_{III} = \lim_{r\to 0}\sqrt{2\pi r}\,\sigma_{bt}(r,0) \tag{3.34}$$

### 3.5 Energy Release Rate

Linear fracture mechanics presupposes existence of a crack and examines the conditions under which crack growth occurs. For a crack to propagate, the rate of elastic energy release should at least be equal the rate of energy needed for creation of a new crack surface. The energy balance between the

strain energy in the structure and the work needed to create a new crack surface can be expressed using the *energy release rate* (*G*) as follows:

$$G = G_C \tag{3.35}$$

*G* is defined as:

$$G = -\frac{d\Pi}{da} \tag{3.36}$$

where $\Pi$ is the strain energy and *a* is the crack area. *G* depends on the geometry of the structure and the current loading. $G_c$ is called the fracture toughness of the material. It is a material property and determined by experiments. Note that the energy release rate is not a time derivative but a rate of change in potential energy with crack area. An important feature of Equation 3.35 is that it can be used as a fracture criterion; a crack starts to grow when *G* reaches the critical value $G_c$.

The connection between the energy release rate and the stress intensity factors is given by [21]:

$$G = G_I + G_{II} + G_{III} = \frac{1}{E^*}(K_I{}^2 + K_{II}{}^2) + \frac{1}{2\mu}K_{III}{}^2 \tag{3.37}$$

where

$$E^* = E \text{ (For plane stress)} \tag{3.38}$$

and

$$E^* = \frac{E}{(1-\nu^2)} \text{ (For plane strain)} \tag{3.39}$$

If only mode I loading type exists, where $K_{II}$ and $K_{III}$ are equal to zero, Equation 3.37 becomes:

$$G = \frac{K^2}{E} \text{ (For plane stress)} \tag{3.40}$$

$$G = \left( \frac{1-\nu^2}{E} \right) \cdot K^2 \text{ (For plane strain)} \tag{3.41}$$

### 3.6 J-integral

The J-integral is similar to *G* but is more general and is also used for nonlinear applications. *J* is equivalent to *G* when a linear elastic material model is used.

The J-integral probably offers the best chance to have a single parameter to relate to the initiation of crack propagation. The J-integral was introduced by Rice as a path-independent contour integral for the analysis of cracks. As previously mentioned, it is equivalent to the energy release rate for a linear elastic material model. It is defined in two dimensions as:

$$J = \int_{\Gamma} ((W+T)n_1 - \sigma_{ij} n_i \frac{\partial u_j}{\partial x_1}) d\Gamma \tag{3.42}$$

where *W* is the strain energy density, *T* is the kinetic energy density, $\sigma_{ij}$ is the stress tensor and $u_j$ is the displacement vector. The $x_1$ direction is the same as the x direction in the local crack tip system in Figure 3.8. The integration path $\Gamma$ is a curve surrounding the crack tip, see Figure 3.8. The J-integral is independent of the path $\Gamma$ as long as it starts and ends at the two sides of the crack face and no other singularities are present within the path. This is an

important feature for the numerical evaluation since the integral can be evaluated using results away from the crack tip.

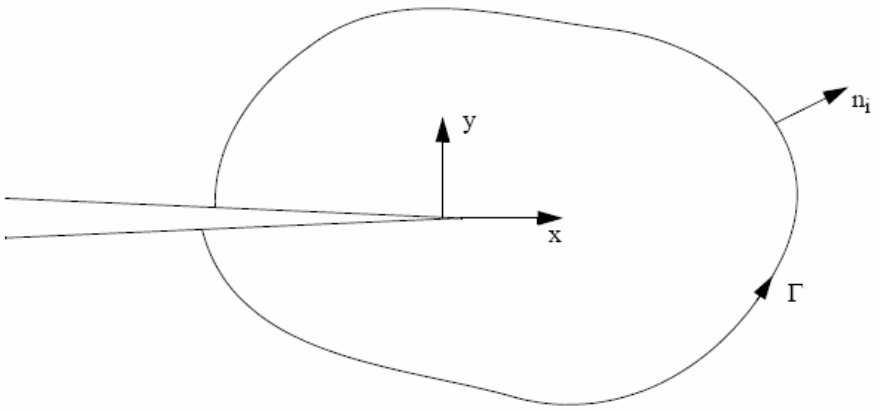


Figure 3.8 Definition of the J-integral

### 3.7 Numerical Evaluation of the J-integral

The J-integral evaluation in MSC.Marc is based upon the domain integration method. Since, it is difficult to define the integration path $\Gamma$, some simplifications are done in finite element analysis. In the domain integration method for two dimensions, the line integral is converted into an area integration over the area inside the path $\Gamma$. This conversion is exact for the linear elastic case and also for the nonlinear case if the loading is proportional, that is, if no unloading occurs. By choosing this area as a set of elements, the integration is straightforward using the finite element solution. In two dimensions, the converted expression is

$$^{-}J = \int_{A} (\sigma_{ij} \frac{\partial u_j}{\partial x_1} - W\delta_{1i}) \frac{\delta q_1}{\delta x_i} dA \qquad (3.43)$$

for the simplified case of no thermal strains, body forces or pressure on the crack faces. *A* is the area inside $\Gamma$ and $q_1$ is a function introduced in the conversion into an area integral. The function $q_1$ can be chosen fairly general, as long it is equal to one at the crack tip and zero on $\Gamma$ [37].

This thesis is concerned with semi-elliptical surface cracks arbitrarily inclined to the free surface of fillet welded joint toes and root subjected to mixed mode loading condition. Therefore, the estimated J-integral values for fillet welded joints will allways be for mixed mode loading type. Since it gives exact solutions for linear elastic case, the J-integral values will be calculated by using commercial finite element analysis software MSC.Marc.

# CHAPTER 4

# FINITE ELEMENT MODELING

## 4.1 Introduction

Finite Element Analysis (FEA) is a computer simulation technique used in engineering analysis. It uses a numerical technique called the finite element method (FEM). The finite element method (FEM) is a computer technique for solving partial differential equations. By using this technique the stresses, deflections and reaction forces etc in objects can be estimated. The technique involves dividing the object into relatively small elements whose individual behavior is easily calculated. The behavior of all of the small elements is then put together to estimate the stresses and deflections in the entire object.

In finite element analysis, the design is discretized or subdivided into a series of elements that are connected by nodes. Material properties and element properties are specified to represent the physical properties of the model. Boundary conditions and applied loads are then defined to represent the operating environment for which the design is to be subjected. Finite element analysis is a simulation tool that enables engineers to simulate the behavior of a structure [44].

In general, there are three phases in finite element analysis:

- Pre-processing (defining the finite element model and environmental factors to be applied to it)
- Analysis solver (solution of finite element model)
- Post-processing of results (using visualization tools)

Finite element analysis is an important part of the overall design process, serving to verify or validate a design prior to its manufacture. However it is important that the results from finite element analysis are always examined carefully. The credibility of the results should always be checked by carrying out experiments whenever possible.

### 4.2 Problem Definition

There are a large number of commercial computer programs available today that are specially designed for creating and analyzing finite element models. Many of these computer programs are highly sophisticated in their ability to generate a model, solve it and finally analyze the results.

Modeling is the most time consuming and human controlled phase of finite element analysis. Modeling can be defined as the simulation of a physical structure or physical process by means of a substitute analytical or numerical construct. It is not simply preparing a mesh of nodes and elements. Modeling require that the physical action of the problem be understood well enough to choose suitable kinds of elements, and enough of them, to represent the physical action adequately. It requires to avoid badly shaped elements and too large to represent important variations of the field quantity (displacement field or stress field). At the other extreme it is desired to avoid waste of analyst time and computer resources associated with over-refinement, that

is, using many more elements than needed to adequately represent the field and its gradient [45].

The optimization of earthmoving machinery attachments requires lots of analyses to be performed. However, it takes too much time to model the critical parts (such as boom and arm etc) of the machines. Therefore, few pre-processors are prepared for modeling the earthmoving machinery attachments automatically. One of these pre-processors is described in the thesis study performed by Yener [47]. In the thesis study of Yener, finite element analyses of excavator boom are carried out automatically. A prepared GUI lets the user set the parameters of the boom geometry and performs the analyses by using MSC.Marc behind it. The program defines the geometric and material properties, boundary conditions and other related parameters automatically. However, while modeling the boom geometry quadrilateral thick shell elements are used. This is due to the reason that the main aim of the study is to optimize the general stress distribution of the boom and lots of analyses must be performed for the optimization, which means that the solution time must be as low as possible. Thus, the prepared programs for earthmoving machinery components do not involve welded joints on them. However, according to the performed tests the failures occurring on the attachments are mainly due to the defects on welded joints and they must be well examined to obtain the optimum attachment geometry.

In this thesis, a prepared GUI will be used to convert the user-selected local shell region to solid region with the desired weld shape and to implement a semi elliptical surface crack into the weld toe and root at different inclination angles. The program will automatically take the geometric and material properties from the global model and it will use the sub-modeling technique for boundary condition application. Although the prepared program is a general use program for box cross section corner joints, only the boom and arm of the HMK 300 LC excavator will be studied in the scope of this study.

### 4.3 Sub-modeling

If the local stress field is of interest this requires a detailed finite element model in order to give sufficiently accurate results. In a large or geometrically complex structure it is often not possible to model whole structure with such accuracy, since this would involve a great deal of modeling work and result in a model that was difficult to work with. In such cases it is often a good solution to analyze the local stresses using a sub-model.

The sub-modeling approach involves creating a relatively coarse model to calculate the global stresses in the structure. In this model the weld can either be totally ignored or just be modeled roughly. Once the stresses have been calculated in the global model, a local model (sub-model) is constructed to model the area in question separately and give the degree of accuracy that is needed to resolve the stresses correctly. An example of this is shown in Figure 4.1. The deformations that are obtained from calculations using the global finite element model are then used as boundary conditions for the local model. This allows the local stresses at the weld to be calculated with a good degree of accuracy without taking up excessive computer time.

A typical structural zooming analysis contains two steps:

1. Global run to obtain a post file containing global results.
2. Local run to define kinematic boundary conditions in the local model and to obtain refined results in the local model.

This procedure can be repeated as many times as desired. Any local analysis can be the global analysis of next level refinement.

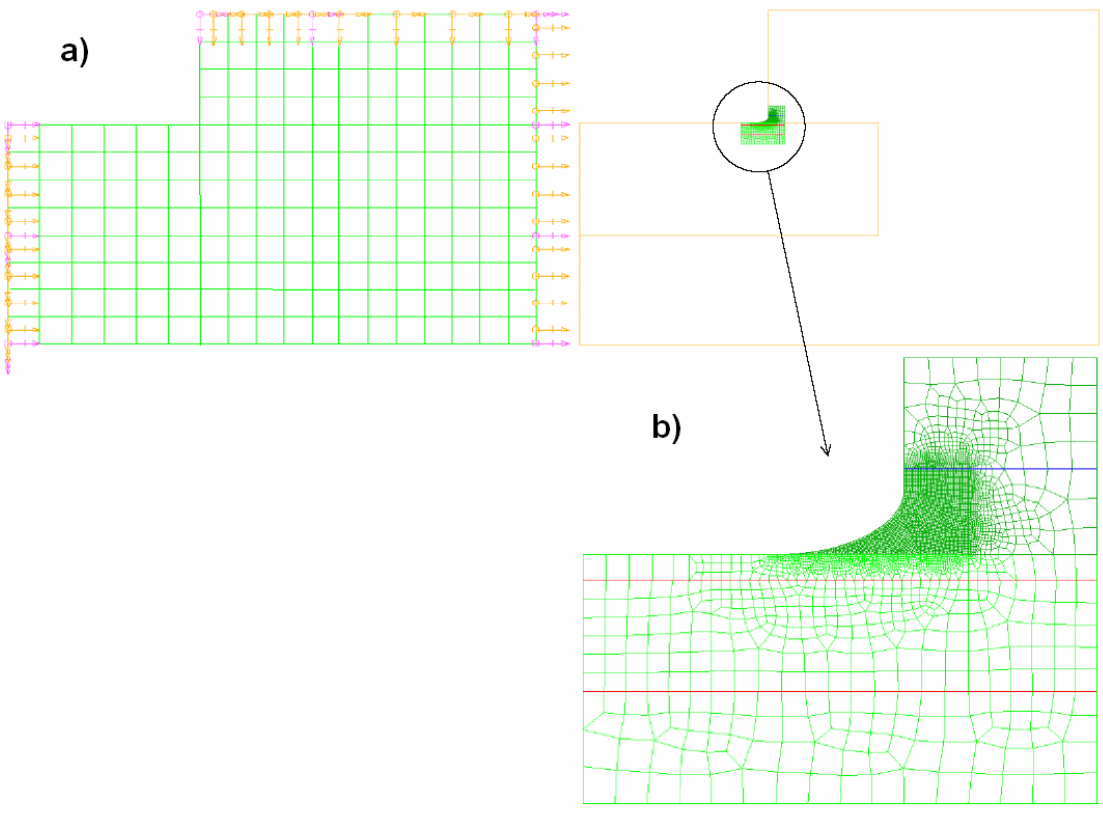


Figure 4.1 a) Global Model b) Local Model [48]

Aside from the obvious benefits of giving more accurate results in a region of the model, the sub-modeling technique has other advantages:

- It reduces, or even eliminates, the need for complicated transition regions in finite element models.
- It enables the user to experiment with different designs for the region of interest without requiring a complete re-analysis of the entire model
- It provides adequate mesh refinement

The sub-modeling technique used in this study is a little bit different from standard sub-modeling techniques used in commercial finite elements software.

The steps included in this study are as follows:

1. Automatic model formation of boom and arm geometry by using prepared GUI in Hidromek Ltd. Sti. and analysis of global model having quadrilateral thick shell elements as element type.
2. Selection of the interested local region.
3. Setting the weld and crack implementation parameters in GUI prepared for this study.
4. Conversion of local quadrilateral shell meshed model to 20-noded hex meshed solid model.
5. Application of set weld parameters to solid model.
6. Implementation of semi elliptical surface cracks either to one of the weld toe or to weld root.
7. Transfer of material properties from global model.
8. Definition of kinematic boundary condition application points.
9. Application of specially prepared tyings to shell-to-solid transition region.
10. Analysis of the sub-model.

The steps mentioned above will be explained in detail below.

### 4.3.1 Global Model

The first step of sub-modeling requires a complete analysis of global model. In this work, the boom and arm of HMK 300 LC excavator will be used as the global model. The global models will be prepared by using GUI prepared in Hidromek Ltd. Sti. It is assumed that material behavior is linear and strains are small. Therefore, linear elastic analysis will be carried out. Sheet metal

parts of the boom and arm are modeled by using quadrilateral thick shell elements. In the analysis only the boom and arm are realistically modeled. Hydraulic cylinders, arm, bucket and connecting linkage are modeled using beam elements (Figure 4.2).

The most critical boundary condition of an excavator is assumed to be when the machine is subjected to maximum digging force at maximum digging force position (Figure 4.6). The maximum digging force calculation of an excavator is defined in standard SAE J1179 [49].

Maximum digging force of an excavator can be calculated in two ways. First when the bucket cylinder is active and the second when the arm cylinder is active, see Figure 4.3.

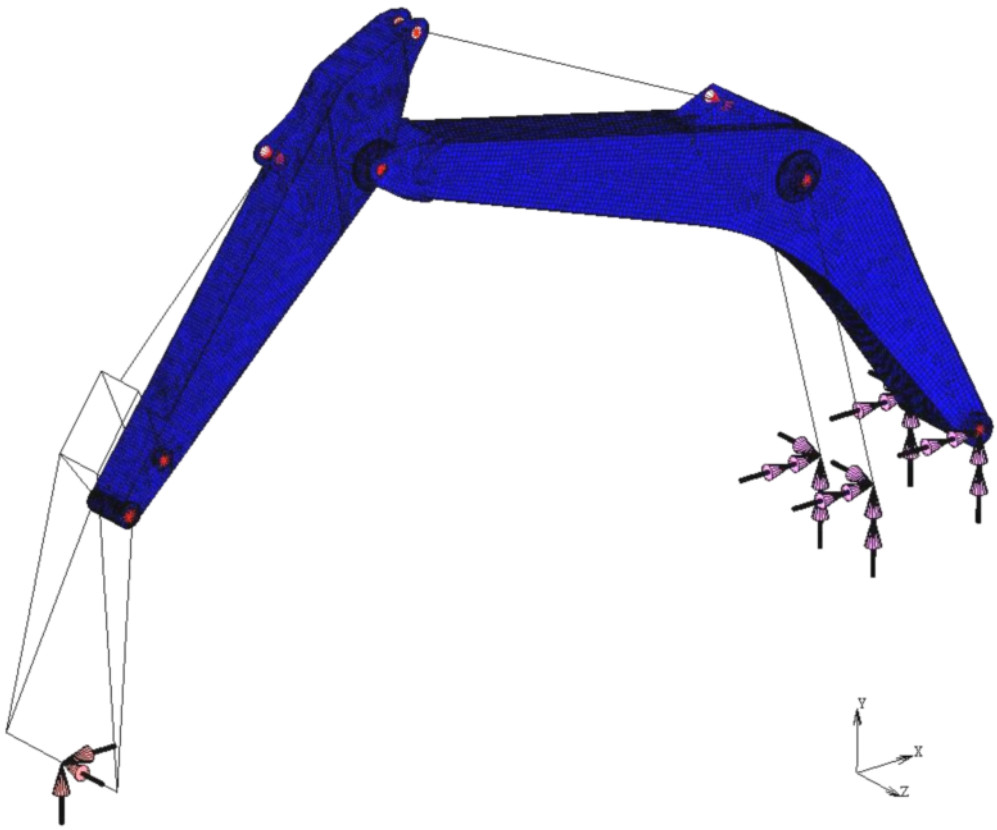


Figure 4.2 FEA Model of Excavator Mechanism

In this study, arm breakout force is taken to be the maximum digging force as the global model boundary condition. In order to see the effect of lateral loads on cracks, the global analyses are done by including the lateral loads and not including them. Figure 4.4 shows an example of global model analysis result including the lateral loads in boundary conditions.

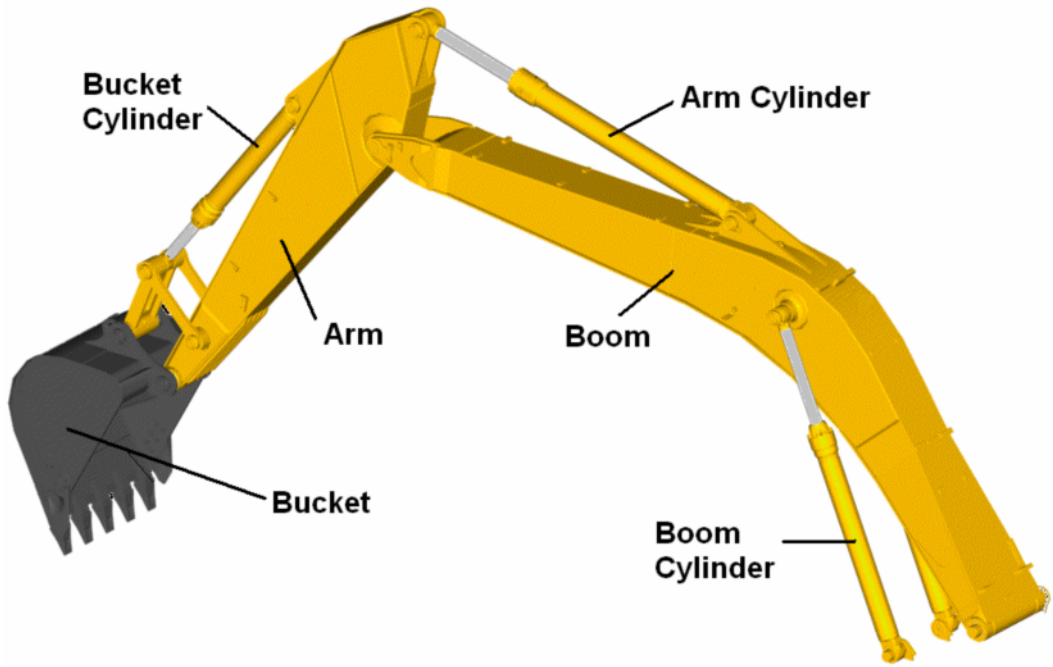


Figure 4.3 Basic Parts of Excavator

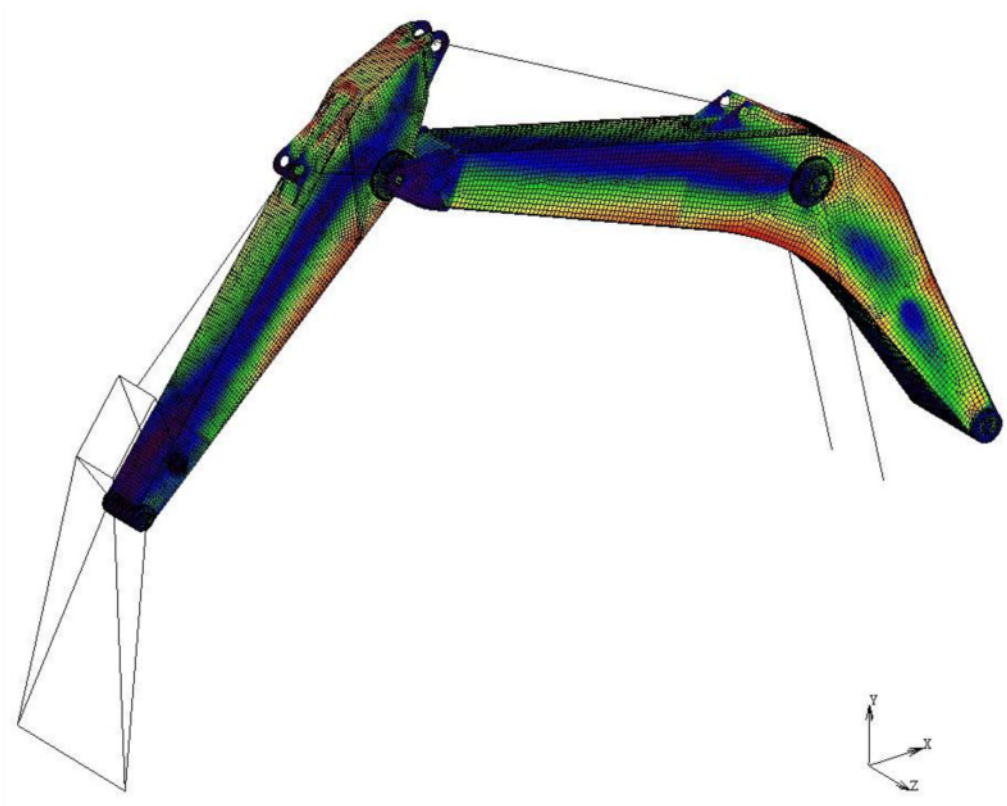


Figure 4.4 Von Mises Stress Map for Shell Outer Layer

#### 4.3.1.1 Boundary Conditions

##### 4.3.1.1.1 Bucket Breakout Force

The bucket breakout force is the available force at the tip of the teeth created by the bucket cylinder. Maximum breakout force is reached when the available tooth force reaches its maximum.

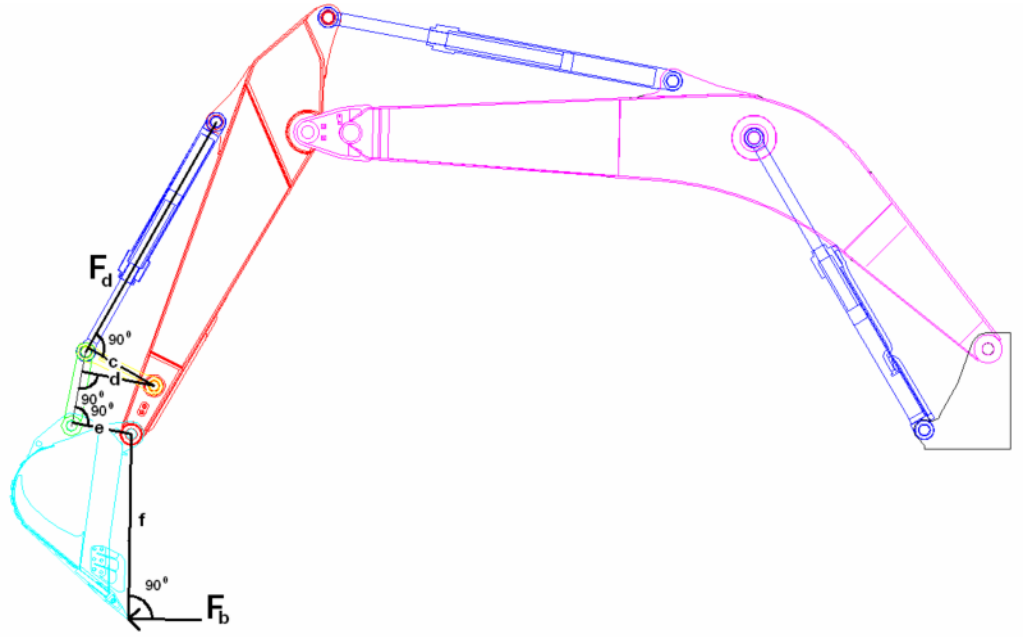


Figure 4.5 Bucket Breakout Force Position

$$F_d = P.\pi \frac{D_d^{\,2}}{4} \tag{4.1}$$

$$F_b = \frac{F_d.c.e}{d.f} \tag{4.2}$$

$F_d$ – Bucket cylinder force

$P$ – Working pressure of bucket cylinder

$D_d$ – Bucket cylinder diameter

$F_b$ – Bucket breakout force

$c$ – Perpendicular distance bucket cylinder axis - lever pivot

$d$ – Perpendicular distance connecting link axis - lever pivot

$e$ – Perpendicular distance connecting link axis - bucket pivot

$f$ – Radius bucket pivot - tooth lip

#### 4.3.1.1.2 Arm Breakout Force

The digging force is the available force at the tip of the bucket teeth created by the arm cylinder(s). Maximum digging force is calculated with dimension "g" at its maximum and with the bucket in a position calculated for maximum bucket breakout force.

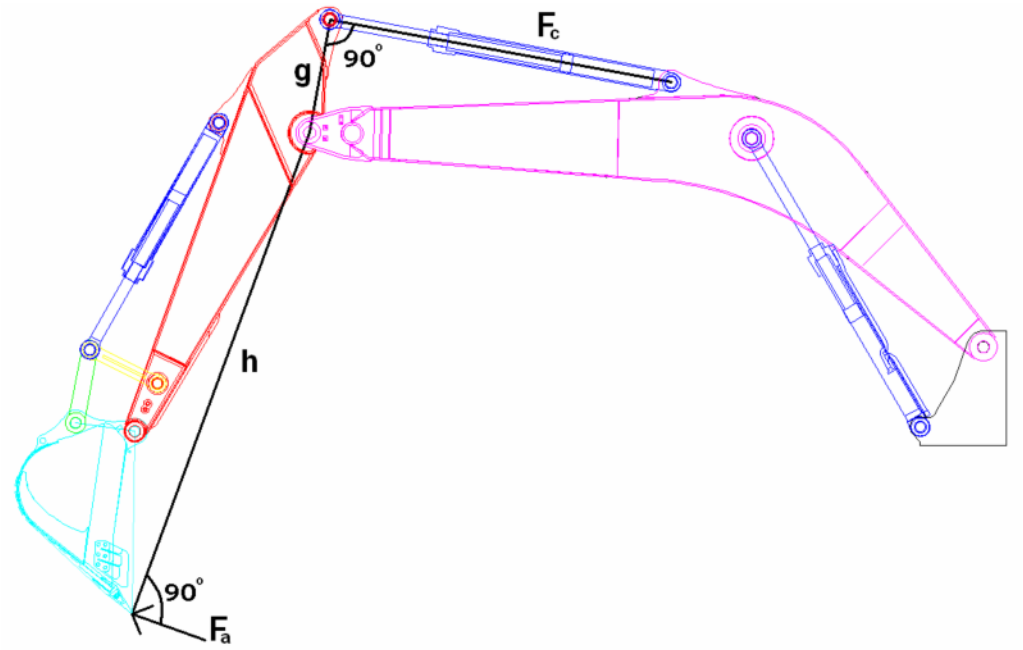


Figure 4.6 Arm Breakout Force (Digging Force) Position

$$F_c = P.\pi \frac{D_c^{\,2}}{4} \tag{4.3}$$

$$F_a = \frac{F_c.g}{h} \tag{4.4}$$

$F_c$ – Arm cylinder force

$P$ – Working pressure of arm cylinder

$D_c$ – Arm cylinder diameter

$F_a$ – Arm breakout force

$g$ – Perpendicular distance arm cylinder axis - arm pivot

$h$ – Distance arm pivot - tooth tip

#### 4.3.1.1.3 Lateral Force

Upper part of an excavator is capable of full rotation about the center of the chassis by means of a hydraulic system. This system is capable of applying a moment 'M' limited by the capacity of hydraulic oil motor-swing unit. This moment causes a lateral force 'F' at the tip of the bucket (Figure 4.7). Therefore, in finite element analysis, this lateral force must be included. However, to see the effect of lateral force on cracks, analysis will be divided into two groups: the analysis including lateral force and not including lateral force.

#### 4.3.1.1.4 Other Boundary Conditions

In finite element analysis, pivot joints of boom and boom cylinder on the chassis will be fixed in all directions except joint rotation direction (Figure 4.2).

To learn more about the global model analysis the thesis written by Yener [47] can be examined.

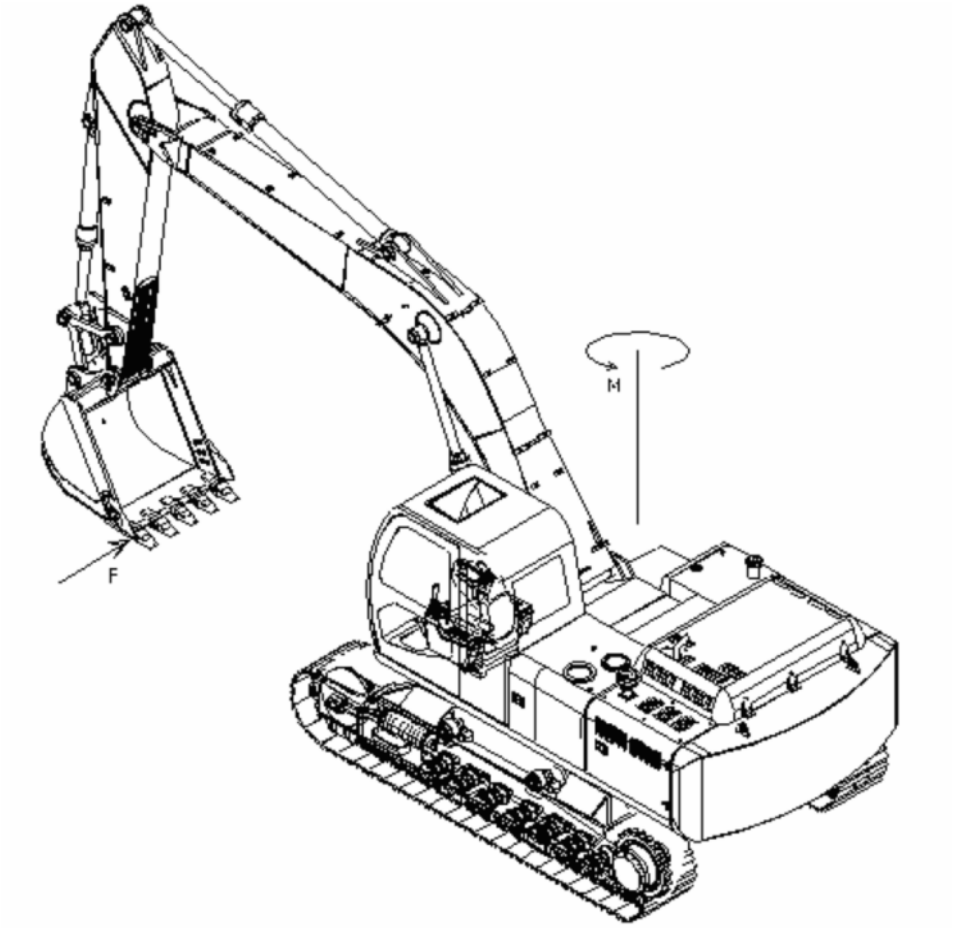


Figure 4.7 Lateral Force on the Bucket

### 4.3.2 Local Region Selection

Local region selection is of great importance for examining the cracks in critical regions. There are some limitations while selecting the local region on global model. First, this study includes only the corner joints of box cross section, therefore the selected region must be on the corner. Second, the selected region junction nodes should follow a linear path on the global model. Third, thickness transition regions should not be selected as local model regions. Although the prepared computer code is for general use, this study will only be interested in excavator boom and arm. Figure 4.8 shows

the selection possibilities (thick black lines) according to the specified limitations mentioned above.

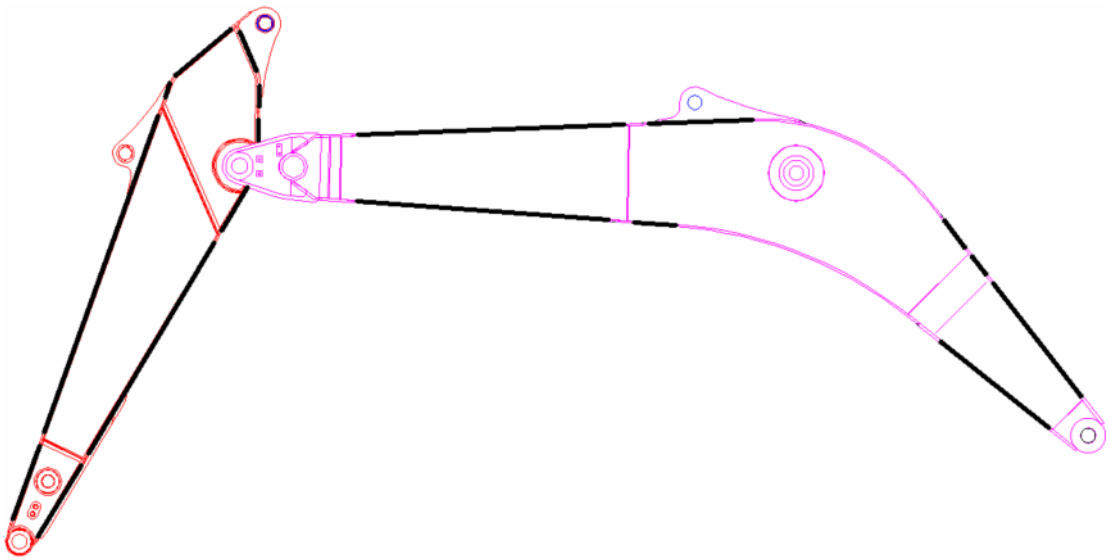

Figure 4.8 Selection Possibilities on Excavator Boom and Arm

### 4.3.3 Parameters

The parameters of local models are divided into two groups: weld parameters and crack parameters. In the following, the parameters are explained in detail.

#### 4.3.3.1 Weld Parameters

In the analyses, the weld shapes are always assumed to be in triangular, either isosceles or scalene, shape. In GUI, the set weld parameters differ with respect to the weld application side selection of the user. If the user

wants to apply one sided weld to created solid models the parameters that defines the weld geometry are (Figure 4.9):

Leg1 – Vertical leg length of the weld
Leg2 – Horizontal leg length of the weld
RD – Root Depth (determines the penetration depth of the weld)

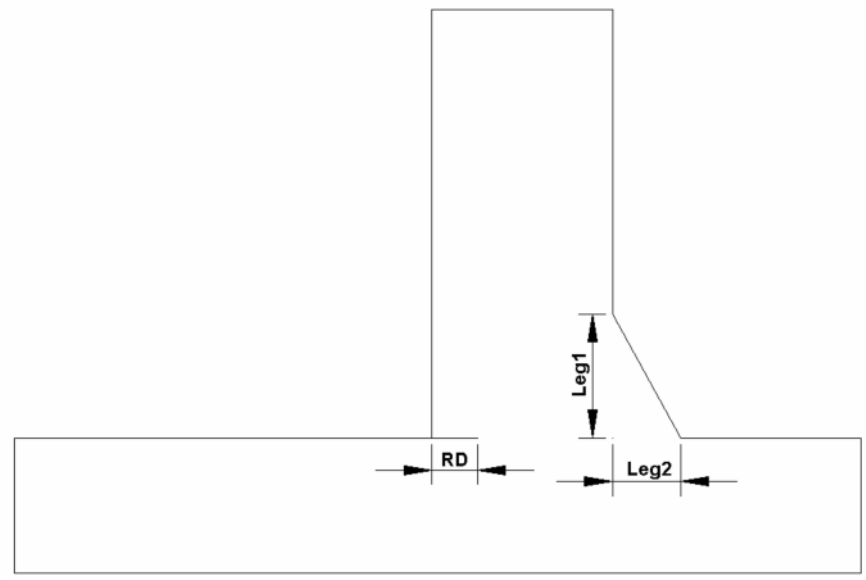


Figure 4.9 One Sided Weld Parameters

If the user wants to apply the weld to both sides of the solid model, the parameters are as follows (Figure 4.10, Figure 4.11):

Leg1 – Vertical leg length of the outer weld
Leg2 – Horizontal leg length of the outer weld
Leg_1 – Vertical leg length of the inner weld
Leg_2 – Horizontal leg length of the inner weld

MCD – Middle Crack Distance (determines the penetration depth of the weld)

MCL – Middle Crack Length (determines the penetration depth of the weld)

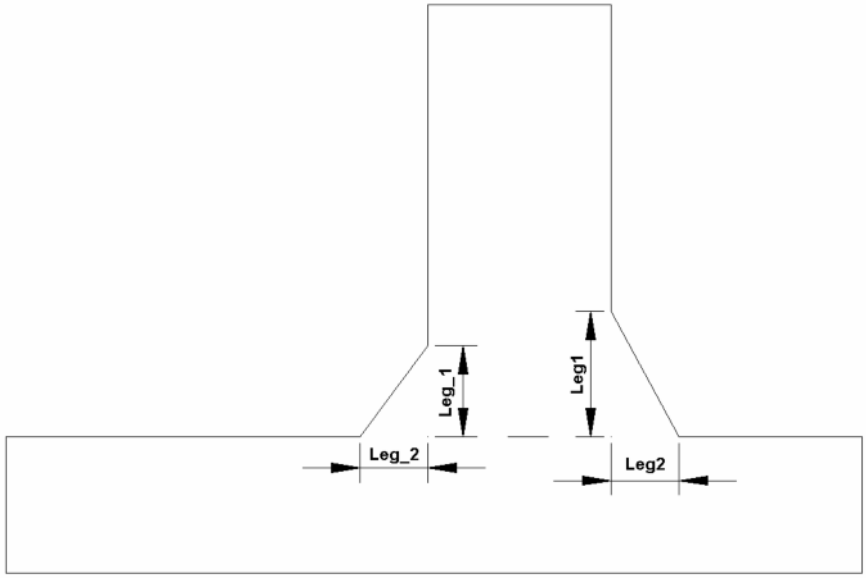


Figure 4.10 Two Sided Weld Geometry Parameters

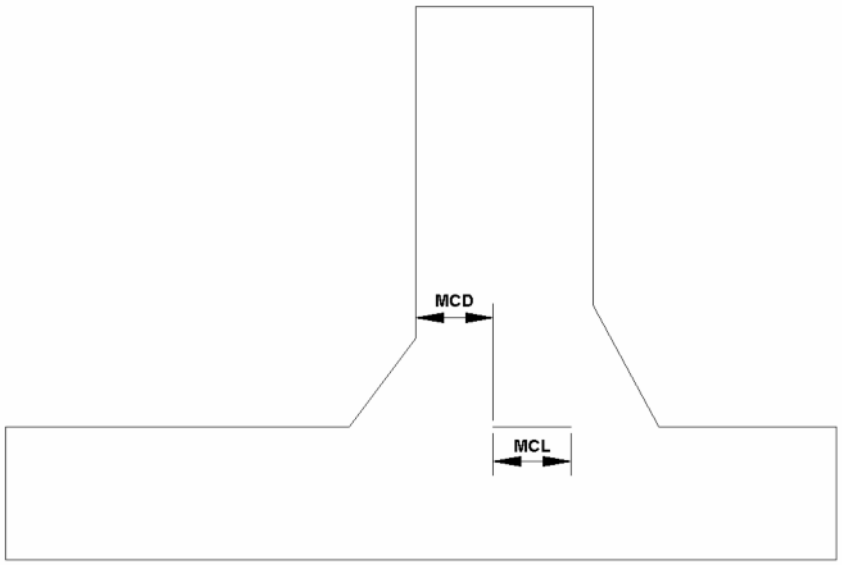


Figure 4.11 Two Sided Weld Penetration Depth Parameters

#### 4.3.3.2 Crack Parameters

In real life applications the most dominant fatigue cracks are semi elliptical surface cracks. A semi elliptic surface crack can be defined by two parameters (Figure 4.12):

a – Half surface crack length
b – Crack depth

If half surface crack length (a) is equal to the crack depth (b) the cracks shape becomes an exact circle. In present work semi elliptic surface cracks are placed into toes and root of local solid models. The analyses are done for various inclination angles ranging from $0^0$ to $90^0$ at weld toe and $0^0$ to $180^0$ at weld root (Figure 4.13).

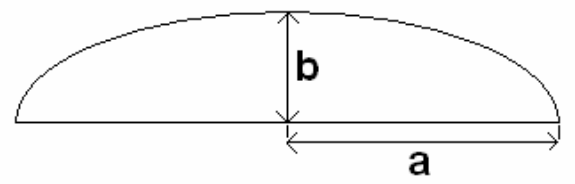


Figure 4.12 Semi Elliptic Crack Parameters

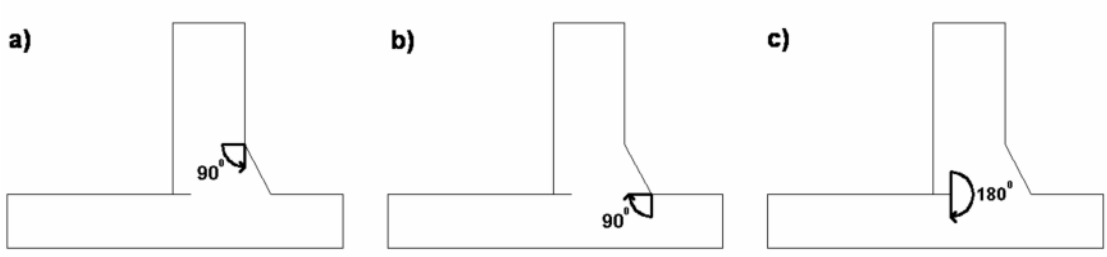


Figure 4.13 Crack Inclination Angle Ranges a) Crack at Weld Toe 1 b) Crack at Weld Toe 2 c) Crack at Weld Root

### 4.3.4 Shell-to-Solid Conversion Method

As mentioned before, sheet metal parts of the global model are modeled by using quadrilateral thick shell elements. Shell-to-Solid conversion method simply forms a crack block and positions it to the specified location. Then, the weld shape is formed and shell model is converted to solid model (Figure 4.14). The local solid model consists of 20-node isoparametric three dimensional brick elements (Figure 4.15). In fracture analysis, in order to simulate the square-root strain singularity around the crack front, collapsed 20-node isoparametric three dimensional brick elements are utilized. These elements are depicted in Figure 4.16 [43]. The representation of collapsed 20-node isoparametric elements at weld to crack front start can be seen in Figure 4.17.

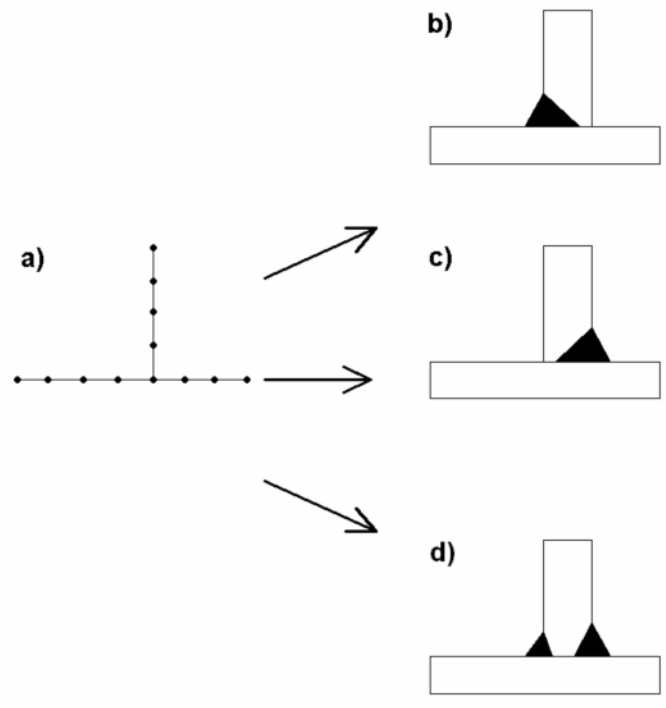


Figure 4.14 Shell-to-Solid Conversion Possibilities a) Shell Model b) Solid Model Welded from Inner Side c) Solid Model Welded from Outer Side d) Solid Model Welded from Both Sides

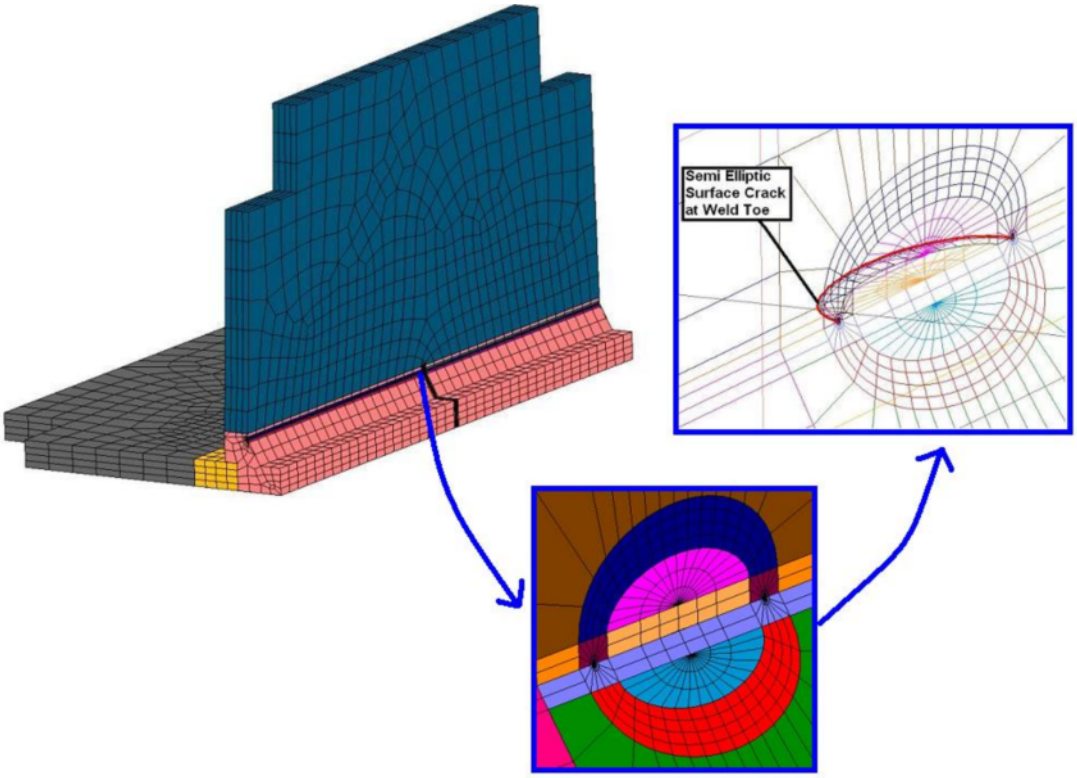


Figure 4.15 Semi Elliptic Surface Crack at Weld Toe

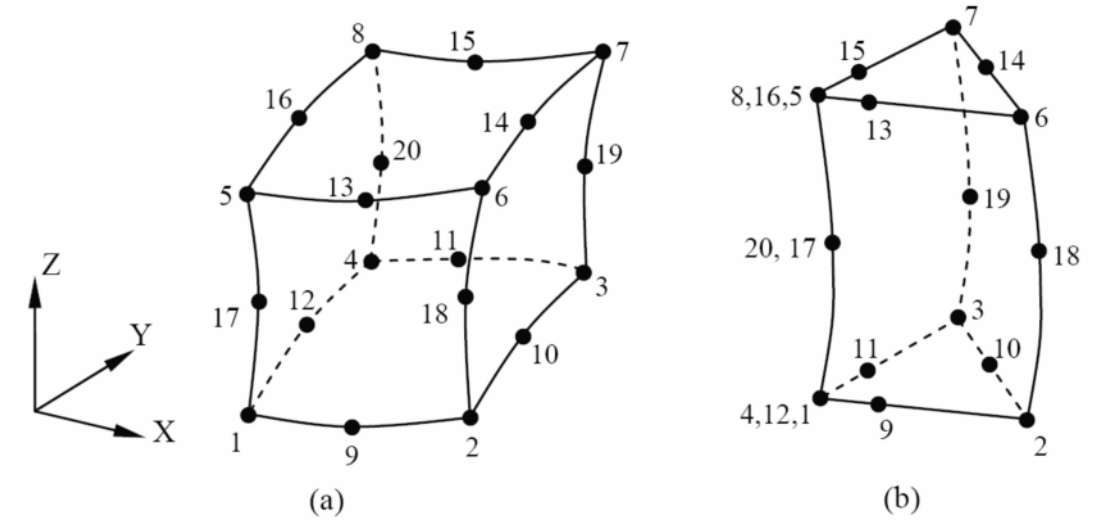


Figure 4.16 a) 20-node Isoparametric Brick Element b) Collapsed 20-node Isoparametric Brick Elements

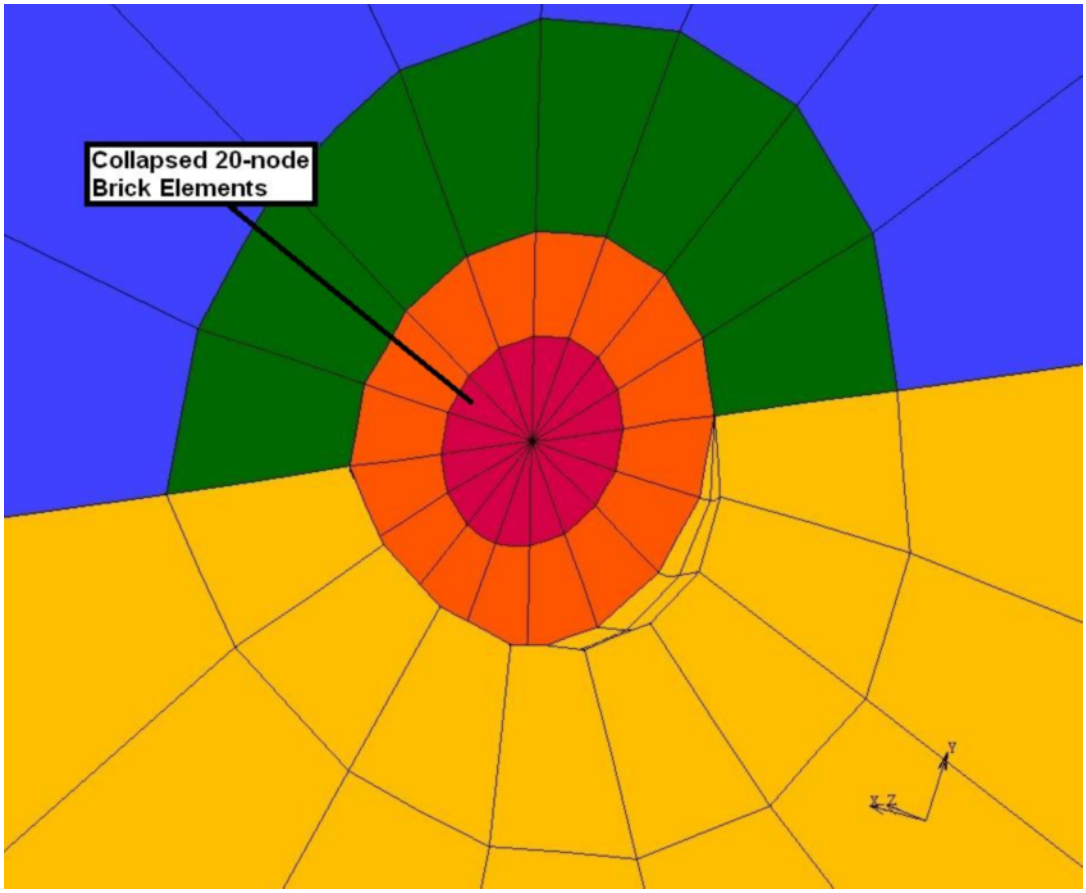


Figure 4.17 Collapsed 20-node Isoparametric Brick Elements at Weld Toe Crack Front Start

### 4.3.5 Material Properties

The computer code is prepared such that it takes all material properties from the global model (Table 4.1, Table 4.2). In addition, the material properties of the welded connections are assumed to be the same with the global model.

Table 4.1 Material Properties of the Steel Used in Global Model Analyses

| Material Type | Yield Strength (MPa) | Tensile Strength (MPa) | Elongation (%) | E (MPa) | Poisson's Ratio | Density ($kg/m^3$) |
|---|---|---|---|---|---|---|
| St-52 | 355 | 510 | 21 | 210000 | 0.3 | 7850 |

Table 4.2 Chemical Compositions of the Steel Used in Global Model Analyses

| Material Type | C mass (%) | Si mass (%) | Mn mass (%) | P mass (%) | S mass (%) |
|---|---|---|---|---|---|
| St-52 | 0.22 | 0.55 | 1.60 | 0.035 | 0.035 |

### 4.3.6 Tyings and Local Model Boundary Conditions

The sheet metal parts of the global model are composed of quadrilateral thick shell elements. These elements' nodes have six degrees of freedom, which are global displacements and rotations in three dimensions.

Degrees of freedom per node:

1 = u = global (Cartesian) x-displacement
2 = v = global (Cartesian) y-displacement
3 = w = global (Cartesian) z-displacement
4 = $\alpha_x$ = rotation about global x-axis
5 = $\alpha_y$ = rotation about global y-axis
6 = $\alpha_z$ = rotation about global z-axis

However, 20-node brick elements' nodes have only global displacements (u, v, w) as degrees of freedom. Therefore, if there exists a transition from shell to solid (or vice versa), a proper tying type must be used not to loose the deformation history of the global model nodes. In this work, a similar method to the method used in the study of Ranestad et al. [12] is adopted. In this method, the sub-model is loaded with the deformation history taken from the global shell model. The deformation history of the nodes is applied to constrained nodes (Mid-surface nodes) (Figure 4.18). The other ("follower") nodes on the edge are forced to stay in the plane defined by the nodes in transverse direction (Figure 4.19). This method gives sufficiently precise values far from the boundary condition application points. Therefore, special attention must be paid not to implement cracks very close to the boundaries. This property is also parameterized in prepared computer code and it can be set according to the size of selected region of interest.

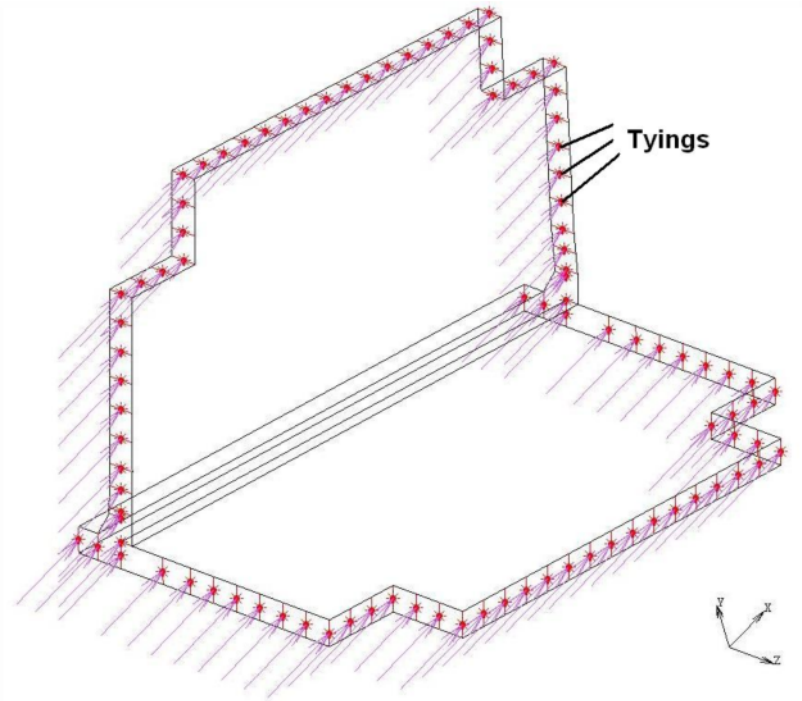


Figure 4.18 Deformation History Applied to Tying Constrained Nodes at Local Model Boundaries

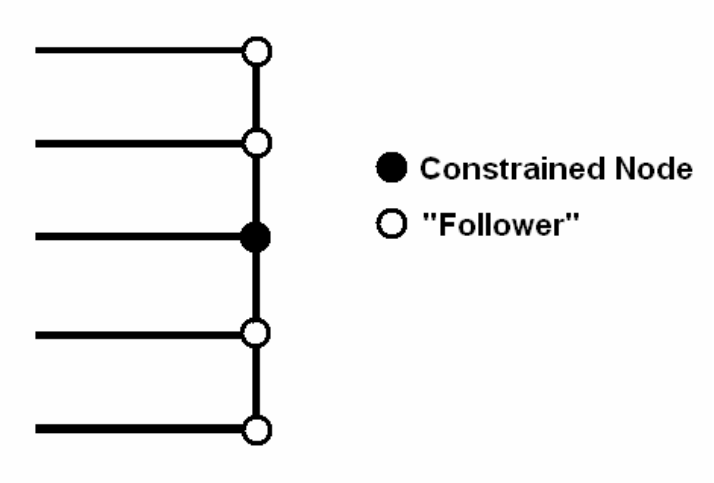


Figure 4.19 Constrained Nodes and the Other (“follower”) Nodes on the Edge are Forced to Stay in the Plane Defined by the Nodes in Transverse Direction

### 4.3.7 J-integral Calculation

As mentioned in section 3.7, J-integral values are calculated in MSC.Marc. The method used in the program is exact for linear cases. Therefore, it can be used for linear analyses of excavator boom and arm. However, to calculate the J-integral some conditions must be satisfied. First, a crack shape must be modeled at the interested location. Second, crack front must be modeled by using quarter-point crack tip elements (Figure 4.16, Figure 4.17). Third, crack front nodes must be defined for J-integral calculation. Crack front nodes are the nodes on the red path shown in Figure 4.15. After satisfying all of the conditions, the analysis of sub-modeled region must be done. The J-integral values of crack front nodes are given in the output file of the performed analysis.

## 4.4 Verification of Finite Element Modeling and J-integral Calculation

### 4.4.1 Verification of Finite Element Modeling

Verification of finite element modeling requires tests to be performed. The performed tests must also have the same boundary conditions with finite element analyses. Finite elements results at some locations must be compared with the test results to verify the model. According to the experimental stress analysis results of HMK 300 LC excavator, maximum deviation from finite element analysis results is 15% (Figure 4.20). Thus, the global model analysis gives sufficiently accurate results.

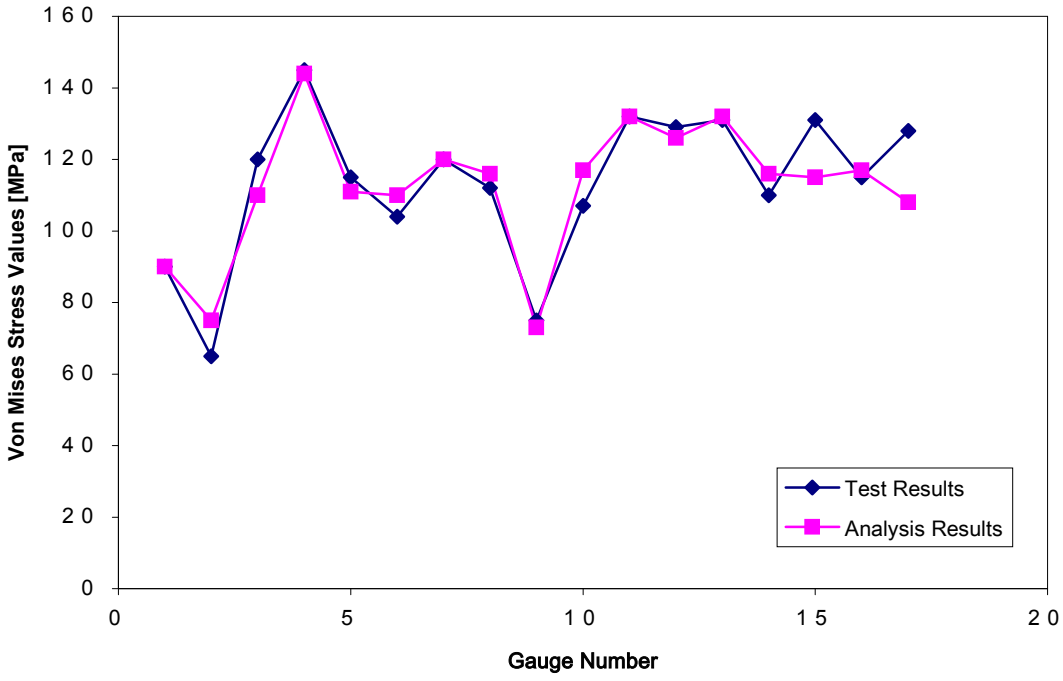


Figure 4.20 Experimental and Finite Element Analysis Results Comparison

### 4.4.2 Verification of J-integral Calculation

To verify the calculated J-integral values, the results in literature are compared with the results obtained in this thesis.

Firstly, embedded circular and elliptical crack solutions of Sneddon [50] and Irwin [51] are investigated. The results are compared and the models are verified.
Secondly, 3D inclined semi elliptical surface cracks in a semi-infinite body under tension are examined. In this context, the solutions of Noda et al. [52] and Isida et al. [53] are compared with the results found by J-integral method.

#### 4.4.2.1 Verification of Embedded Circular and Elliptical Crack Models

Sneddon [50] treated the problem of a circular crack of radius *a* (penny-shaped crack) embedded in an infinite solid subjected to uniform tension (Figure 4.21). He arrived at:

$$K = \frac{2}{\pi} \cdot \sigma \cdot \sqrt{\pi \cdot a} \tag{4.5}$$

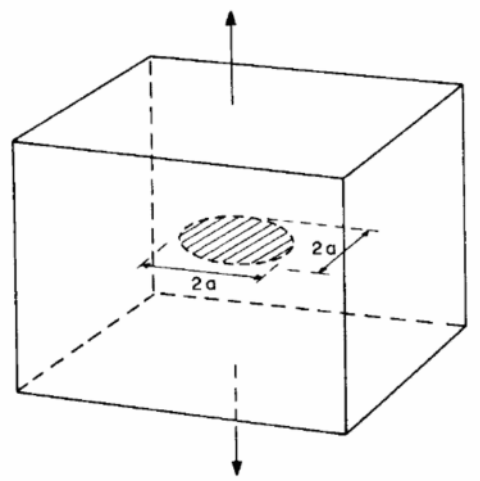


Figure 4.21 Embedded Penny-shaped Crack

If plane strain assumption is assumed to exist, Mode-I stress intensity factor can be calculated by using J-integral values as follows:

$$K_I = \sqrt{\frac{E}{1-\nu^2} J} \tag{4.6}$$

In the analyses, it is seen that the size of the collapsed 20-node brick elements and the size of the solid cube has a vital effect on the solutions. Therefore, to obtain more accurate results the edge of the solid cube is increased up to forty times the circular crack radius (a) and the size of the collapsed brick elements surrounding the crack front is decreased up to one over twenty-five times the circular crack radius. Since the model is symmetric, in finite element analysis half of the model is used to calculate the J-integral values (Figure 4.22, Figure 4.23). Calculated J-integral values are all the same at the crack front nodes. To be able to compare the present results with the bibliographical ones, dimensionless SIF and J-integral are introduced

$$K_I^* = \frac{K_I}{\sigma \cdot \sqrt{\pi \cdot a}} \tag{4.7}$$

where $K_I$ is the real SIF, $\sigma$ the applied stress and *a* the crack radius or crack depth and

$$J^* = \frac{J}{(\sigma^2 \cdot \pi \cdot a / E)} \tag{4.8}$$

where *J* is the real J-integral value, $\sigma$ the applied stress, *a* the crack radius or crack depth and *E* modulus of elasticity (Table 4.3).

Table 4.3 Details and Comparison for a Penny-shaped Crack Analysis

| *E* (MPa) | Poisson's Ratio ($\nu$) | *a* (mm) | $\sigma$ (MPa) | J-integral Value ($J^*$) | Present Study ($K_I^*$) | Sneddon's Solution ($K_I^*$) | Difference (%) |
|---|---|---|---|---|---|---|---|
| 210000 | 0.3 | 50 | 100 | 0.3684 | 0.6362 | 0.6366 | 0.0596 |

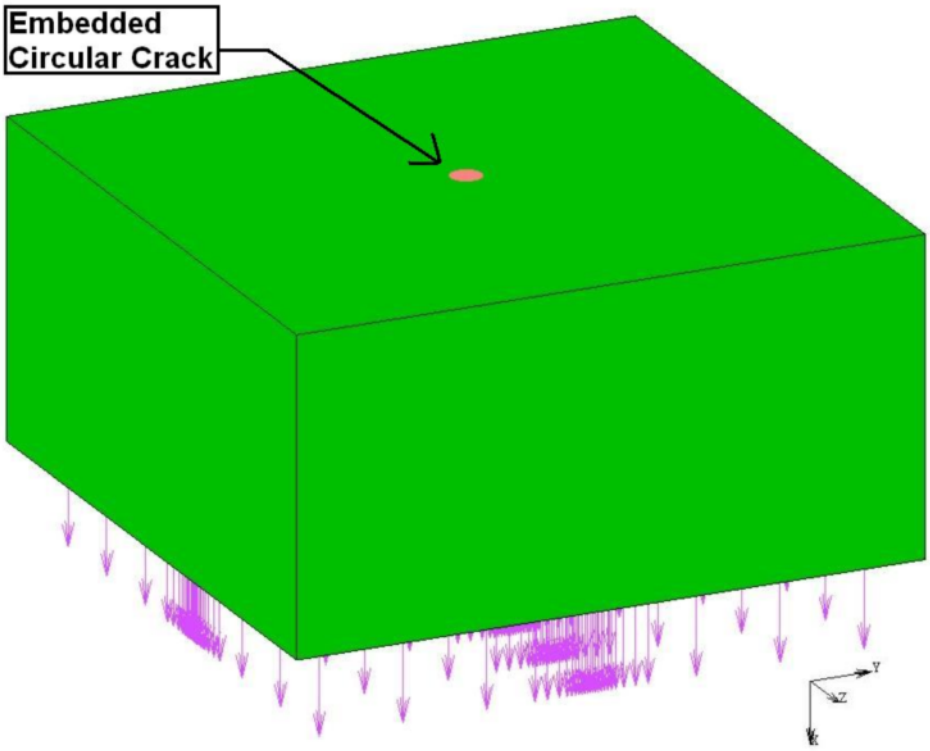


Figure 4.22 General View of Embedded Circular Crack

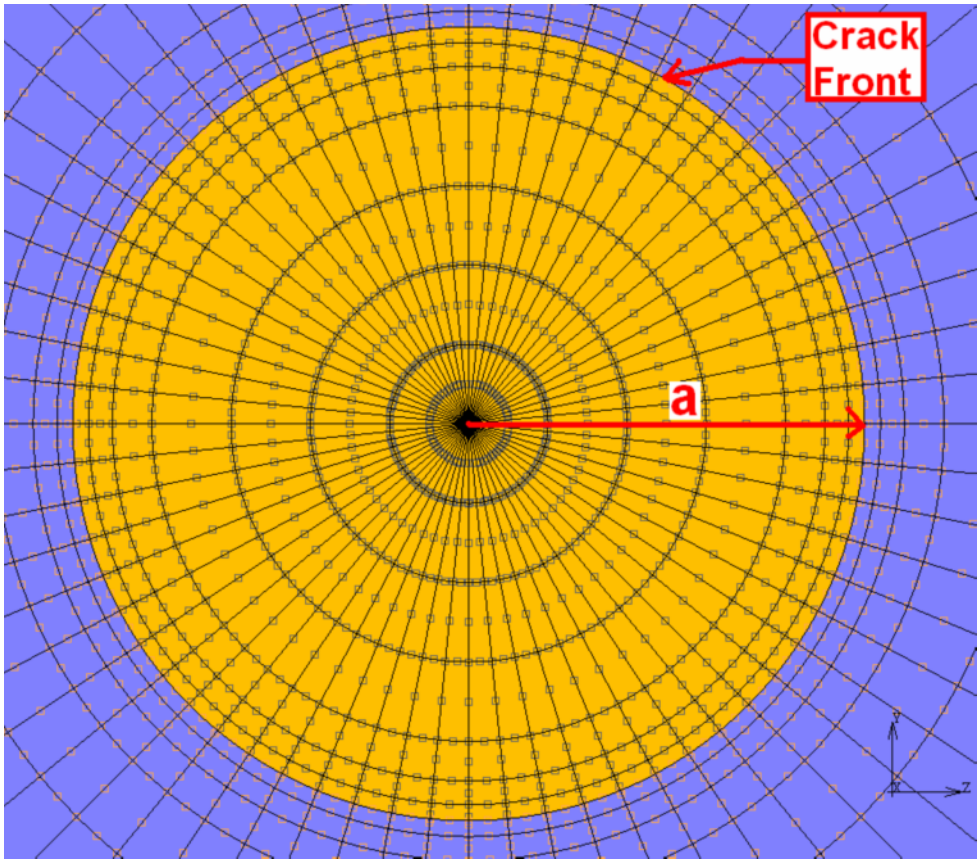


Figure 4.23 Close-up View of Embedded Circular Crack

A solution for an embedded elliptical flaw not being available, Irwin [51] derived a useful expression on the basis of the stress field around the crack front of an elliptical crack in an infinite body in remote tension. The calculated SIF values showed that they vary around the crack front. The results of Irwin's analysis is:

$$K = \frac{\sigma \cdot \sqrt{\pi \cdot a}}{E(\phi)} \cdot \left\{ \sin^2 \phi + \frac{a^2}{c^2} \cdot \cos^2 \phi \right\}^{1/4} \qquad (4.9)$$

where *a, c,* $\phi$ are as shown in Figure 4.24, and *E* ($\phi$) is the elliptical integral:

$$E(\phi) = \int_0^{\pi/2} \left\{ 1 - \left[ 1 - \frac{a^2}{c^2} \right] \cdot \sin^2 \phi \right\}^{1/2} \cdot d\phi \qquad (4.10)$$

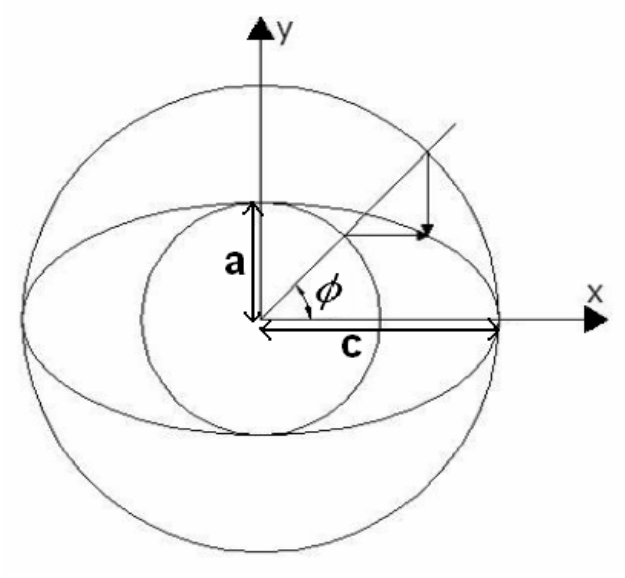


Figure 4.24 Parametric Representation of a Point on an Ellipse

In Irwin's solution the maximum value of SIF is obtained on minor axis, and the minimum value of the SIF is obtained on major axis of the elliptical crack. In the analysis, embedded elliptical crack dimensions are 125 mm as major axis and 50 mm as minor axis. The solution of eq. (4.10) is calculated by using MATLAB for the specified major and minor axis values. The details of the analysis and the normalized SIF comparison of Irwin's solution and the present study can be seen in Table 4.4 and Table 4.5.

To decrease the size effect of the solid cube and collapsed brick elements the edge of the solid cube is increased up to sixty times the elliptical crack minor axis (a) and the size of the collapsed brick elements surrounding the

crack front is decreased up to one over twenty-five times the elliptical crack minor axis (Figure 4.25). Since the model is symmetric, in finite element analysis half of the model is used to calculate the J-integral values.

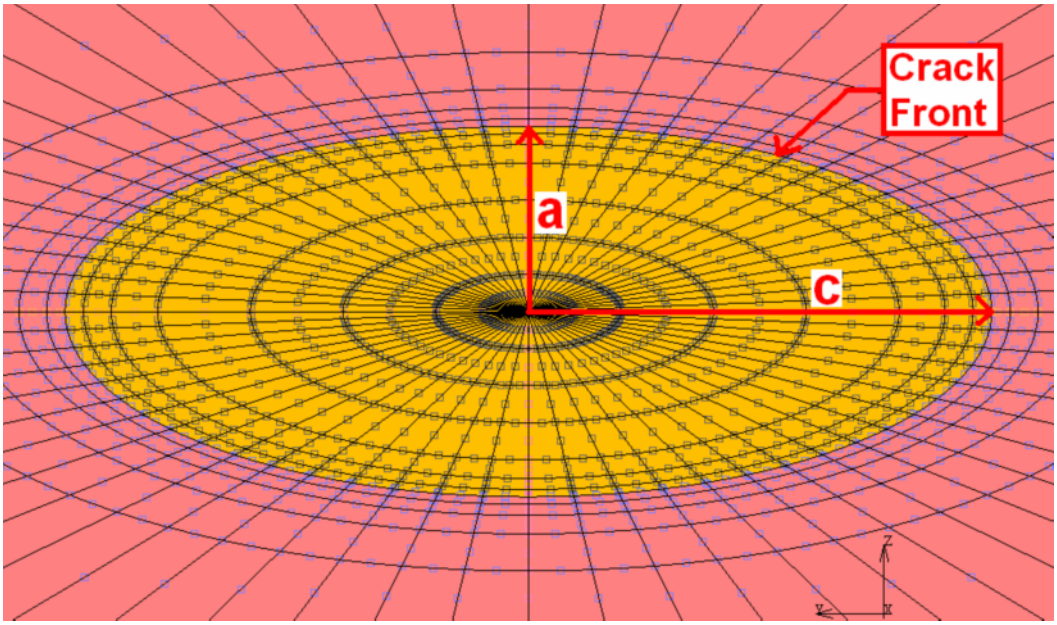


Figure 4.25 Close-up View of Embedded Elliptic Crack

Table 4.4 Details for Elliptical Crack Analysis

| *E* (MPa) | Poisson's Ratio ($\nu$) | *a* (mm) | *c* (mm) | $\sigma$ (MPa) | E($\phi$) |
|---|---|---|---|---|---|
| 210000 | 0.3 | 50 | 125 | 100 | 1.1507 |

Table 4.5 Normalized SIF Comparison for an Elliptical Crack

| $\phi$ (degree) | Present Study | Irwin's Solution | Difference (%) |
|---|---|---|---|
| 0.00 | 0.5523 | 0.5496 | 0.4886 |
| 5.64 | 0.5594 | 0.5565 | 0.5284 |
| 10.96 | 0.5773 | 0.5740 | 0.5725 |
| 16.27 | 0.6034 | 0.5991 | 0.6991 |
| 21.68 | 0.6340 | 0.6291 | 0.7633 |
| 27.14 | 0.6662 | 0.6610 | 0.7800 |
| 32.54 | 0.6982 | 0.6924 | 0.8332 |
| 37.89 | 0.7287 | 0.7222 | 0.8969 |
| 43.26 | 0.7568 | 0.7499 | 0.9110 |
| 48.15 | 0.7822 | 0.7730 | 1.1706 |
| 54.14 | 0.8045 | 0.7982 | 0.7829 |
| 59.98 | 0.8236 | 0.8192 | 0.5291 |
| 65.31 | 0.8393 | 0.8353 | 0.4796 |
| 70.62 | 0.8513 | 0.8482 | 0.3641 |
| 75.94 | 0.8601 | 0.8581 | 0.2415 |
| 80.24 | 0.8655 | 0.8637 | 0.2020 |
| 90.00 | 0.8678 | 0.8690 | -0.1379 |

#### 4.4.2.2 Verification of 3D Inclined Semi Elliptical Surface Crack Models

In the study of Noda et al. [52], a singular integral equation method is applied to calculate the stress intensity factor along crack front of a 3D inclined semi-elliptical surface crack in a semi-infinite body under tension. The results show that their method yields smooth variations of mixed modes stress intensity factors along the crack front accurately for various geometrical conditions. In their study one of the parameters examined is the effect of inclination angle ($\psi$) on SIF (Figure 4.26, Figure 4.27). In this manner, they calculated mode I, II and III stress intensity factors at different inclination angles. Their results showed that, it is difficult to obtain accurate results for large inclination angles

($\psi$ > 45 degrees), because the effect of free surface on the results is complicated.

The study of Noda et al. gives SIF values at each mode for different inclination angles (Table 4.8). In this study, to make a comparison, the given SIF values will be converted to normalized mixed mode J-integral values through eq. (4.11) [21] and eq. (4.8):

$$J = J_I + J_{II} + J_{III} = \frac{1}{E^*}(K_I{}^2 + K_{II}{}^2) + \frac{1}{2\mu} K_{III}{}^2 \qquad (4.11)$$

where $E^*$ is defined in eq. (3.39) and $\mu$ is defined in eq. (3.6). The details of the analysis can be seen in Table 4.6.

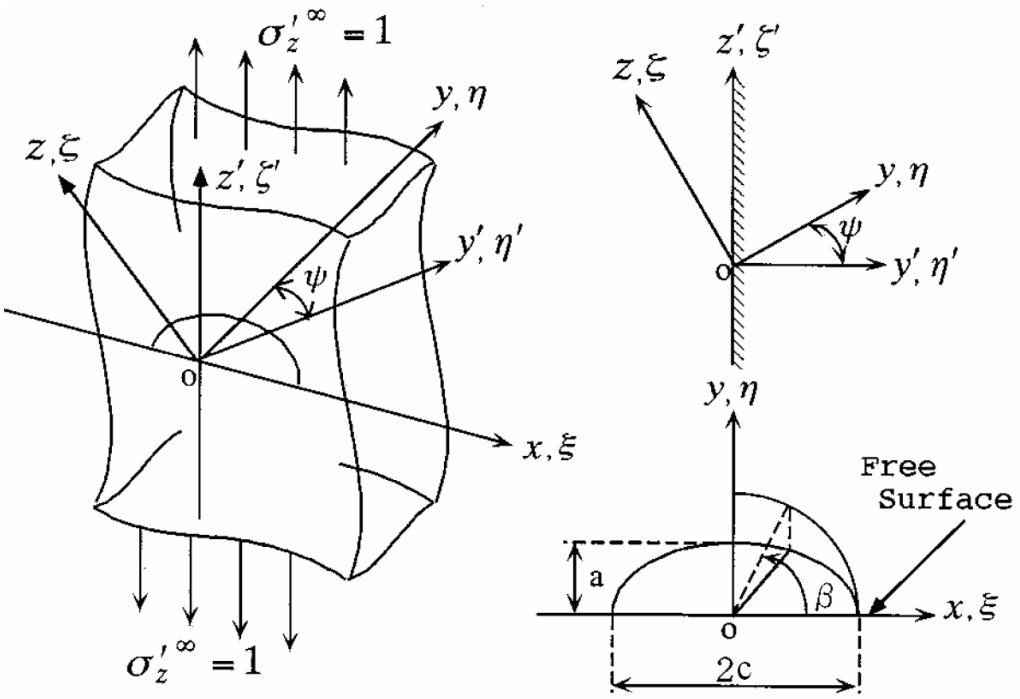


Figure 4.26 An Inclined Semi Elliptical Surface Crack in a Semi-infinite Body

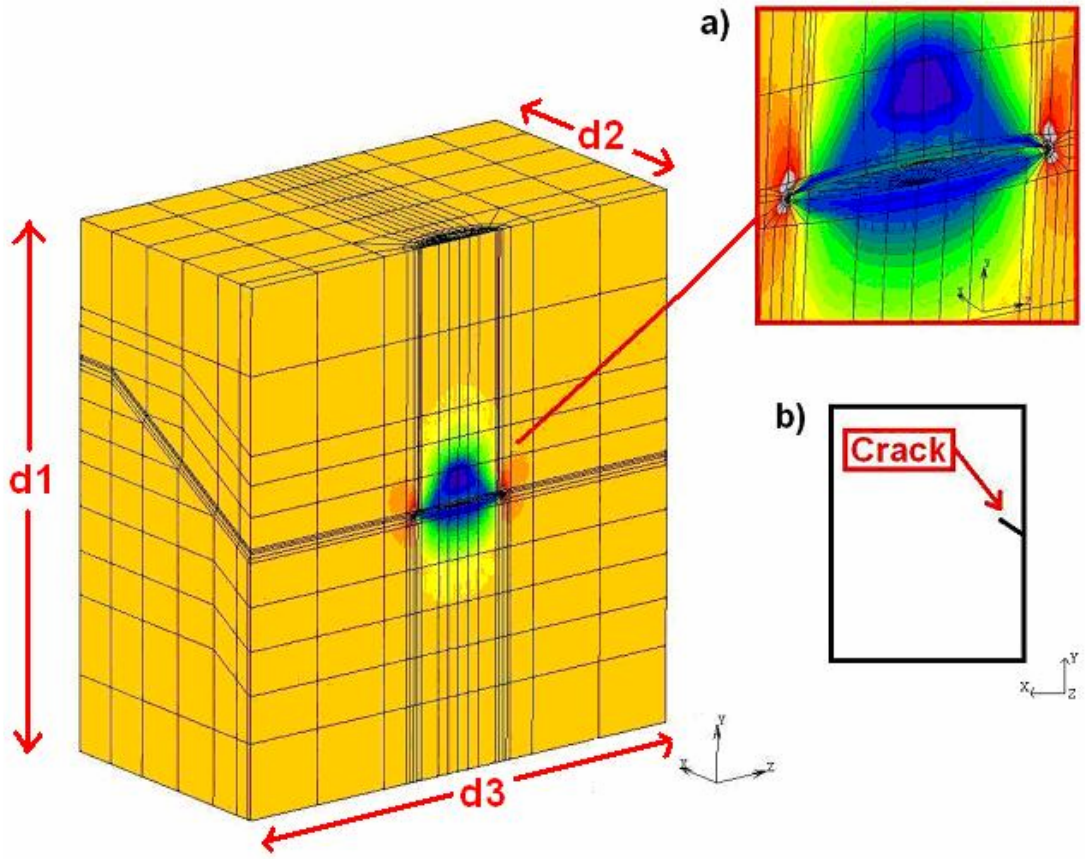


Figure 4.27 General View of an Inclined Semi Elliptical Surface Crack Von Mises Stress Distribution a) Over Deformed Shape of the Crack Mouth b) Side View of the Loaded Cube Showing the Inclined Crack

Table 4.6 Details for Noda's Solution

| *E* (MPa) | Poisson's Ratio (ν) | a (mm) | *a/c* | $\sigma$ (MPa) | d1 (mm) | d2 (mm) | d3 (mm) |
|---|---|---|---|---|---|---|---|
| 210000 | 0.3 | 1 | 0.5 | 1 | 20 | 10 | 20 |

Isida et al. [53] also studied semi-elliptical surface cracks arbitrarily inclined to the free surface of a semi-infinite solid subjected to tension. They calculated the SIF at the maximum depth point ($\beta = 90^0$) of the crack front at different inclination angles. The calculated SIF values are converted to normalized J-integral values by using eq. (4.11) and eq. (4.8). The details and the comparison of their study and the present study are given in Table 4.7 and in Table 4.9.

Table 4.7 Details for Isida's Solution

| $E$ (MPa) | Poisson's Ratio ($\nu$) | a (mm) | $\beta$ (degree) | $\sigma$ (MPa) |
|---|---|---|---|---|
| 210000 | 0.3 | 1 | 90 | 1 |

## 4.5 Conclusion

As can be seen from the comparison tables 4.3, 4.5, 4.8 and 4.9, computed stress intensity factors and J-integral values are approximately the same with referred values. However, the results differ near the free surface where the inclination angle is large. This is a commonly encountered problem as can be seen in literature. From these results, it can be said that the J-integral method adopted in this study gives sufficiently accurate results and can be used to calculate the mixed mode J-integral values around crack front of inclined semi-elliptical surface cracks at weld toe and root of the parts.

Table 4.8 Normalized J-integral Value Comparisons for Inclined Semi Elliptical Surface Cracks

| $\beta$ (degree) | $\psi$ = 15 (degree) | | | $\psi$ = 30 (degree) | | |
|---|---|---|---|---|---|---|
| | Present Study | Noda's Solution | Difference [%] | Present Study | Noda's Solution | Difference [%] |
| 16.62 | 0.4278 | 0.4145 | 3.1126 | 0.3389 | 0.3376 | 0.3607 |
| 30.77 | 0.4756 | 0.4697 | 1.2329 | 0.3855 | 0.3871 | 0.4325 |
| 42.80 | 0.5343 | 0.5312 | 0.5795 | 0.4355 | 0.4411 | 1.2891 |
| 53.43 | 0.5860 | 0.5826 | 0.5829 | 0.4790 | 0.4863 | 1.5234 |
| 63.16 | 0.6271 | 0.6218 | 0.8340 | 0.5132 | 0.5205 | 1.4272 |
| 72.34 | 0.6560 | 0.6494 | 1.0094 | 0.5375 | 0.5444 | 1.2997 |
| 81.20 | 0.6732 | 0.6658 | 1.1019 | 0.5520 | 0.5588 | 1.2409 |
| 90.00 | 0.6789 | 0.6715 | 1.0874 | 0.5568 | 0.5637 | 1.2377 |

| $\beta$ (degree) | $\psi$ = 45 (degree) | | | $\psi$ = 60 (degree) | | |
|---|---|---|---|---|---|---|
| | Present Study | Noda's Solution | Difference [%] | Present Study | Noda's Solution | Difference [%] |
| 16.62 | 0.2119 | 0.2359 | 11.2976 | 0.0952 | 0.1424 | 49.5080 |
| 30.77 | 0.2575 | 0.2737 | 6.3199 | 0.1290 | 0.1636 | 26.7915 |
| 42.80 | 0.3004 | 0.3160 | 5.1794 | 0.1602 | 0.1916 | 19.6312 |
| 53.43 | 0.3356 | 0.3516 | 4.7908 | 0.1854 | 0.2166 | 16.8549 |
| 63.16 | 0.3618 | 0.3787 | 4.6698 | 0.2038 | 0.2358 | 15.6774 |
| 72.34 | 0.3801 | 0.3975 | 4.5690 | 0.2168 | 0.2491 | 14.9267 |
| 81.20 | 0.3912 | 0.4088 | 4.5091 | 0.2245 | 0.2572 | 14.5595 |
| 90.00 | 0.3948 | 0.4129 | 4.5985 | 0.2270 | 0.2601 | 14.5852 |

Table 4.9 Normalized J-integral Value Comparisons for Inclined Semi Elliptical Surface Cracks

| a/c | $\psi$ = 0 (degree) | | | $\psi$ = 15 (degree) | | |
|---|---|---|---|---|---|---|
| | Present Study | Isida's Solution | Difference [%] | Present Study | Isida's Solution | Difference [%] |
| 0.25 | 0.9886 | 0.9505 | 3.8597 | 0.9027 | 0.8949 | 0.8715 |
| 0.35 | - | - | - | - | - | - |
| 0.40 | - | - | - | 0.7695 | 0.7568 | 1.6402 |
| 0.50 | 0.7309 | 0.7095 | 2.9235 | 0.6789 | 0.6704 | 1.2494 |
| 0.60 | - | - | - | 0.6053 | 0.5953 | 1.6625 |
| 0.65 | - | - | - | - | - | - |
| 0.70 | - | - | - | - | - | - |
| 0.75 | 0.5407 | 0.5270 | 2.5403 | - | - | - |
| 0.80 | - | - | - | 0.4774 | 0.4689 | 1.7778 |
| 1.00 | 0.4067 | 0.3964 | 2.5317 | 0.3793 | 0.3749 | 1.1739 |

Table 4.9 (continued)

| a/c | $\psi$ = 30 (degree) | | | $\psi$ = 45 (degree) | | |
|---|---|---|---|---|---|---|
| | Present Study | Isida's Solution | Difference [%] | Present Study | Isida's Solution | Difference [%] |
| 0.25 | 0.7375 | 0.7330 | 0.6166 | - | - | - |
| 0.35 | 0.6689 | 0.6626 | 0.9470 | - | - | - |
| 0.40 | - | - | - | - | - | - |
| 0.50 | 0.5568 | 0.5591 | 0.4033 | 0.3948 | 0.4007 | 1.5028 |
| 0.60 | - | - | - | - | - | - |
| 0.65 | - | - | - | 0.3437 | 0.3406 | 0.9139 |
| 0.70 | 0.4501 | 0.4435 | 1.4765 | - | - | - |
| 0.75 | - | - | - | - | - | - |
| 0.80 | - | - | - | 0.2914 | 0.2882 | 1.1040 |
| 1.00 | 0.3229 | 0.3177 | 1.6170 | 0.2353 | 0.2324 | 1.2268 |

# CHAPTER 5

# PARAMETRIC ANALYSES AND NUMERICAL RESULTS

## 5.1 Introduction

This chapter presents the parametric analysis and obtained results by using J-integral method. Although the prepared program is a general use program, this study is mainly focused on the most critical parts (boom and arm) of HMK 300 LC excavator. In this work, each part is examined in two groups. First, global model boundary conditions include the lateral force; and the second, global model boundary conditions do not include the lateral force. In each group, the models are examined in three sub-groups: local solid model welded from outer side, local solid model welded from inner side and local solid model welded from both sides. For this purpose, semi-elliptical surface cracks are placed to the weld toe and weld root of the prepared models for a range of inclination angles ($\psi$). For both sides welded case the root cracks are implemented to the outer side of the root. Eventually, the mixed mode J-integral values are found along the crack front at different crack front position angles ($\beta$).

The boundary conditions of the sub-models are directly taken from the global model. The global model used in this study is verified by the experiments carried out in Hidromek Ltd. Sti. (Section 4.4.1).

In case studies, 252 sub-models are formed for different parameters. The calculated mixed mode J-integral values showing the effect of inclined semi elliptical surface cracks on weld toes and weld root of different welded connections are given in Figures 5.5-5.34 and in Figures 5.40-5.69. The obtained results are non-dimensionalized by using eq. (4.7) and eq. (4.8). Since the sub-model applied stresses are variable around the boundaries of the sub-models, a constant applied stress value (σ) is used during the normalization. The details of the analyses are given in Table 5.1. and Table 5.2.

Table 5.1 Parametric Analyses Material Properties and Crack Parameters

| *E* (MPa) | Poisson's Ratio ($\nu$) | *a* (mm) | *c* (mm) | $\sigma$ (MPa) |
|---|---|---|---|---|
| 210000 | 0.3 | 0.5 | 1 | 100 |

Table 5.2 Parametric Analyses Weld Parameters (mm)

| Leg1 | Leg2 | Root Depth (RD) | Leg_1 | Leg_2 | Middle Crack Distance (MCD) | Middle Crack Length (MCL) |
|---|---|---|---|---|---|---|
| 11 | 6 | 6 | 6 | 6 | 3 | 3 |

## 5.2 Parametric Analyses

The boom and arm of the excavator are the most critical parts of all structure. Since almost all of the earth-moving machineries are exposed to repeated

fluctuating stresses, fatigue cracks occur especially on boom and arm of the machines due to high stresses on these parts. The cracks appear generally on welded connections of sheet metals. Thus, optimization of these parts is a very important procedure for reducing the stresses that the welds are exposed to. However, the shape optimization is not enough alone without proper weld parameters selection. Therefore, this study will examine the weld parameters of an optimized excavator boom and arm in terms of fracture mechanics. In all of the analyses three cases: welding from outside, welding from inside and welding from both sides will be compared to each other. In the following, the details of the boom and arm parametric analyses will be explained.

### 5.2.1 Boom Parametric Analyses

A typical structural zooming (sub-modeling) analysis starts with the global model analysis. This is due to the reason that the displacement type boundary conditions are taken from the global post file. In Figure 5.1 and in Figure 5.2 the stress map of the excavator boom global shell model and the interested regions are shown. The interested region must be at the corner of the box section and must not contain any thickness transition region. Figure 5.3 shows the different sheet metal thicknesses with different colors and the position of the selected region.

When the selection is made, the interested region is in shell form and must be transformed to solid local model. Shell-to-solid conversion procedure, the boundary conditions, weld and crack parameters are explained in detail in Chapter 4. An example to a completed solid local model analysis is given in Figure 5.4. In Figures 5.5-5.34 the normalized *J*-integral values versus inclination angle ($\psi$) for five crack front position angles ($\beta$) are presented.

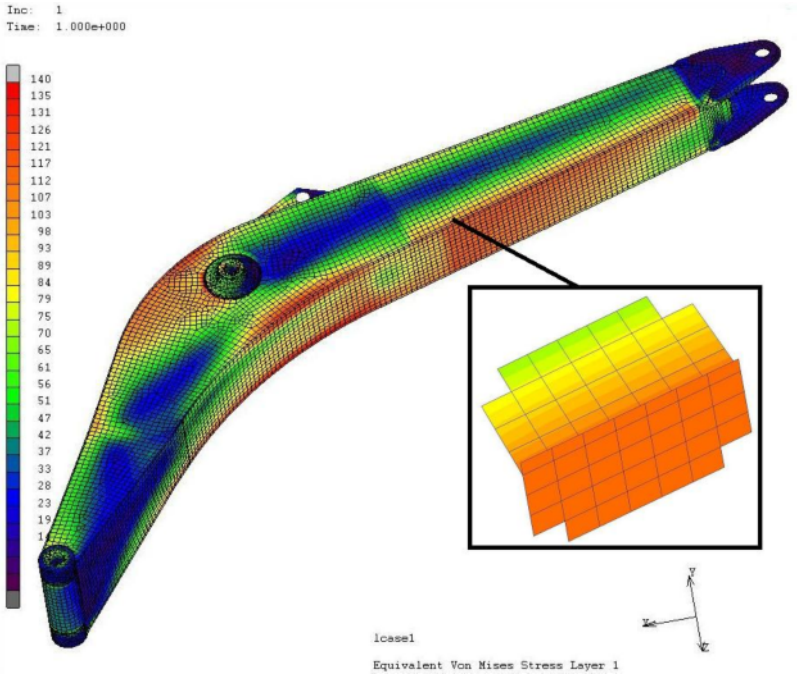


Figure 5.1 Excavator Boom Global Model (Von Mises Stress Outer Layer)

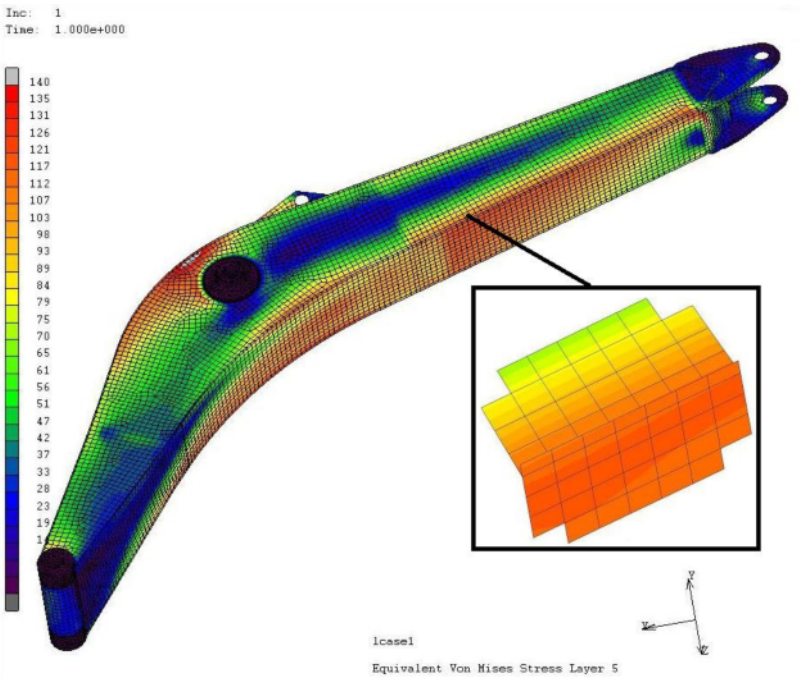


Figure 5.2 Excavator Boom Global Model (Von Mises Stress Inner Layer)

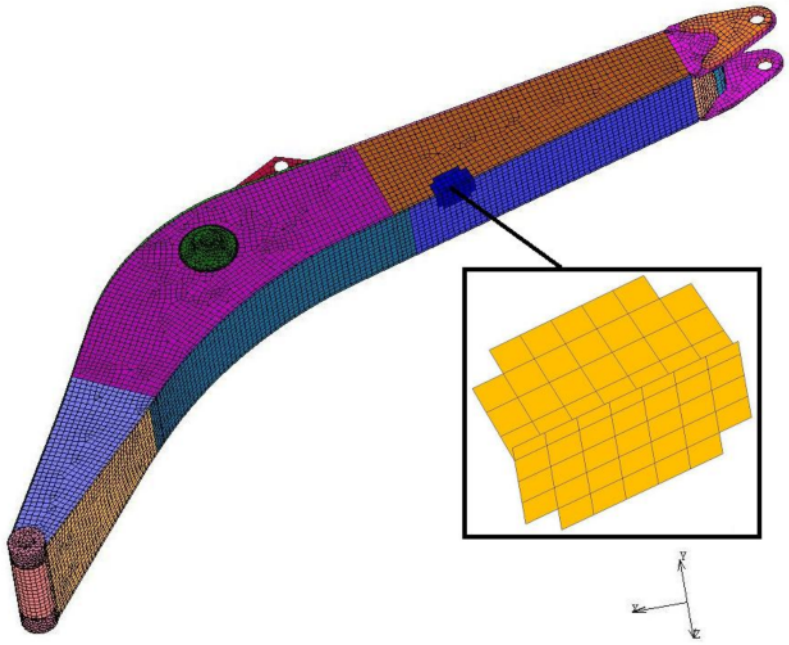

Figure 5.3 Excavator Boom Model Sheet Metals and the Selected Region

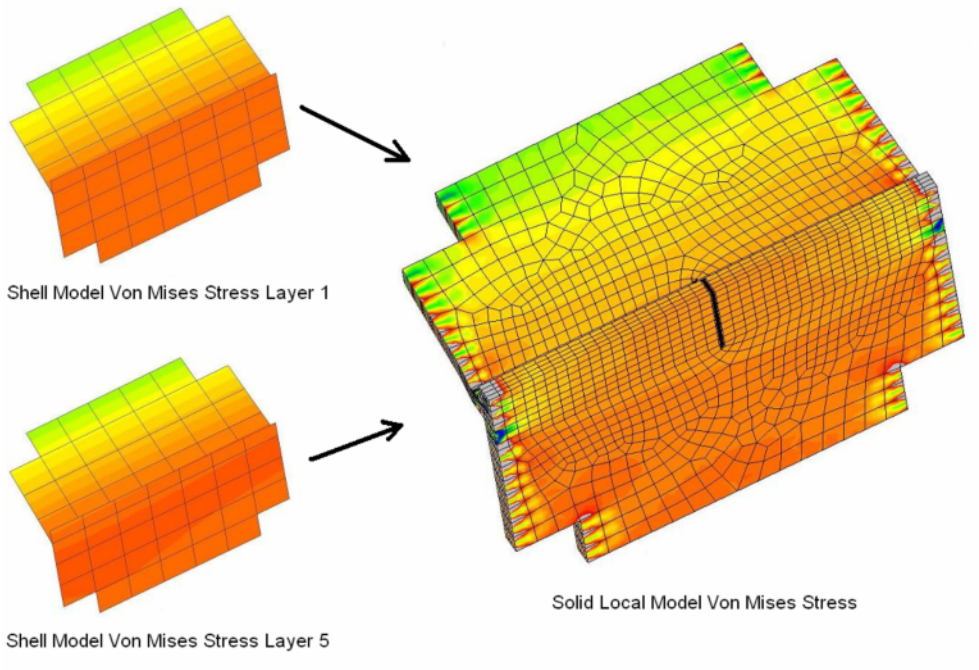


Figure 5.4 Boom Selected Shell Region and Boom Solid Local Model Von Mises Stress Map

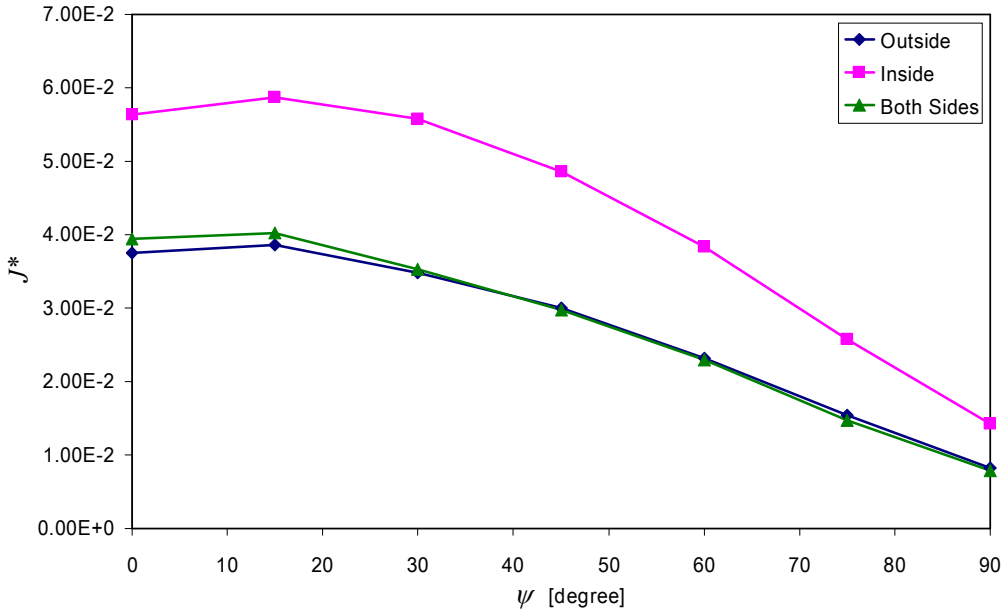


Figure 5.5 Normalized *J*-integral versus Inclination Angle ($\psi$)
(Crack at Weld Toe 1, Lateral Force is Included, $\beta$=31$^0$)

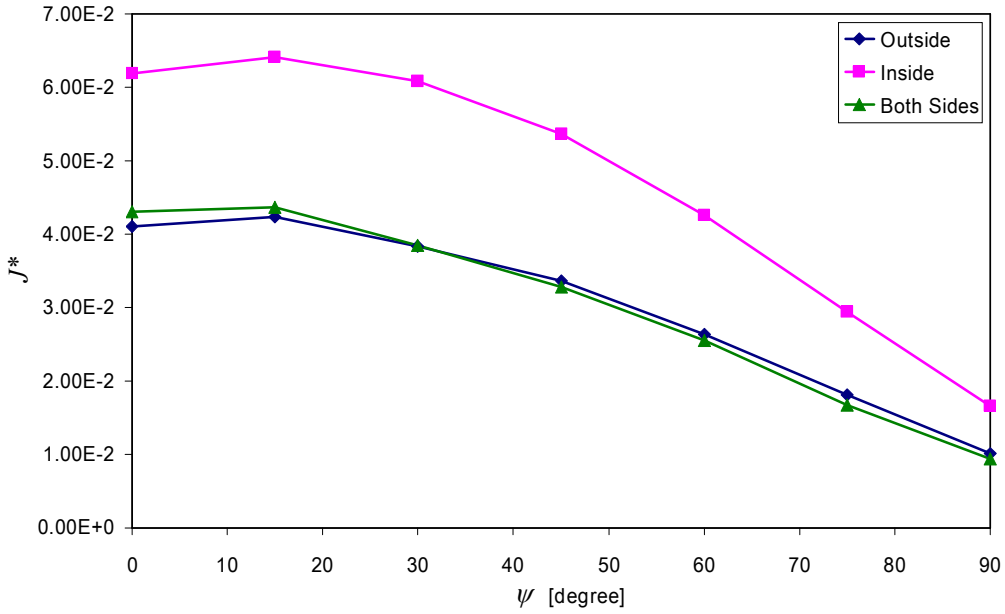


Figure 5.6 Normalized J-integral versus Inclination Angle ($\psi$)
(Crack at Weld Toe 1, Lateral Force is Included, $\beta$=63$^0$)

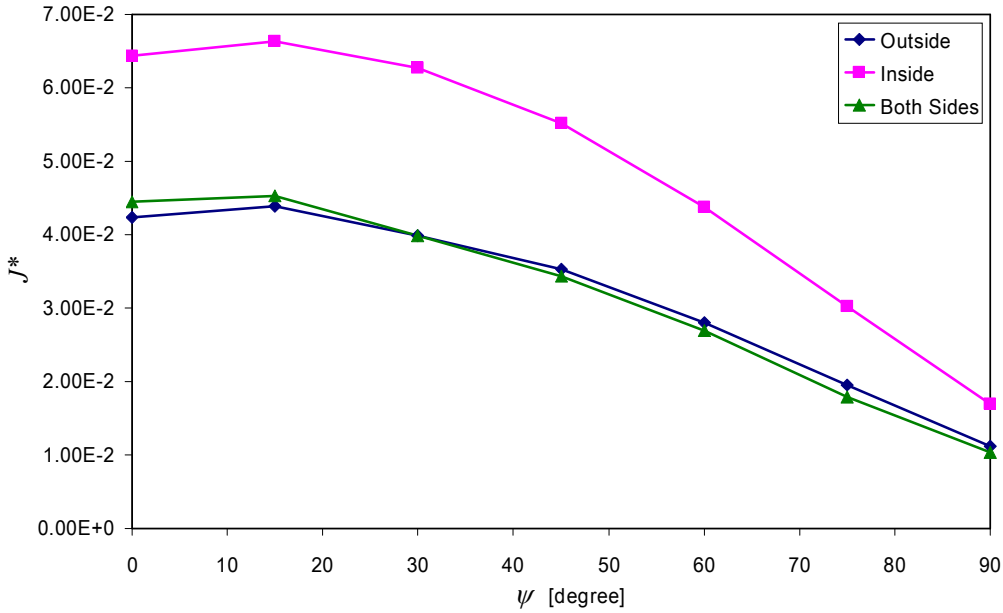


Figure 5.7 Normalized J-integral versus Inclination Angle ($\psi$)
(Crack at Weld Toe 1, Lateral Force is Included, $\beta$=90$^0$)

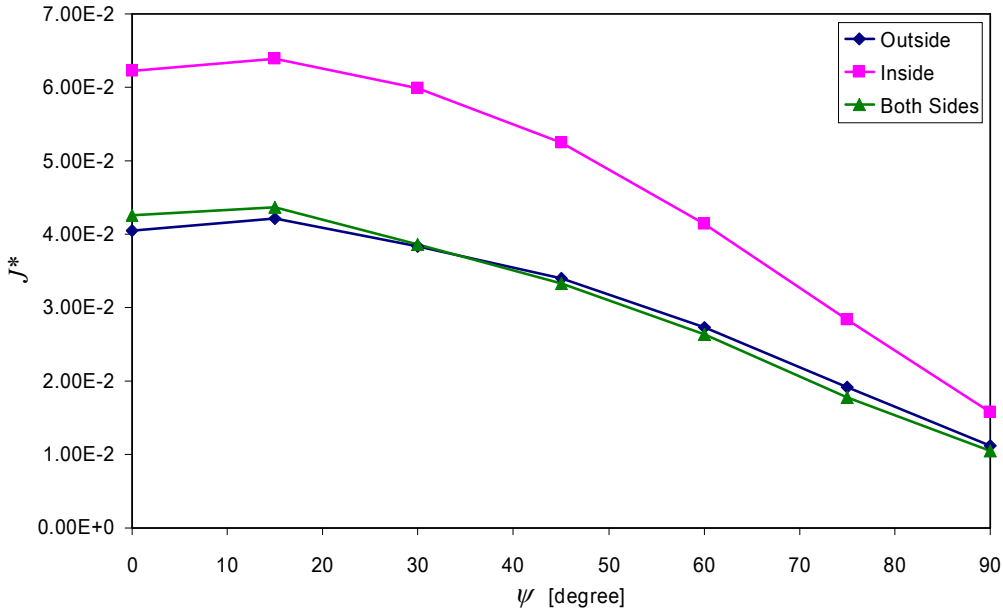


Figure 5.8 Normalized J-integral versus Inclination Angle ($\psi$)
(Crack at Weld Toe 1, Lateral Force is Included, $\beta$=117$^0$)

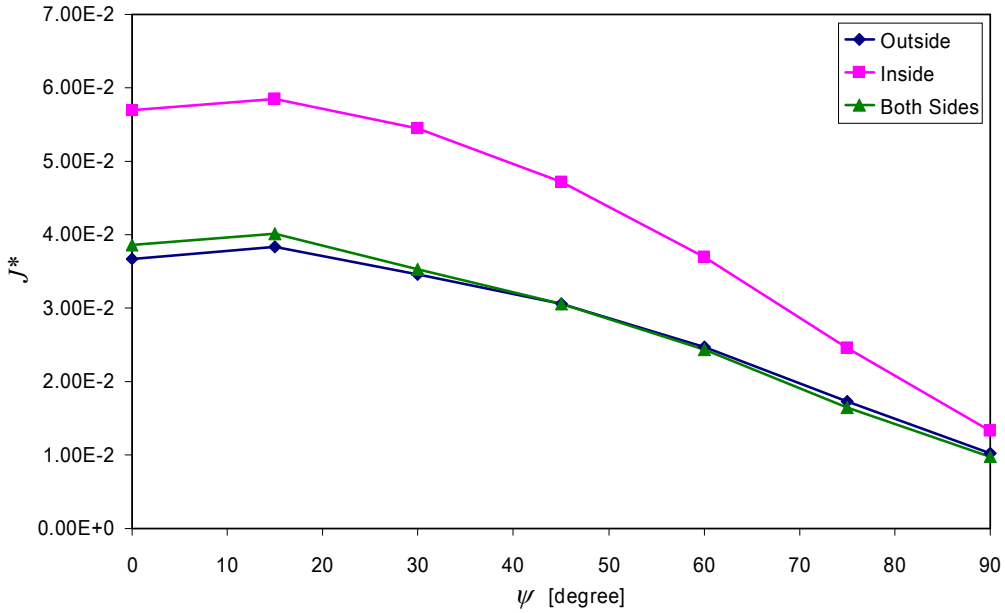


Figure 5.9 Normalized J-integral versus Inclination Angle ($\psi$)
(Crack at Weld Toe 1, Lateral Force is Included, $\beta$=149$^0$)

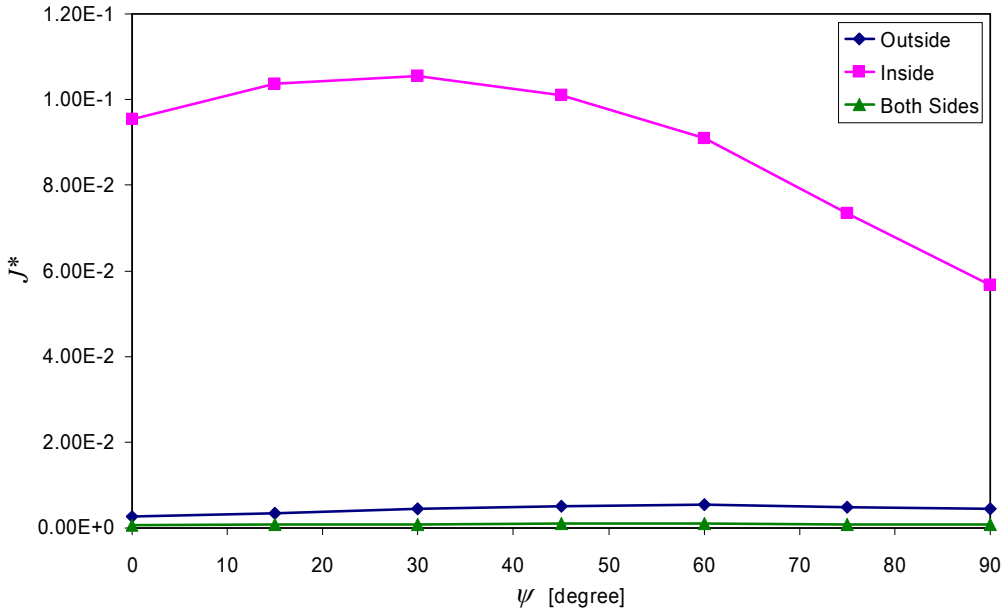


Figure 5.10 Normalized J-integral versus Inclination Angle ($\psi$)
(Crack at Weld Toe 2, Lateral Force is Included, $\beta$=31$^0$)

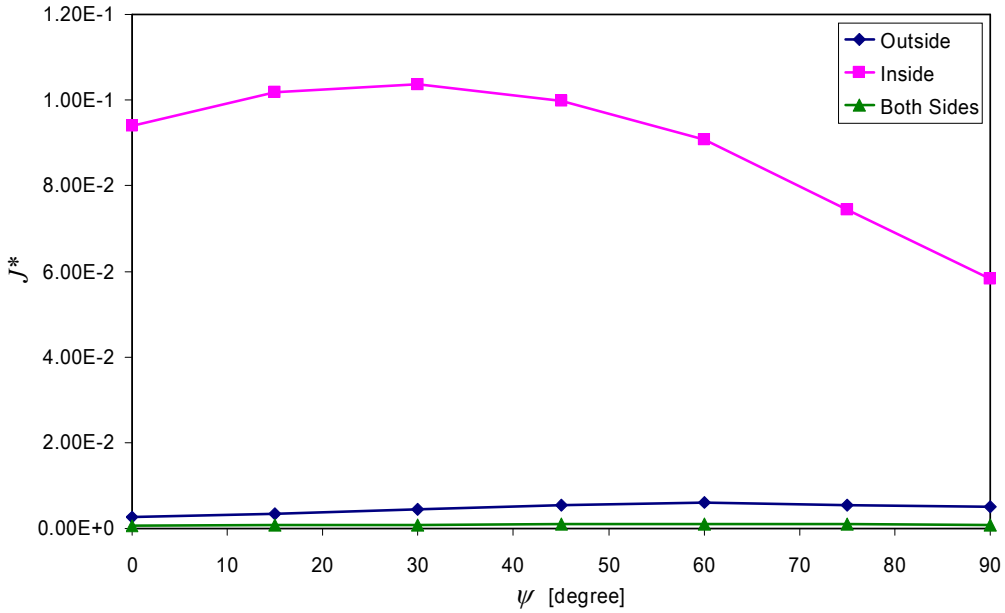


Figure 5.11 Normalized J-integral versus Inclination Angle ($\psi$)
(Crack at Weld Toe 2, Lateral Force is Included, $\beta$=63$^0$)

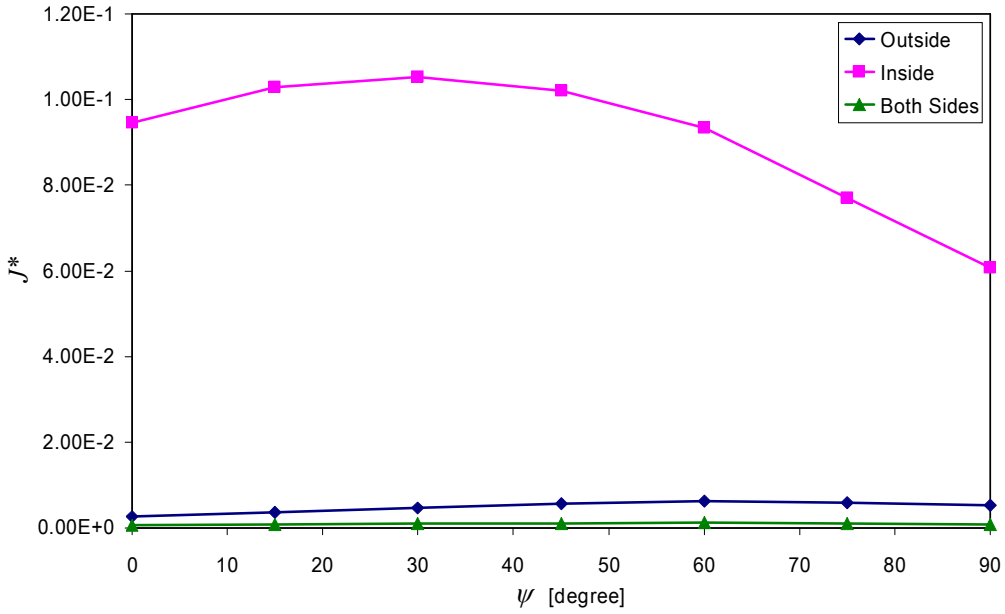


Figure 5.12 Normalized J-integral versus Inclination Angle ($\psi$)
(Crack at Weld Toe 2, Lateral Force is Included, $\beta$=90$^0$)

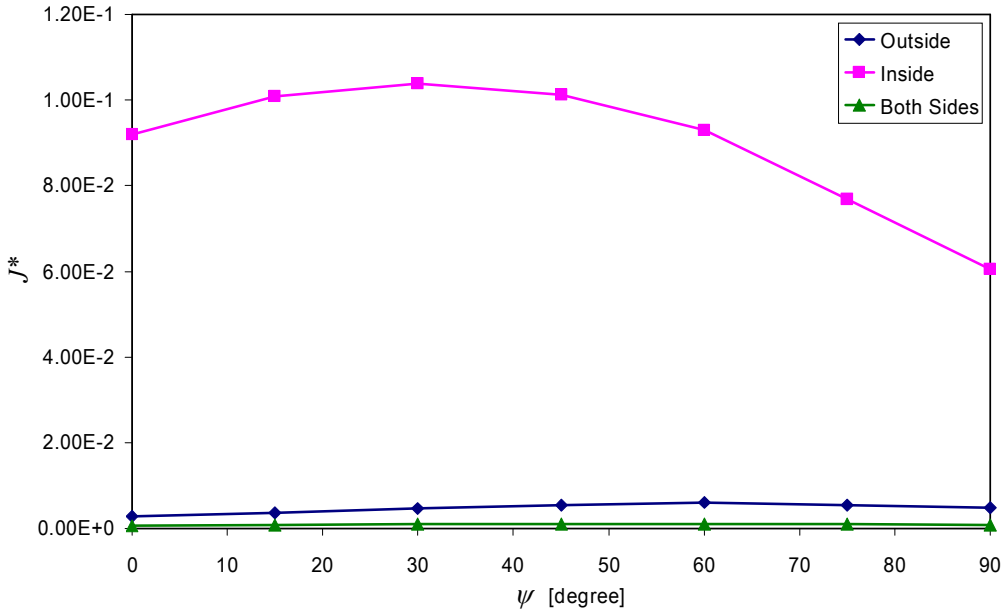


Figure 5.13 Normalized J-integral versus Inclination Angle ($\psi$)
(Crack at Weld Toe 2, Lateral Force is Included, $\beta$=117$^0$)

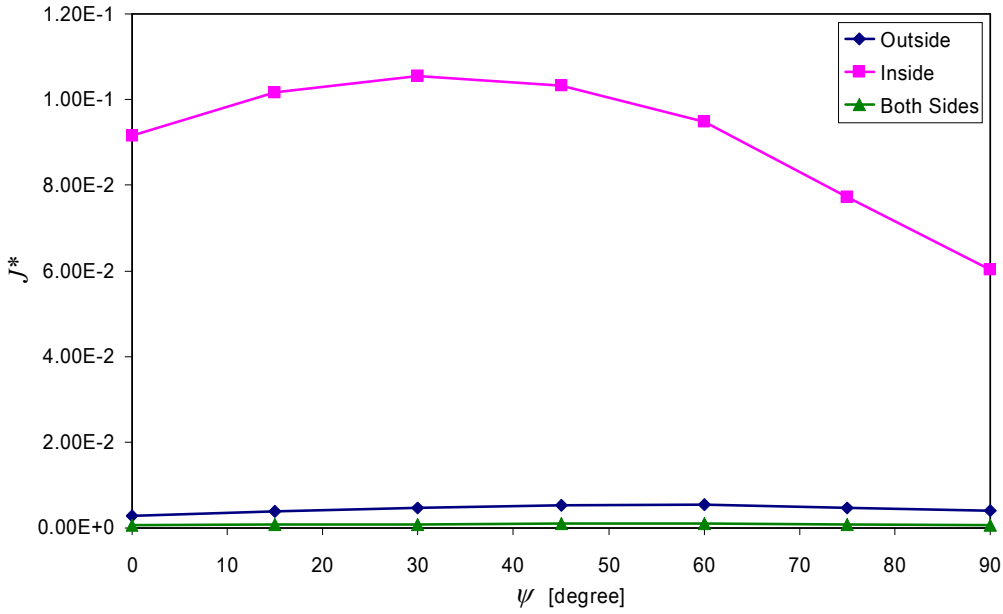


Figure 5.14 Normalized J-integral versus Inclination Angle ($\psi$)
(Crack at Weld Toe 2, Lateral Force is Included, $\beta$=149$^0$)

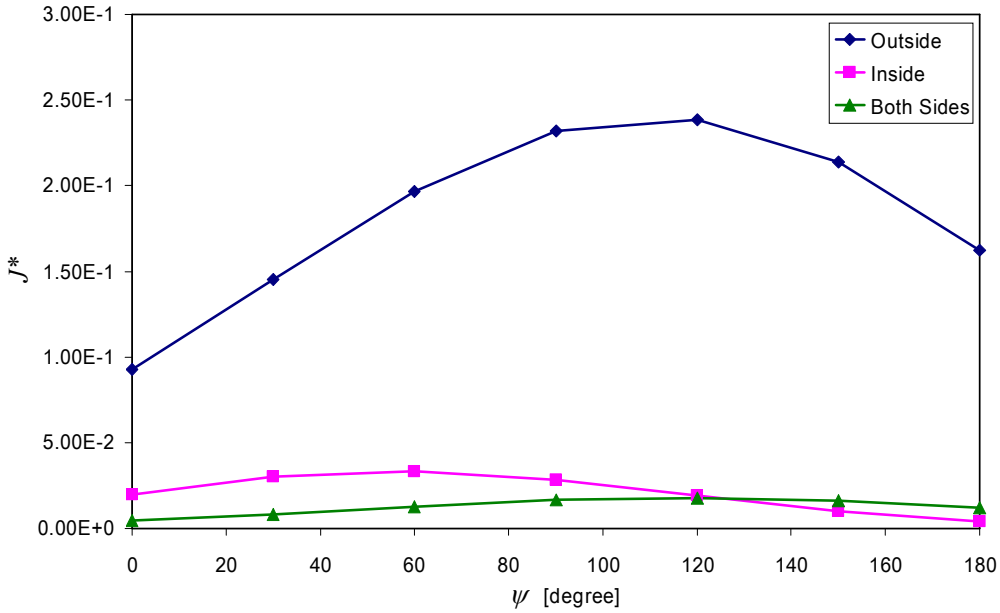


Figure 5.15 Normalized J-integral versus Inclination Angle ($\psi$)
(Crack at Weld Root, Lateral Force is Included, $\beta$=31$^0$)

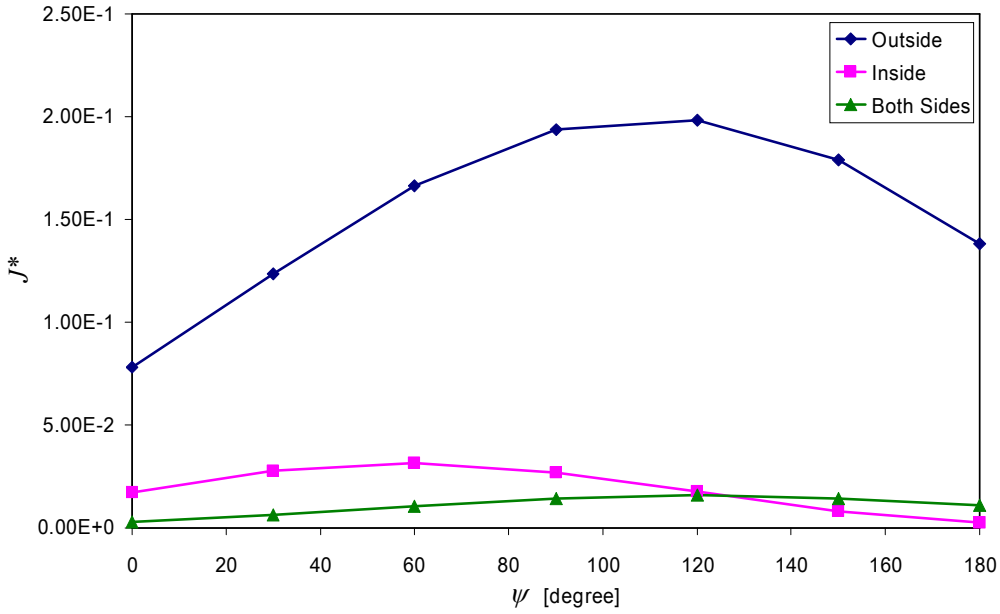


Figure 5.16 Normalized J-integral versus Inclination Angle ($\psi$)
(Crack at Weld Root, Lateral Force is Included, $\beta$=63$^0$)

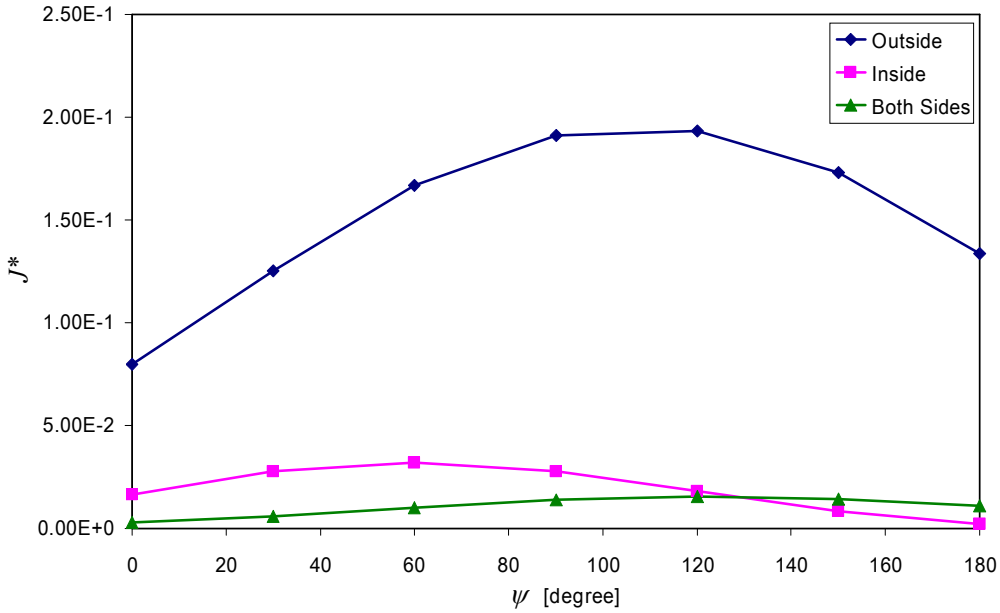


Figure 5.17 Normalized J-integral versus Inclination Angle ($\psi$)
(Crack at Weld Root, Lateral Force is Included, $\beta$=90$^0$)

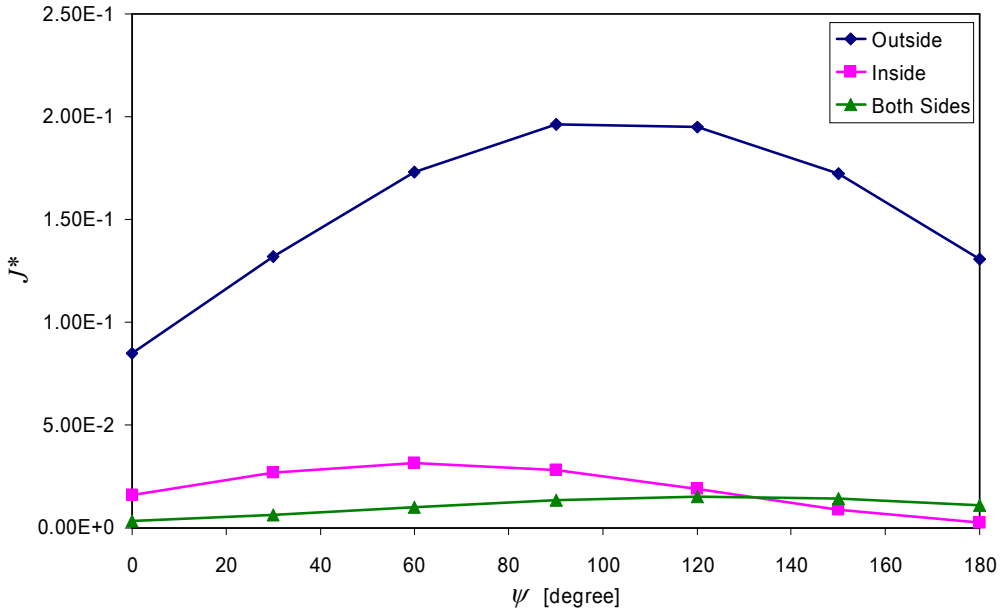


Figure 5.18 Normalized J-integral versus Inclination Angle ($\psi$)
(Crack at Weld Root, Lateral Force is Included, $\beta$=117$^0$)

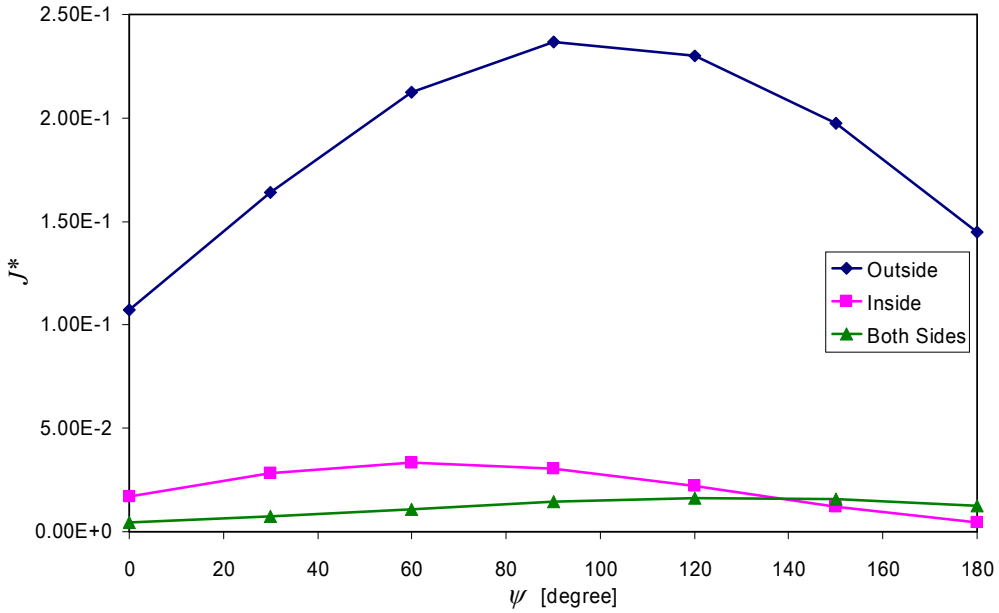


Figure 5.19 Normalized J-integral versus Inclination Angle ($\psi$)
(Crack at Weld Root, Lateral Force is Included, $\beta$=149$^0$)

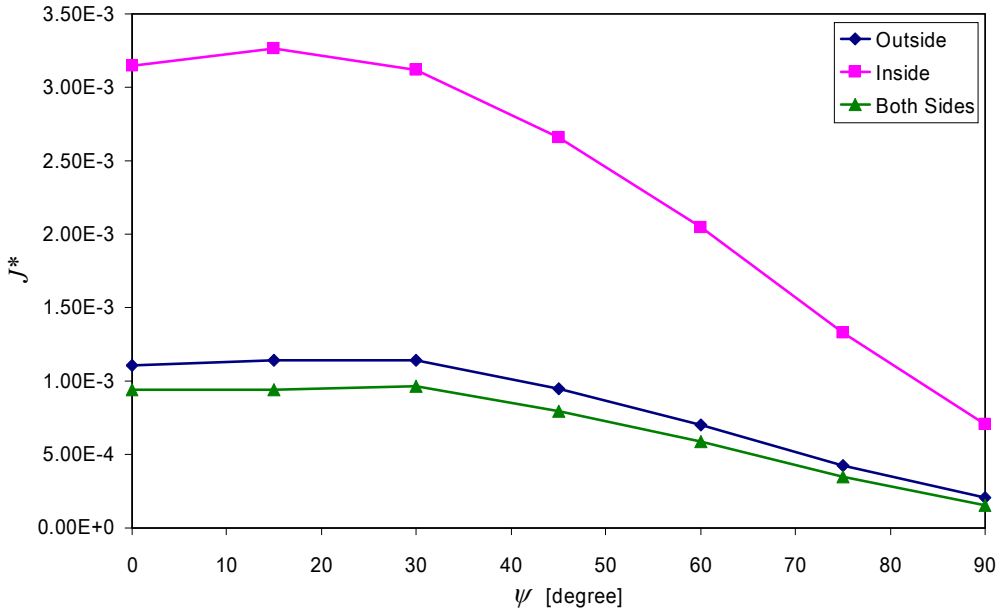


Figure 5.20 Normalized J-integral versus Inclination Angle ($\psi$)
(Crack at Weld Toe 1, Lateral Force is **not** Included, $\beta$=31$^0$)

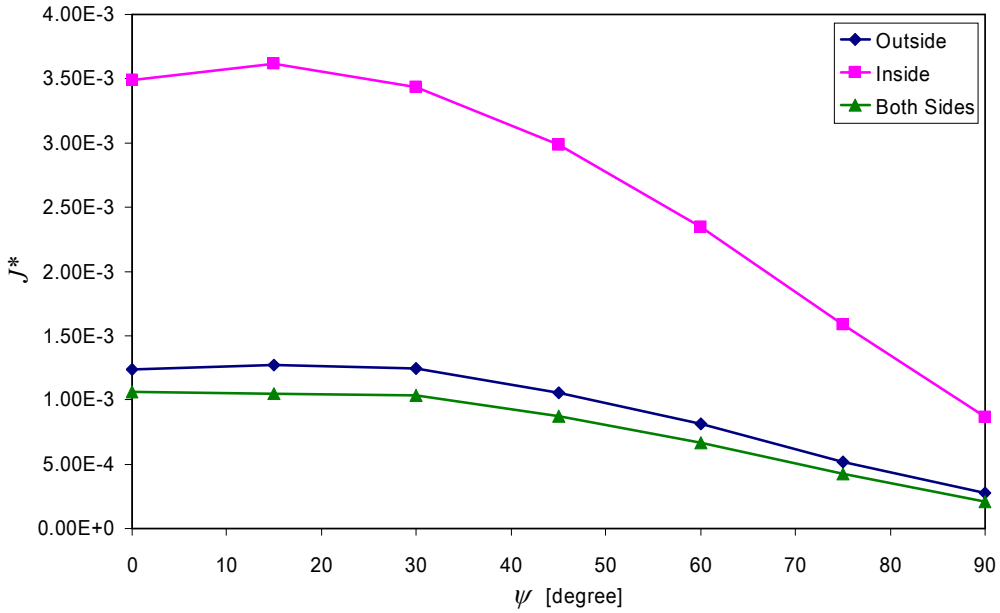


Figure 5.21 Normalized J-integral versus Inclination Angle ($\psi$)
(Crack at Weld Toe 1, Lateral Force is **not** Included, $\beta$=63$^0$)

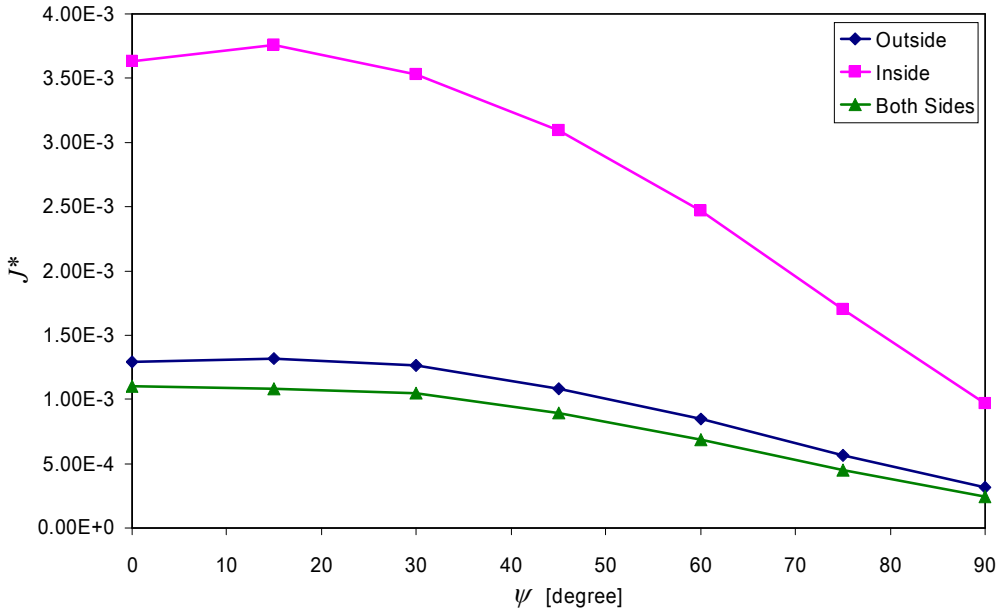


Figure 5.22 Normalized J-integral versus Inclination Angle ($\psi$)
(Crack at Weld Toe 1, Lateral Force is **not** Included, $\beta$=90$^0$)

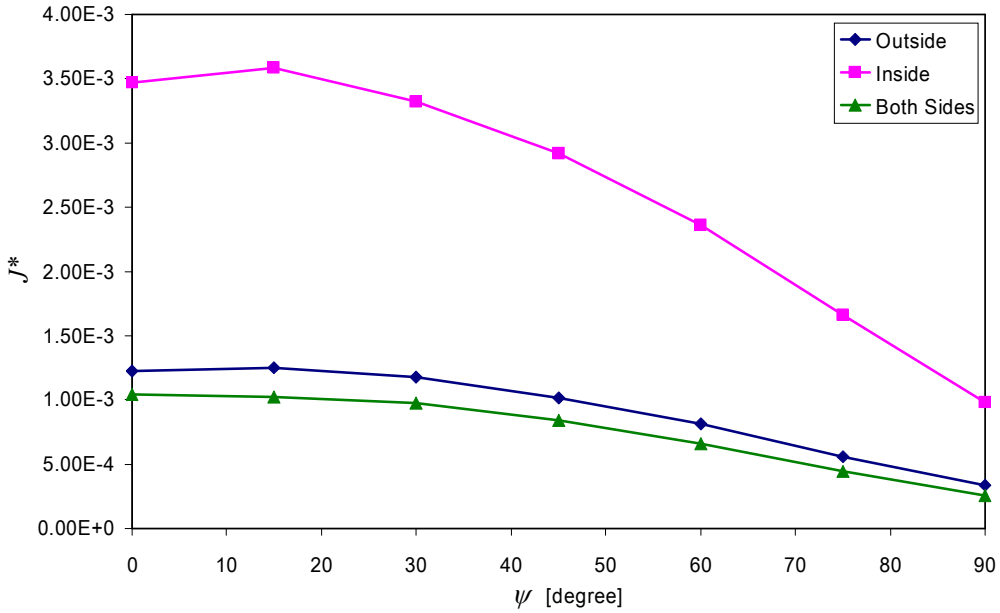


Figure 5.23 Normalized J-integral versus Inclination Angle ($\psi$)
(Crack at Weld Toe 1, Lateral Force is **not** Included, $\beta$=117$^0$)

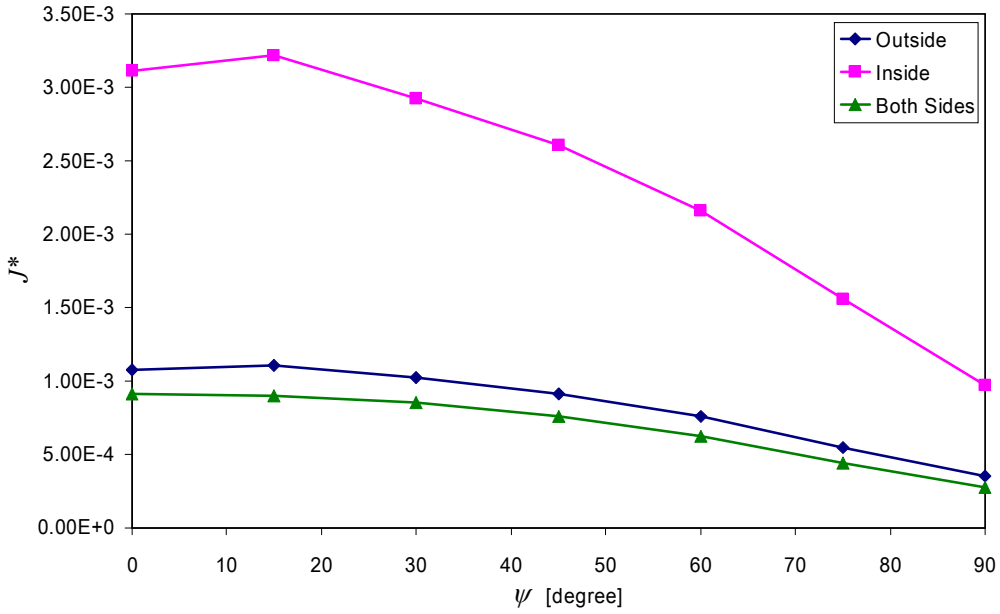


Figure 5.24 Normalized J-integral versus Inclination Angle ($\psi$)
(Crack at Weld Toe 1, Lateral Force is **not** Included, $\beta$=149$^0$)

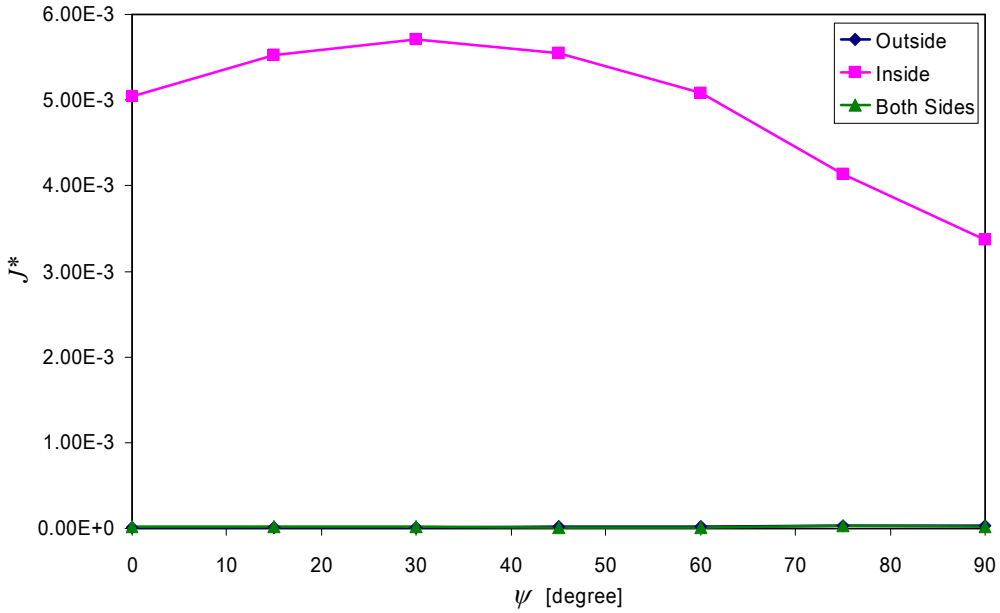


Figure 5.25 Normalized J-integral versus Inclination Angle ($\psi$)
(Crack at Weld Toe 2, Lateral Force is **not** Included, $\beta$=31$^0$)

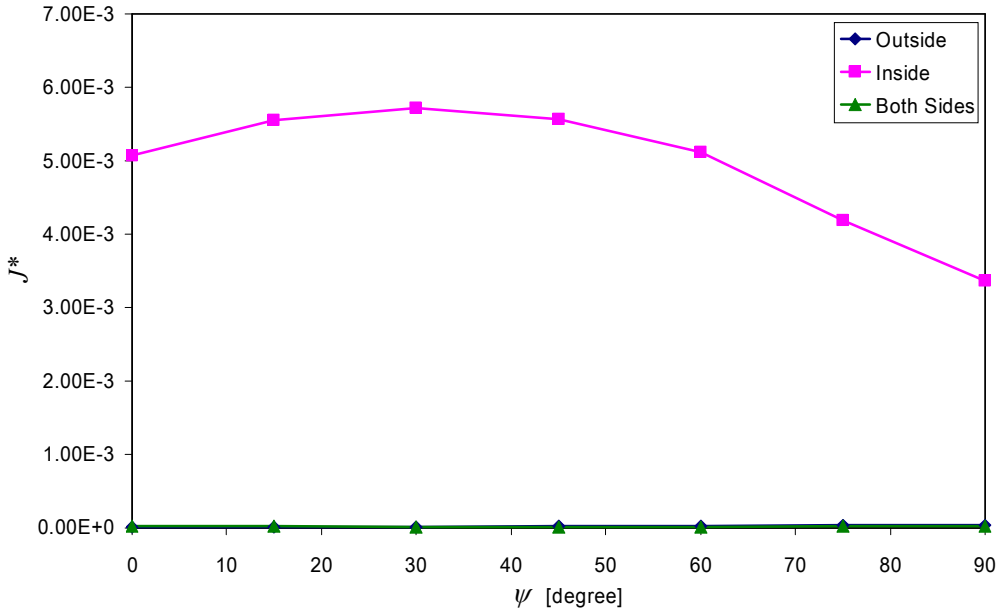


Figure 5.26 Normalized J-integral versus Inclination Angle ($\psi$)
(Crack at Weld Toe 2, Lateral Force is **not** Included, $\beta$=63$^0$)

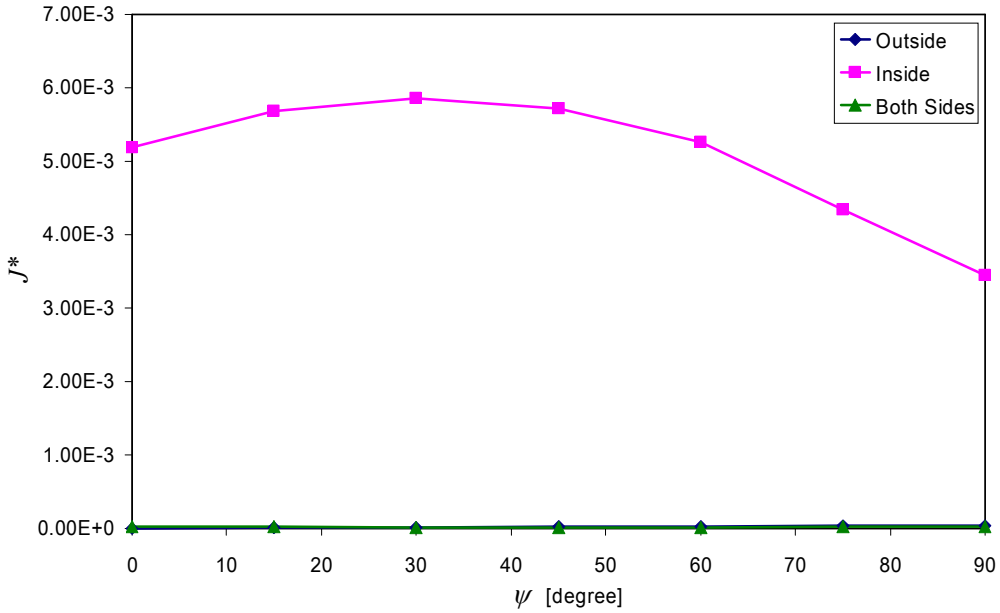


Figure 5.27 Normalized J-integral versus Inclination Angle ($\psi$)
(Crack at Weld Toe 2, Lateral Force is **not** Included, $\beta$=90$^0$)

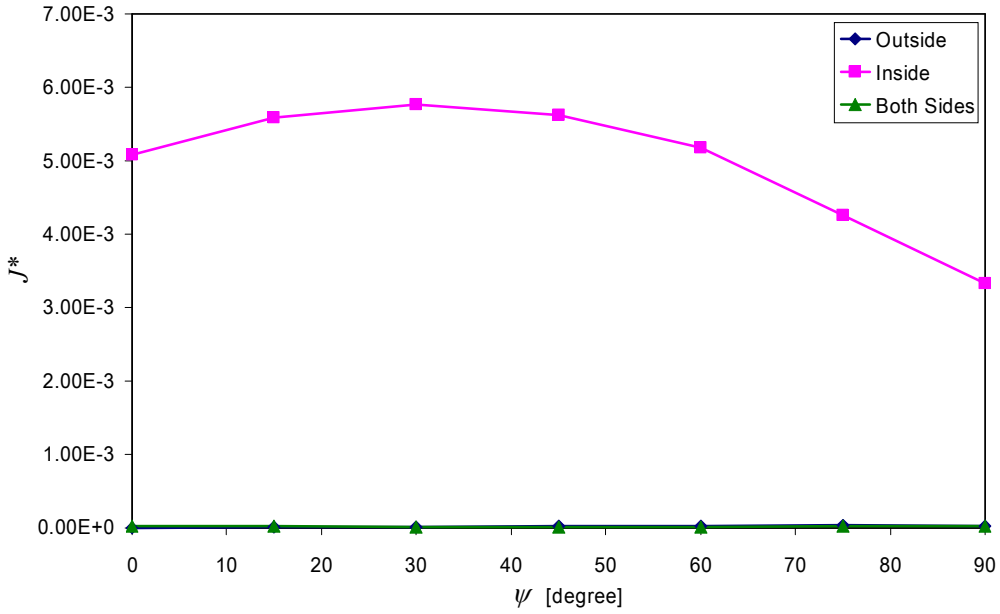


Figure 5.28 Normalized J-integral versus Inclination Angle ($\psi$)
(Crack at Weld Toe 2, Lateral Force is **not** Included, $\beta$=117$^0$)

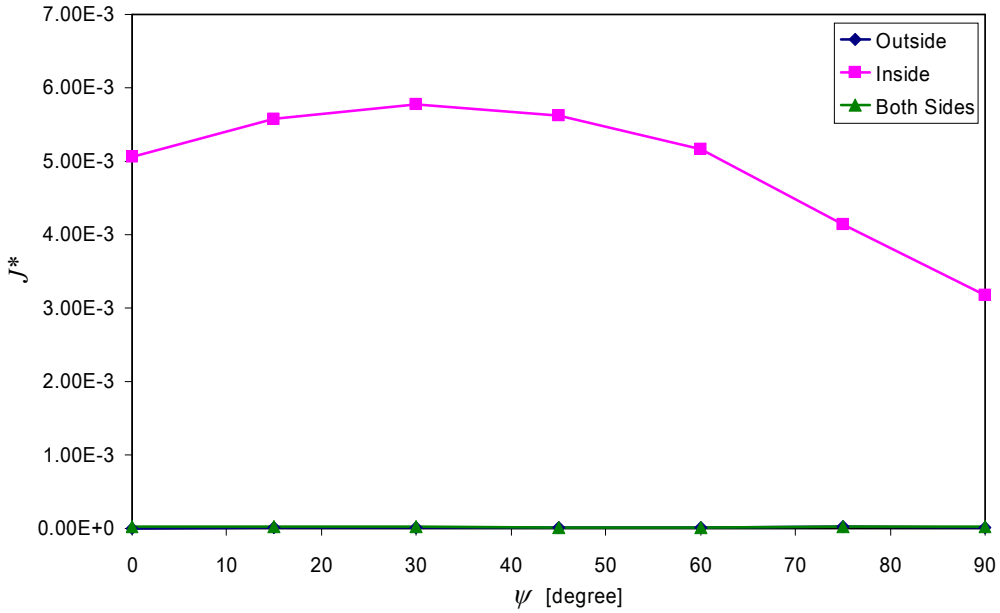


Figure 5.29 Normalized J-integral versus Inclination Angle ($\psi$)
(Crack at Weld Toe 2, Lateral Force is **not** Included, $\beta$=149$^0$)

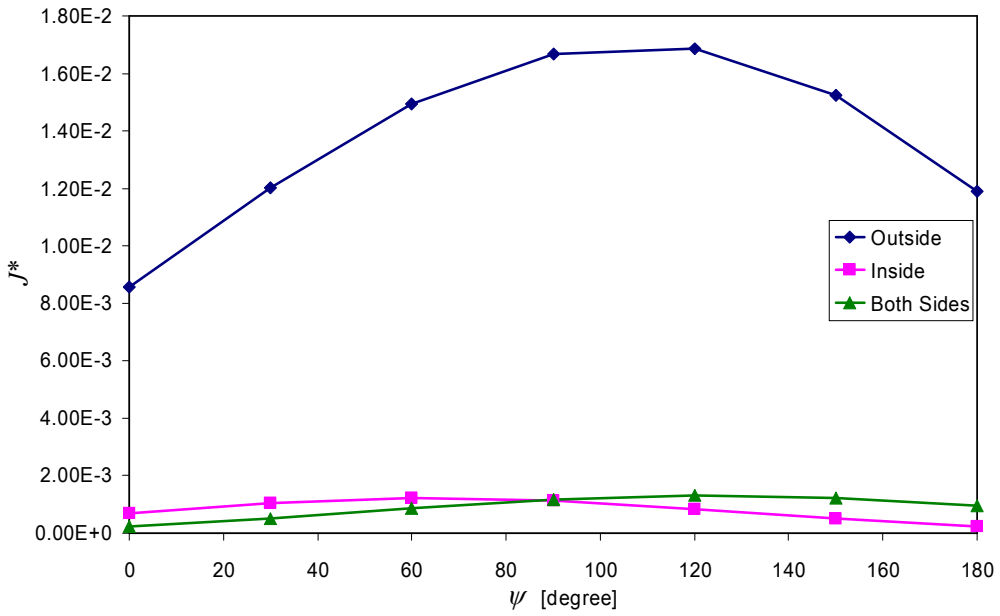


Figure 5.30 Normalized J-integral versus Inclination Angle ($\psi$)
(Crack at Weld Root, Lateral Force is **not** Included, $\beta$=31$^0$)

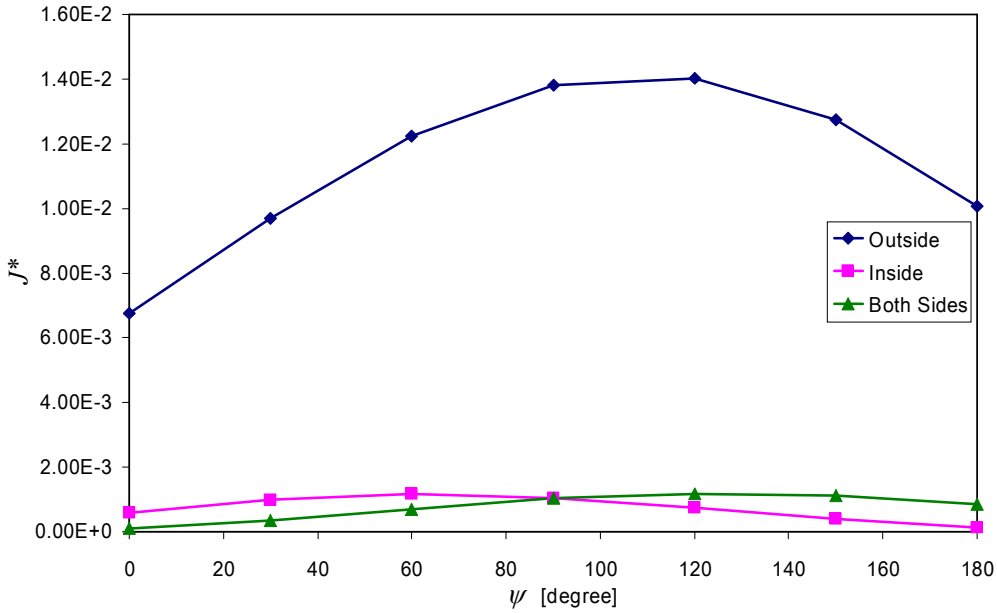


Figure 5.31 Normalized J-integral versus Inclination Angle ($\psi$)
(Crack at Weld Root, Lateral Force is **not** Included, $\beta=63^0$)

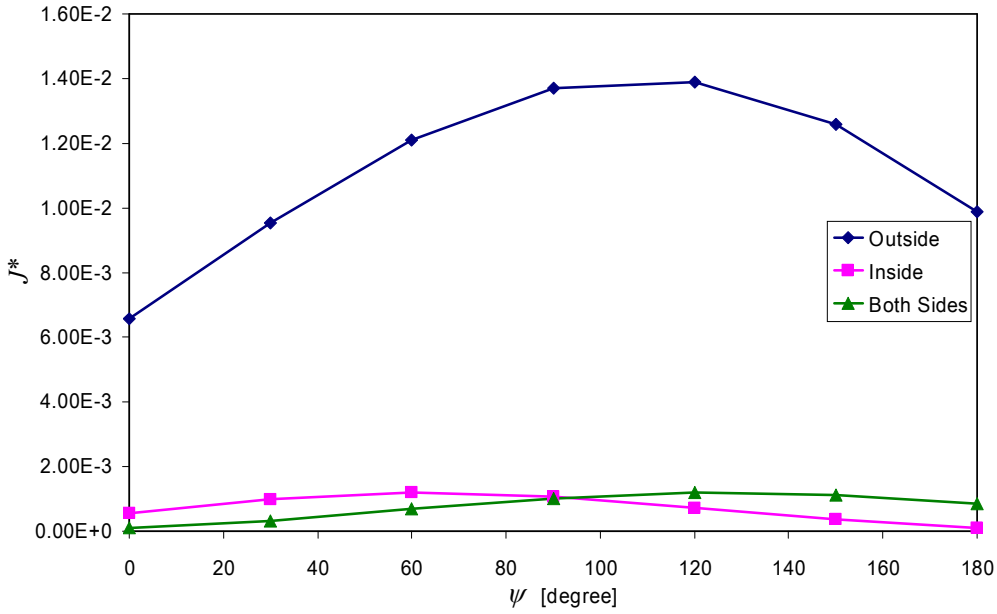


Figure 5.32 Normalized J-integral versus Inclination Angle ($\psi$)
(Crack at Weld Root, Lateral Force is **not** Included, $\beta=90^0$)

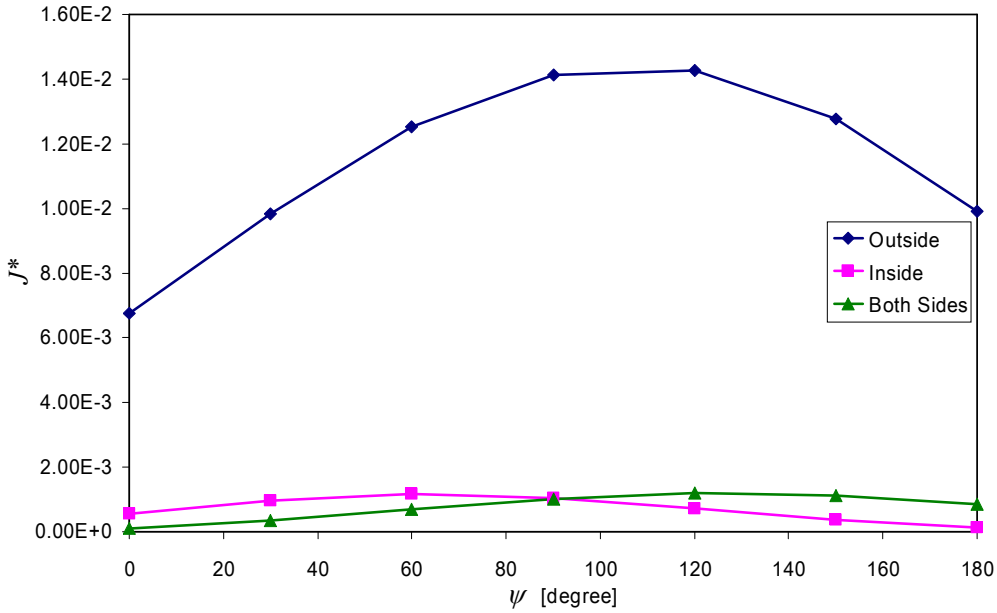


Figure 5.33 Normalized J-integral versus Inclination Angle ($\psi$)
(Crack at Weld Root, Lateral Force is **not** Included, $\beta$=117$^0$)

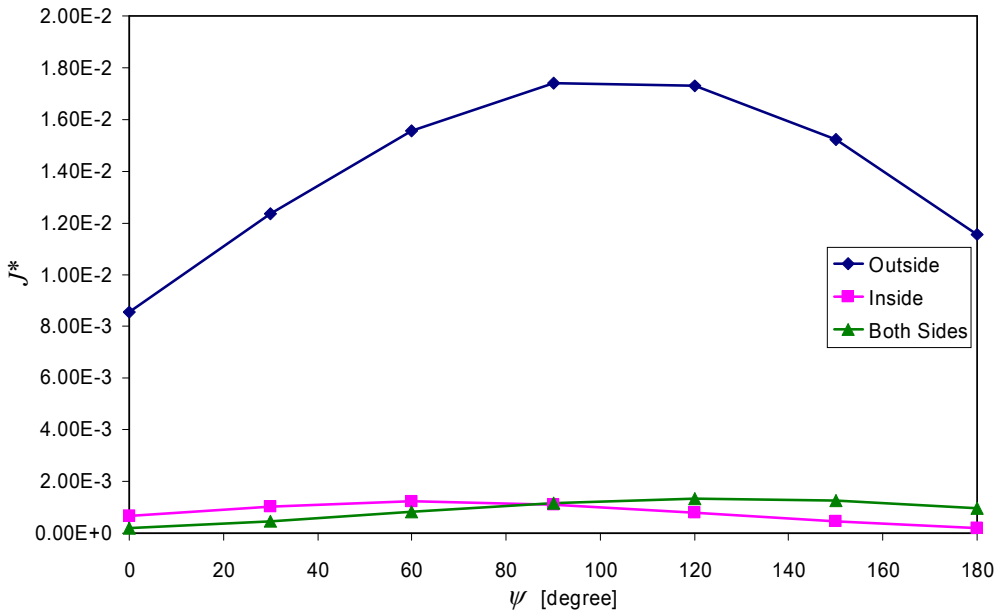


Figure 5.34 Normalized J-integral versus Inclination Angle ($\psi$)
(Crack at Weld Root, Lateral Force is **not** Included, $\beta$=149$^0$)

### 5.2.2 Arm Parametric Analyses

The excavator arm is one of the main components of digging mechanism. It is also exposed to repeated fluctuations, which cause cracks to occur. Figure 5.35 shows a crack encountered during the fatigue tests performed in Hidromek Ltd. Sti. Therefore, this location can be a good starting point for fracture mechanics analyses of excavator arm. The global shell model analysis of the arm will again be the initial step in structural zooming analysis (Figure 5.36, 5.37). The selected region on global shell model is shown in Figure 5.38. Notice that the selected region is at the corner of the box section and does not contain any thickness transition region. An example to the generated solid local model analysis is given in Figure 5.39. The resulting normalized *J*- integral values versus inclination angle ($\psi$) for five crack front position angles ($\beta$) are given in Figures 5.40-5.69.

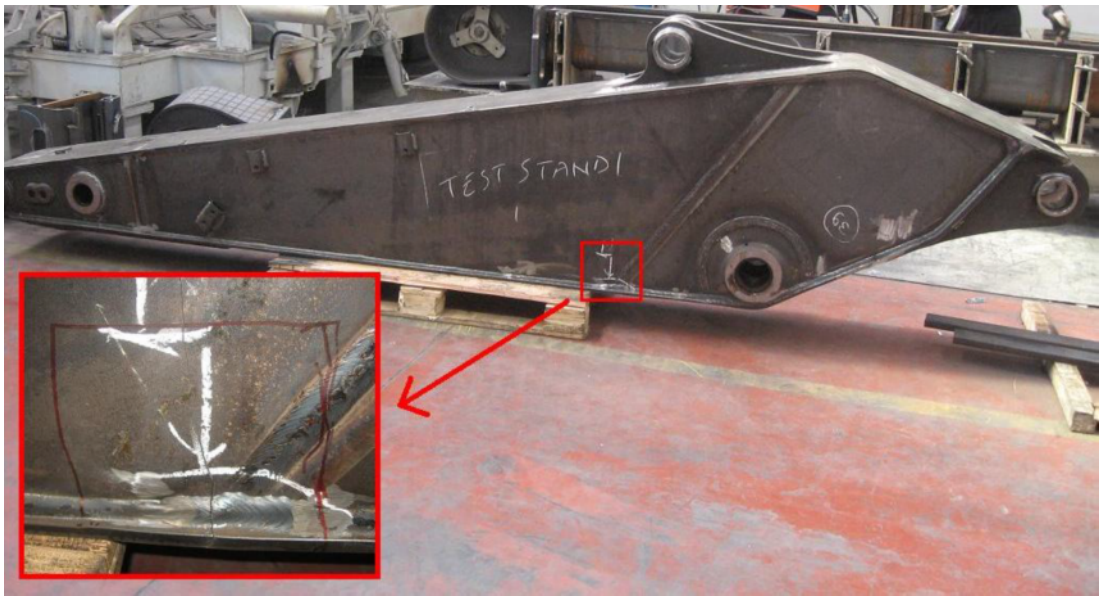


Figure 5.35 A Fatigue Crack Occurred on HMK 300 LC Excavator Arm During the Performed Tests in Hidromek Ltd. Sti.

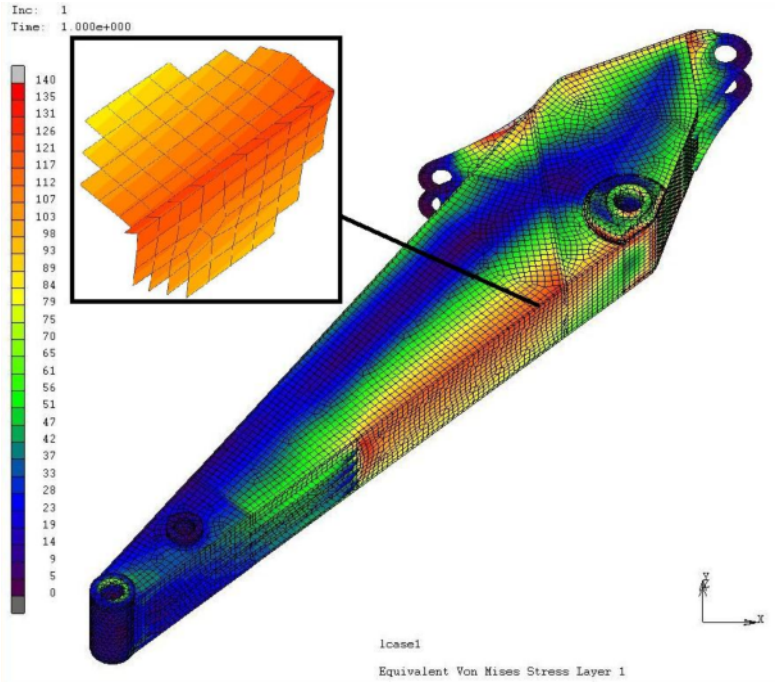


Figure 5.36 Excavator Arm Global Model (Von Mises Stress Outer Layer)

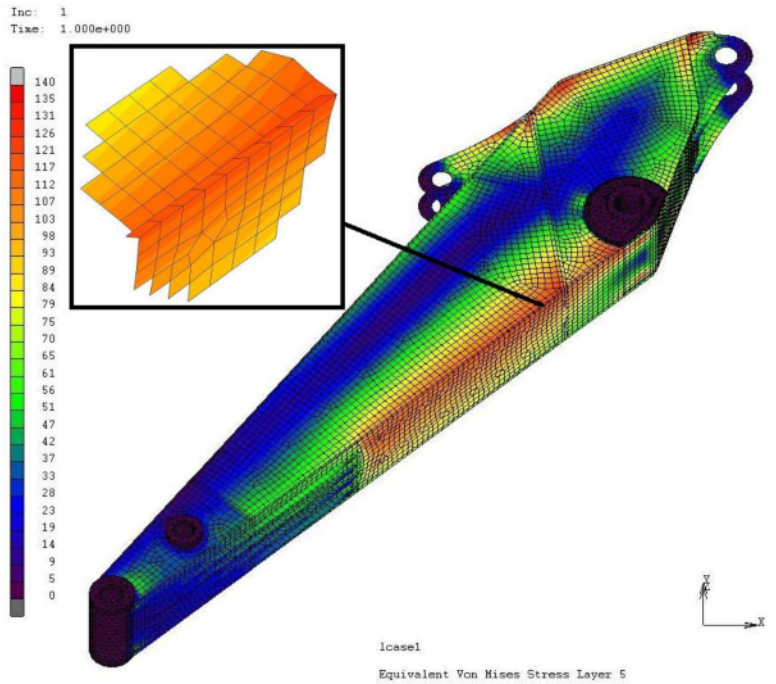


Figure 5.37 Excavator Arm Global Model (Von Mises Stress Inner Layer)

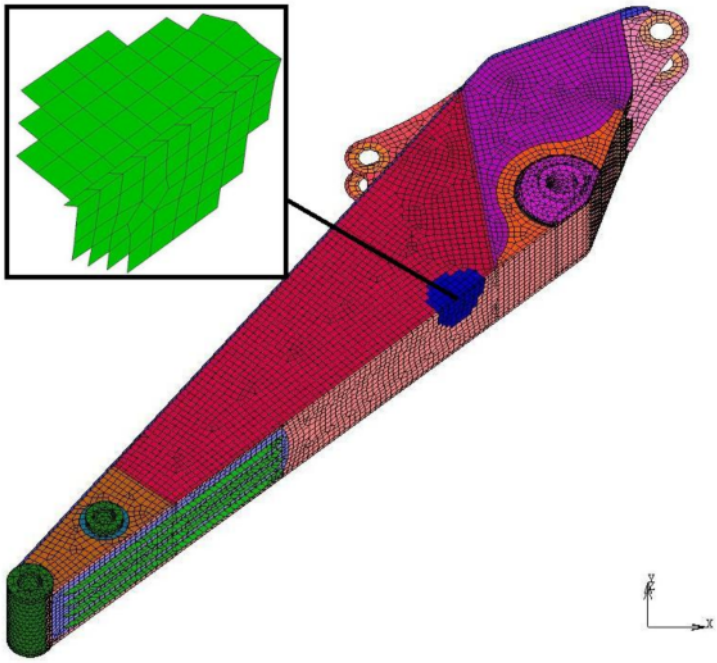

Figure 5.38 Excavator Arm Model Sheet Metals and the Selected Region

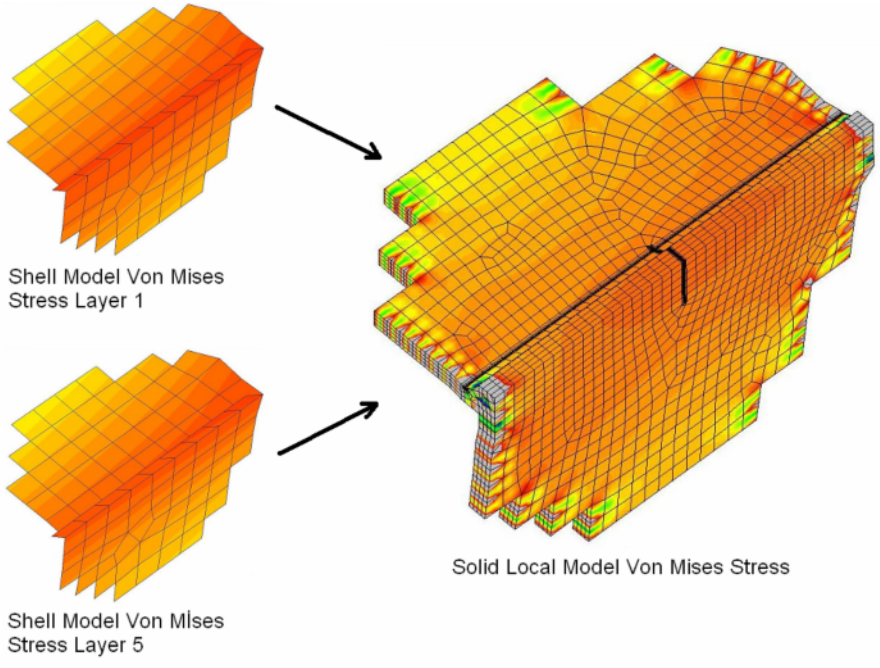


Figure 5.39 Arm Selected Shell Region and Arm Solid Local Model Von Mises Stress Map

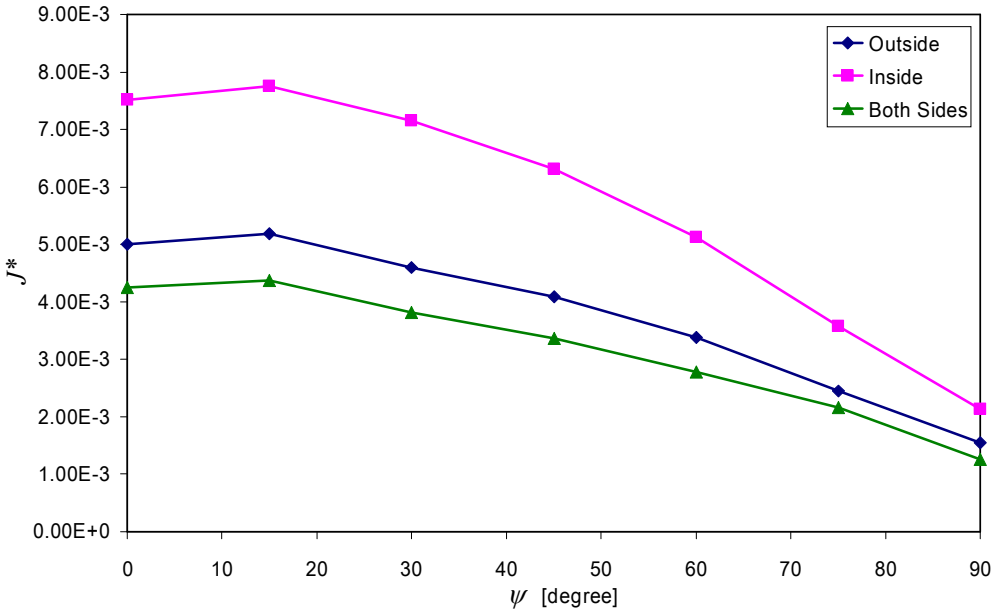


Figure 5.40 Normalized *J*-integral versus Inclination Angle ($\psi$)
(Crack at Weld Toe 1, Lateral Force is Included, $\beta$=31$^0$)

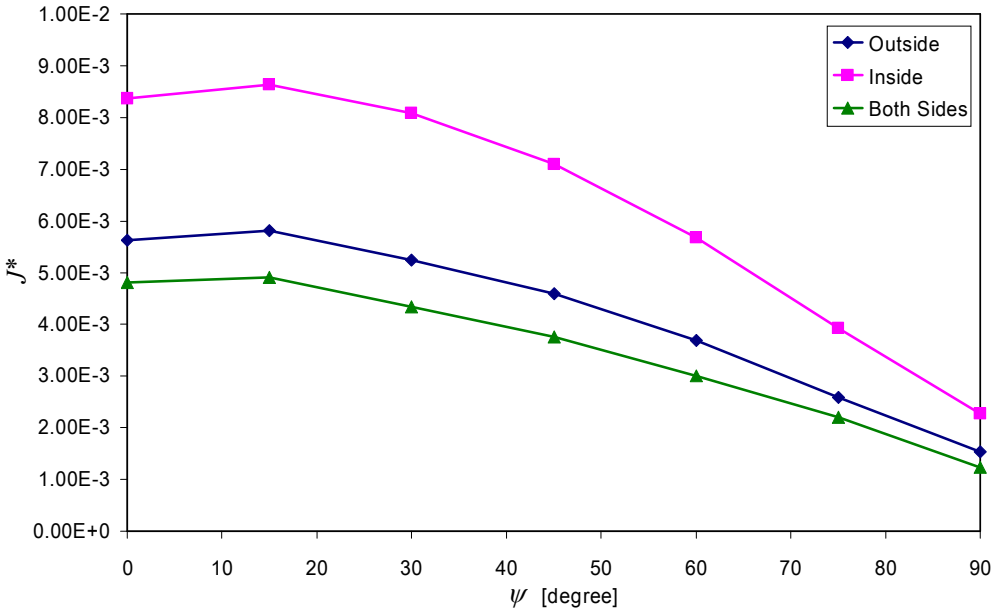


Figure 5.41 Normalized J-integral versus Inclination Angle ($\psi$)
(Crack at Weld Toe 1, Lateral Force is Included, $\beta$=63$^0$)

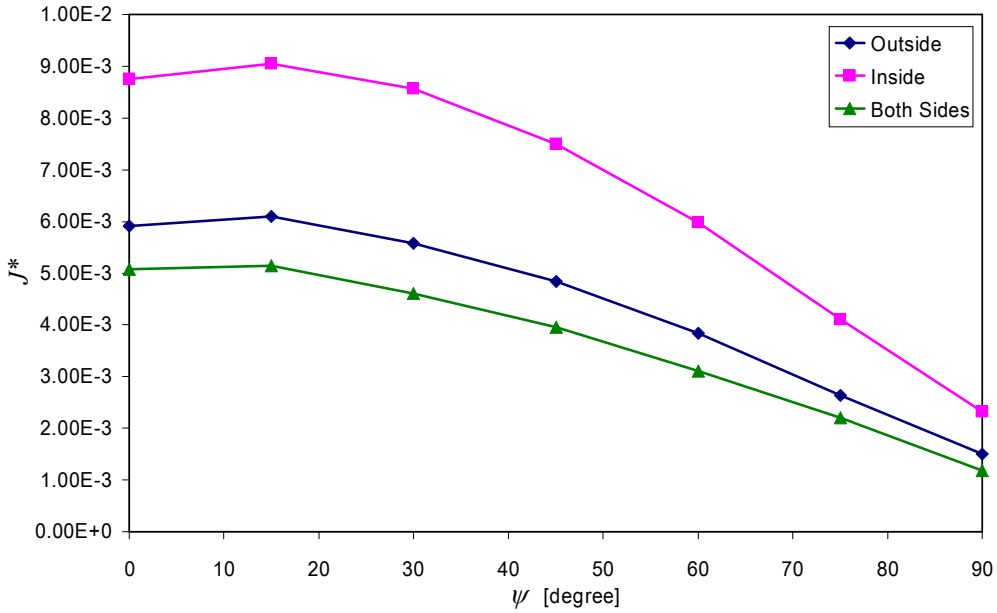


Figure 5.42 Normalized J-integral versus Inclination Angle ($\psi$)
(Crack at Weld Toe 1, Lateral Force is Included, $\beta$=90$^0$)

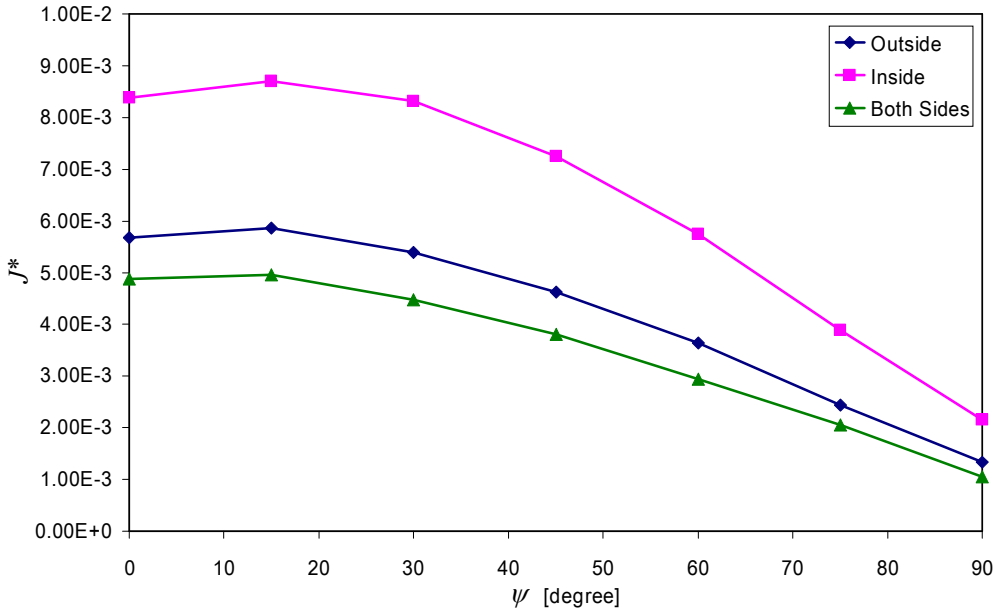


Figure 5.43 Normalized J-integral versus Inclination Angle ($\psi$)
(Crack at Weld Toe 1, Lateral Force is Included, $\beta$=117$^0$)

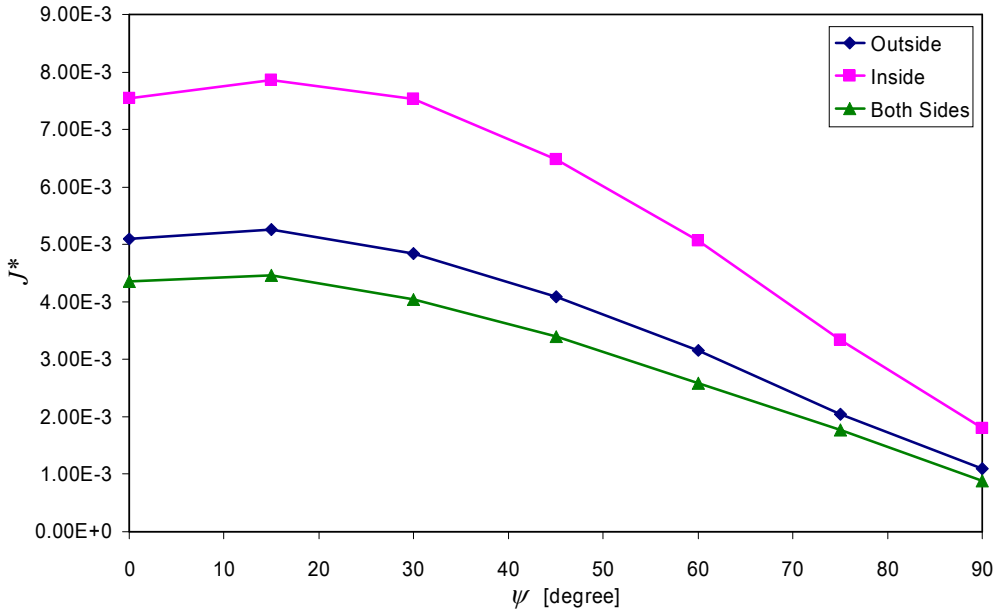


Figure 5.44 Normalized J-integral versus Inclination Angle ($\psi$)
(Crack at Weld Toe 1, Lateral Force is Included, $\beta$=149$^0$)

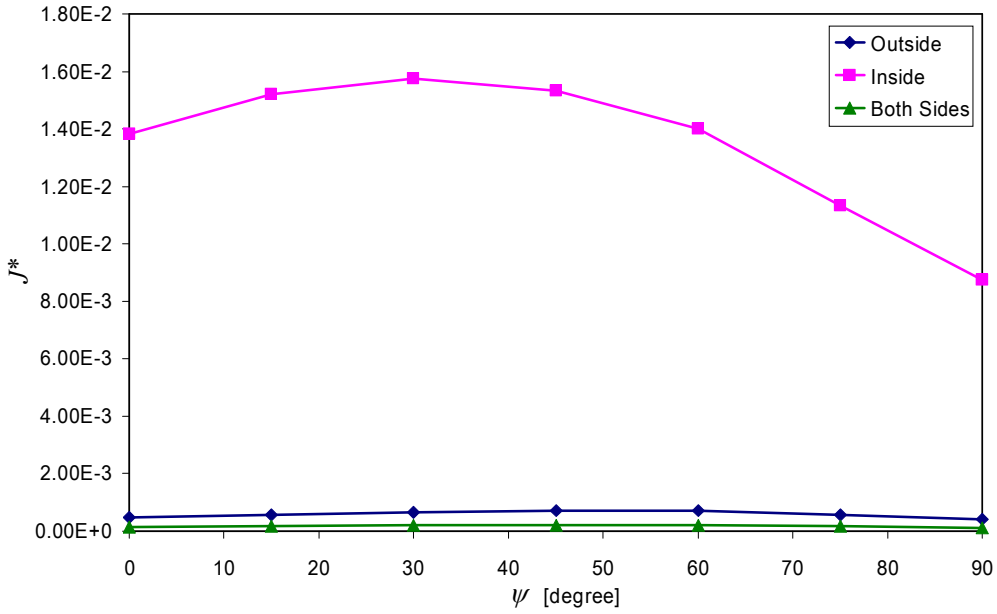


Figure 5.45 Normalized J-integral versus Inclination Angle ($\psi$)
(Crack at Weld Toe 2, Lateral Force is Included, $\beta$=31$^0$)

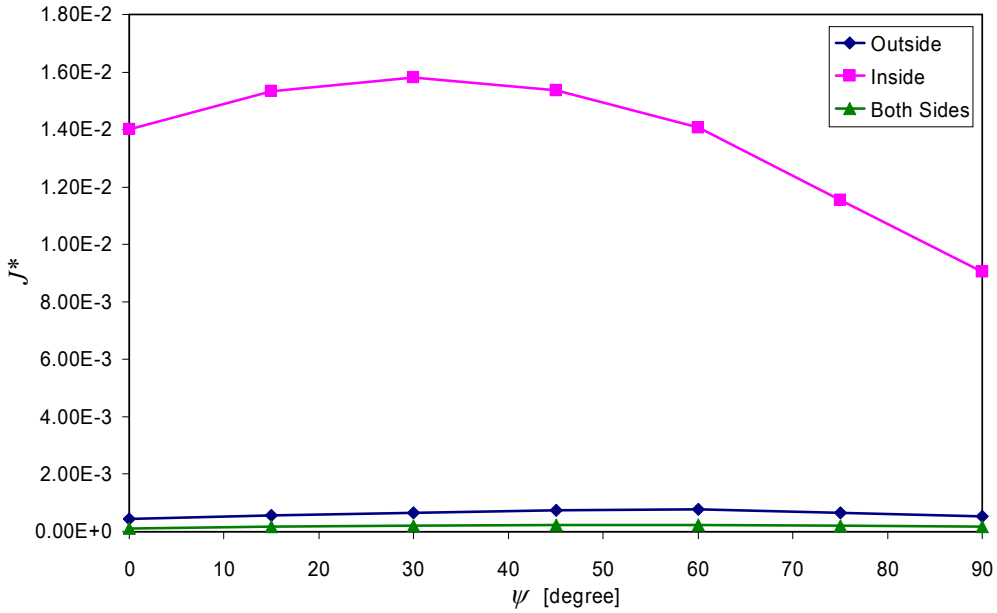


Figure 5.46 Normalized J-integral versus Inclination Angle ($\psi$)
(Crack at Weld Toe 2, Lateral Force is Included, $\beta$=63$^0$)

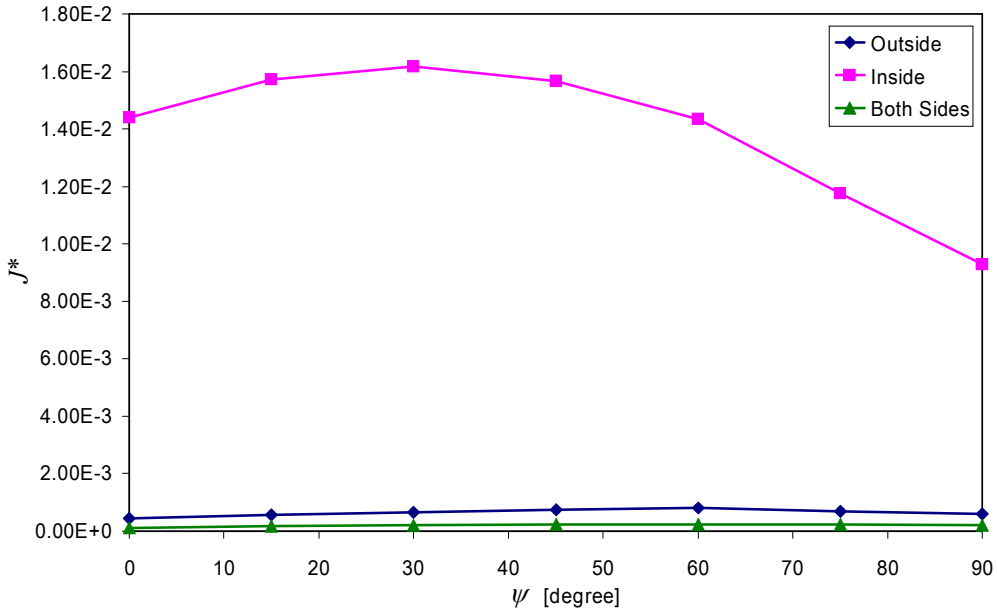


Figure 5.47 Normalized J-integral versus Inclination Angle ($\psi$)
(Crack at Weld Toe 2, Lateral Force is Included, $\beta$=90$^0$)

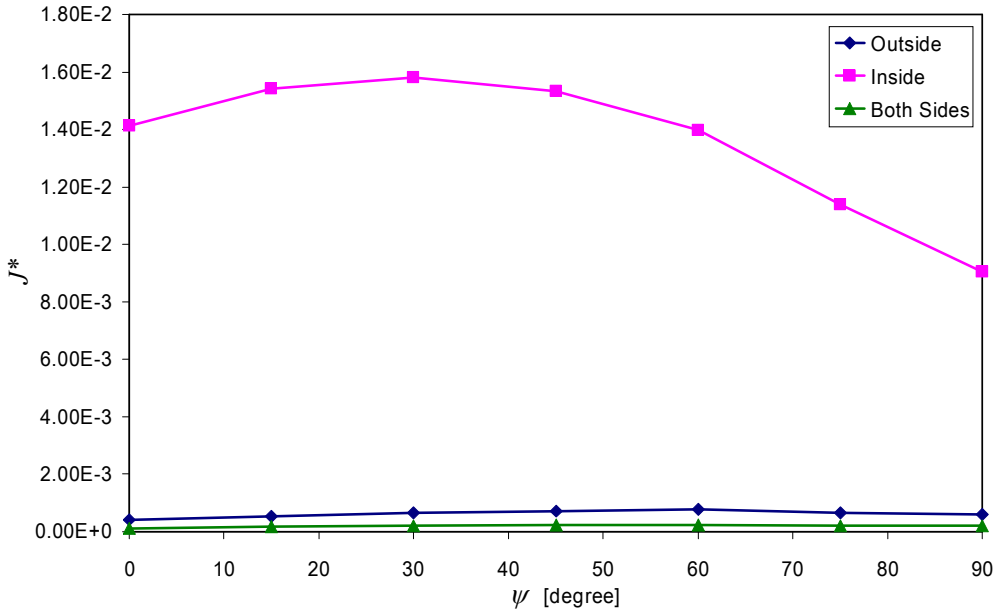


Figure 5.48 Normalized J-integral versus Inclination Angle ($\psi$)
(Crack at Weld Toe 2, Lateral Force is Included, $\beta$=117$^0$)

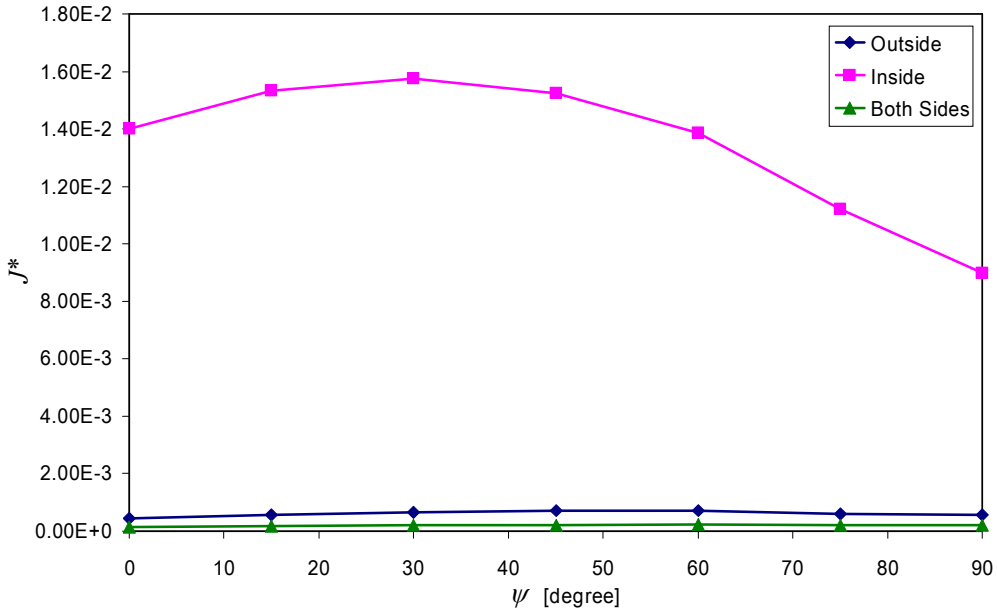


Figure 5.49 Normalized J-integral versus Inclination Angle ($\psi$)
(Crack at Weld Toe 2, Lateral Force is Included, $\beta$=149$^0$)

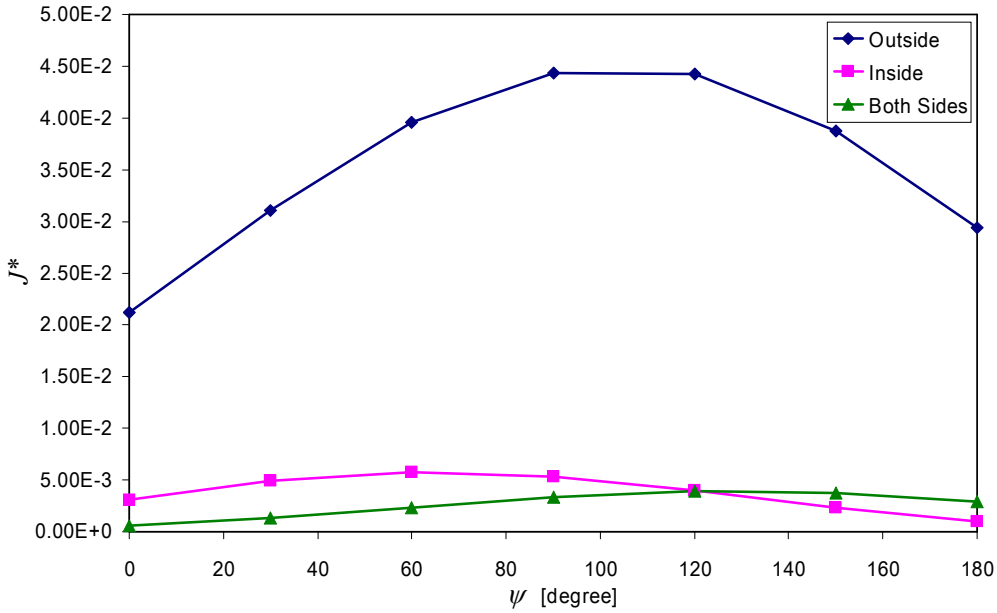


Figure 5.50 Normalized J-integral versus Inclination Angle ($\psi$)
(Crack at Weld Root, Lateral Force is Included, $\beta$=31$^0$)

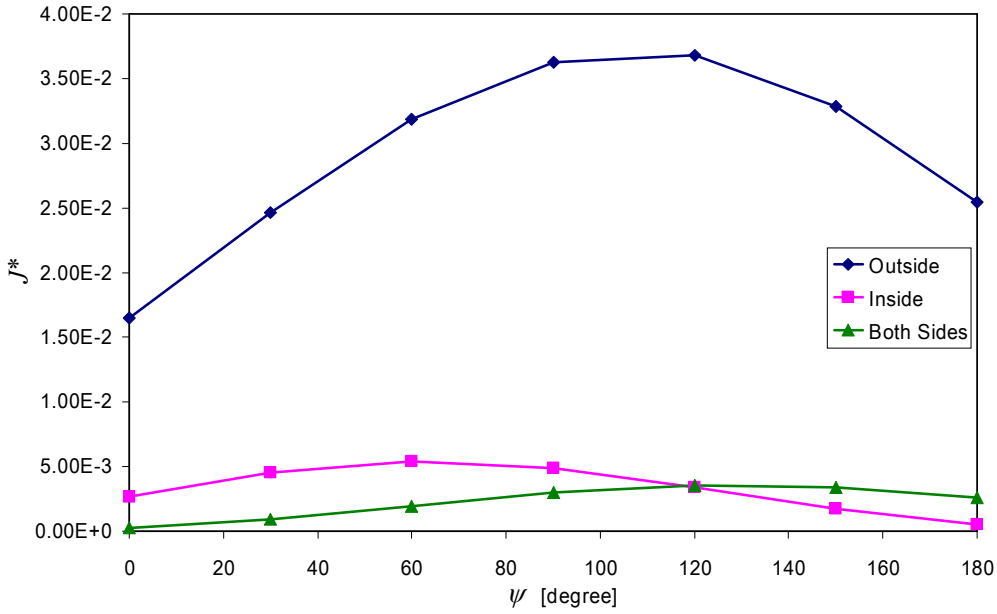


Figure 5.51 Normalized J-integral versus Inclination Angle ($\psi$)
(Crack at Weld Root, Lateral Force is Included, $\beta$=63$^0$)

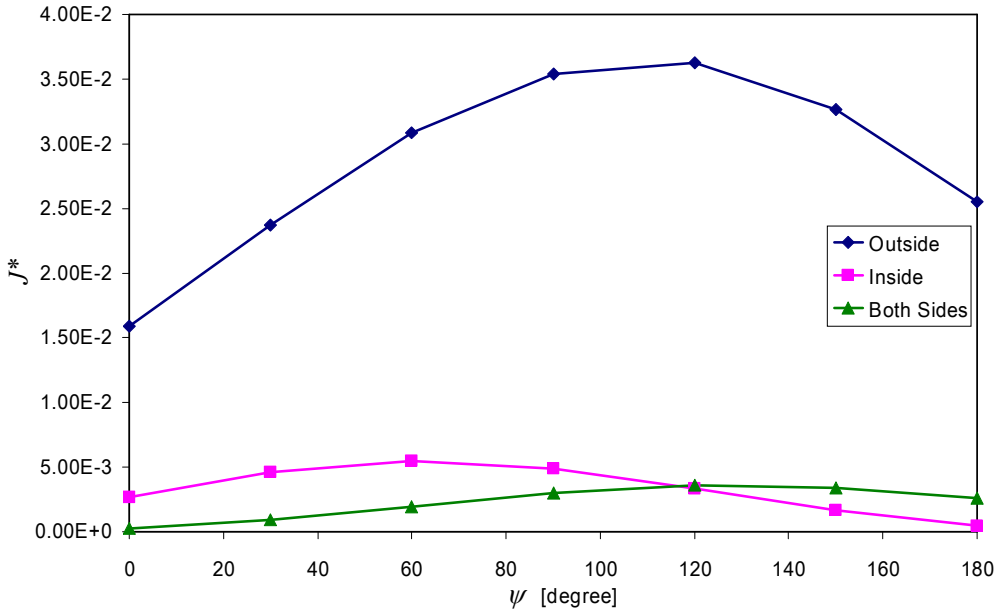


Figure 5.52 Normalized J-integral versus Inclination Angle ($\psi$)
(Crack at Weld Root, Lateral Force is Included, $\beta$=90$^0$)

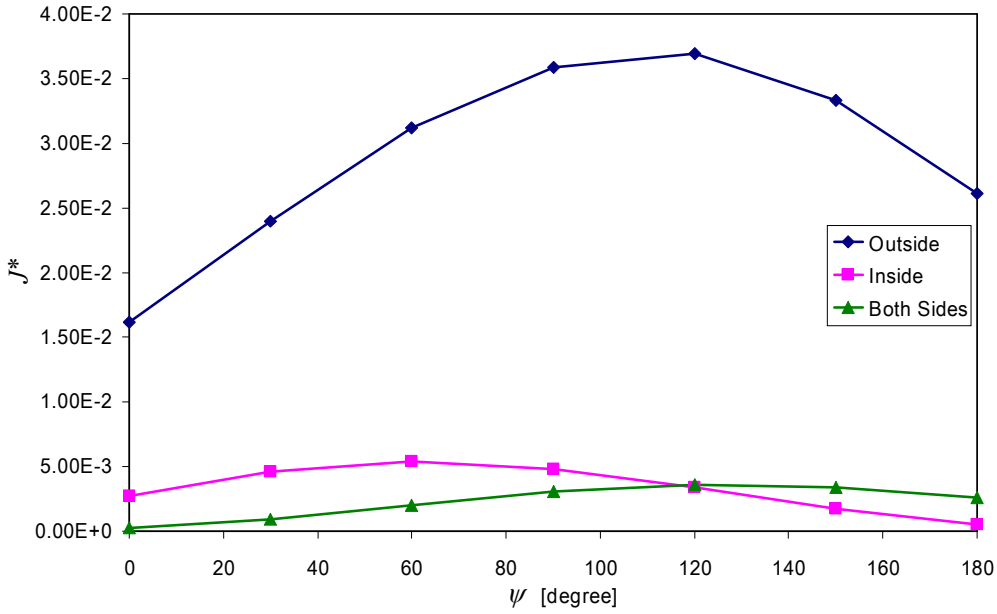


Figure 5.53 Normalized J-integral versus Inclination Angle ($\psi$)
(Crack at Weld Root, Lateral Force is Included, $\beta$=117$^0$)

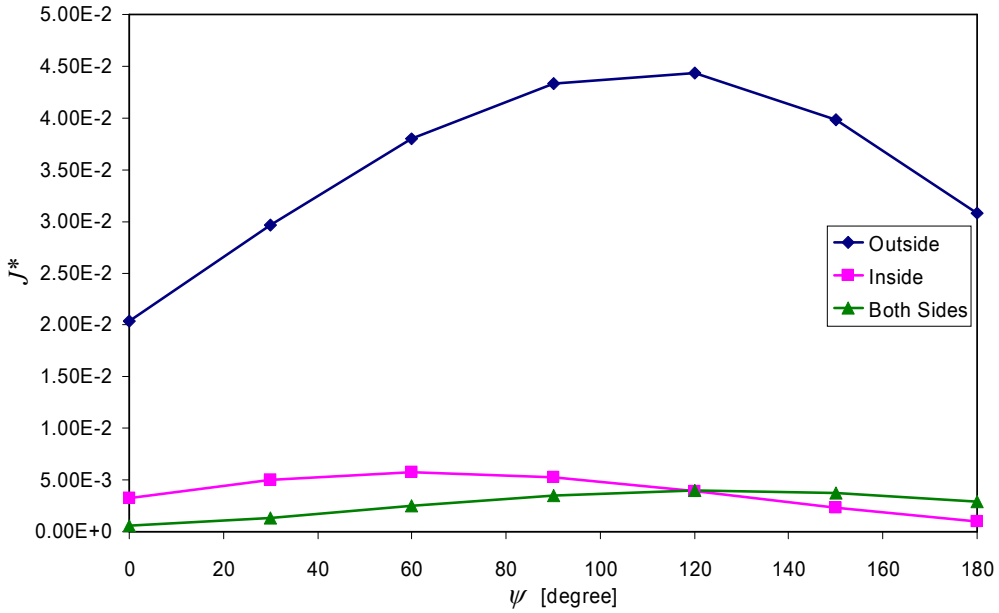


Figure 5.54 Normalized J-integral versus Inclination Angle ($\psi$)
(Crack at Weld Root, Lateral Force is Included, $\beta$=149$^0$)

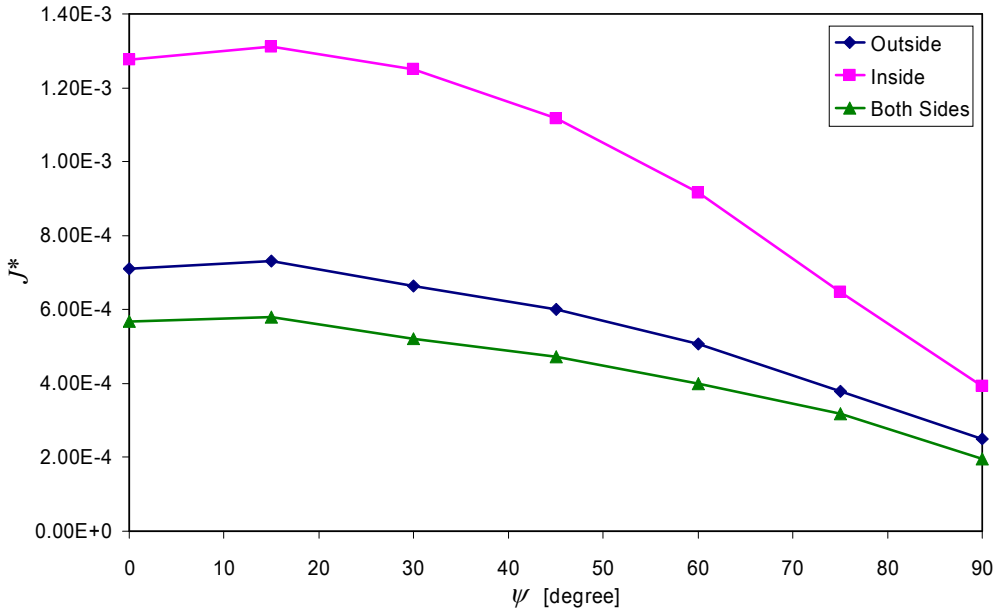


Figure 5.55 Normalized J-integral versus Inclination Angle ($\psi$)
(Crack at Weld Toe 1, Lateral Force is **not** Included, $\beta$=31$^0$)

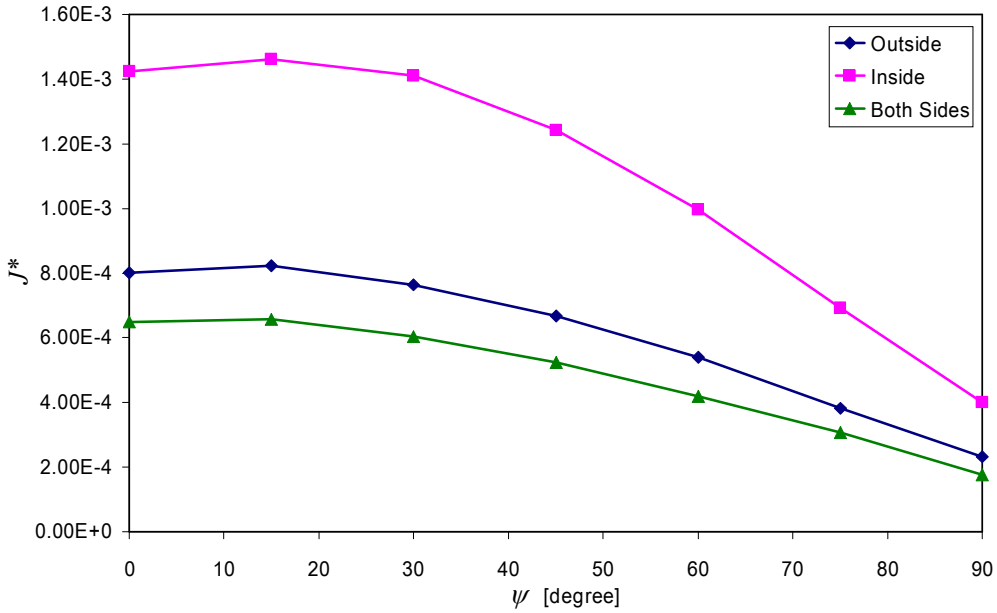


Figure 5.56 Normalized J-integral versus Inclination Angle ($\psi$)
(Crack at Weld Toe 1, Lateral Force is **not** Included, $\beta$=63$^0$)

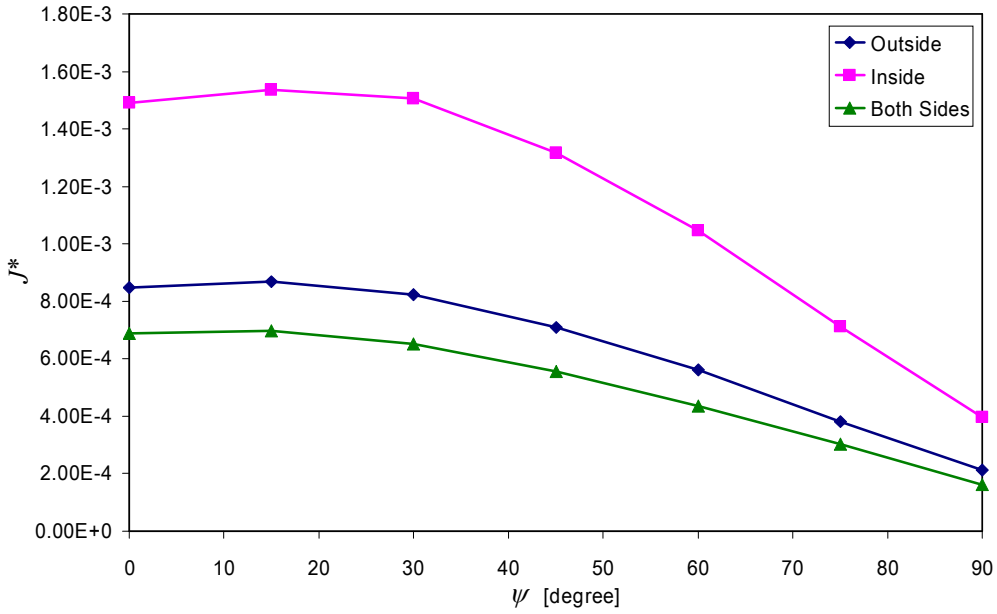


Figure 5.57 Normalized J-integral versus Inclination Angle ($\psi$)
(Crack at Weld Toe 1, Lateral Force is **not** Included, $\beta$=90$^0$)

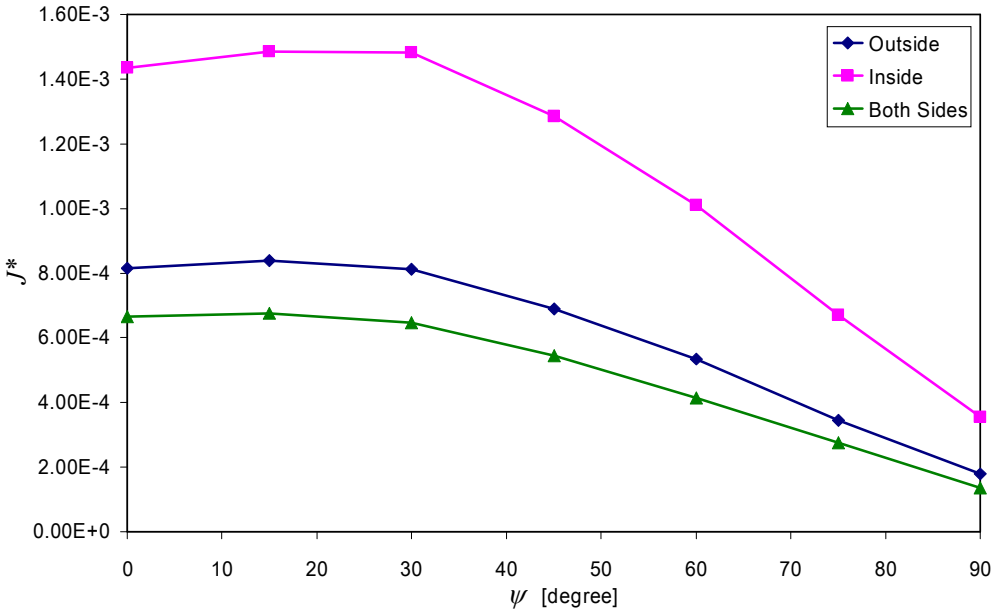


Figure 5.58 Normalized J-integral versus Inclination Angle ($\psi$)
(Crack at Weld Toe 1, Lateral Force is **not** Included, $\beta$=117$^0$)

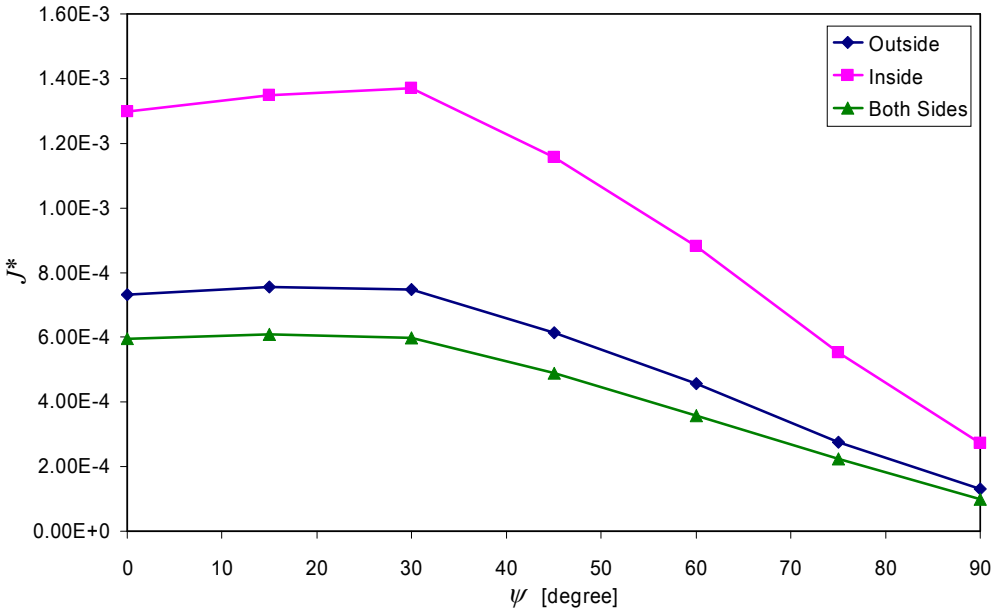


Figure 5.59 Normalized J-integral versus Inclination Angle ($\psi$)
(Crack at Weld Toe 1, Lateral Force is **not** Included, $\beta$=149$^0$)

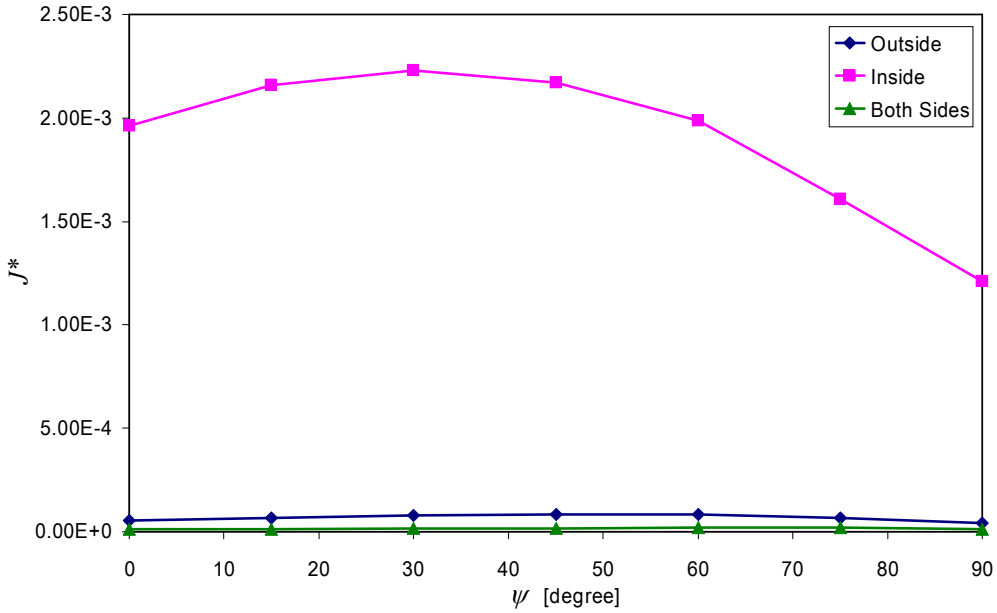


Figure 5.60 Normalized J-integral versus Inclination Angle ($\psi$)
(Crack at Weld Toe 2, Lateral Force is **not** Included, $\beta$=31$^0$)

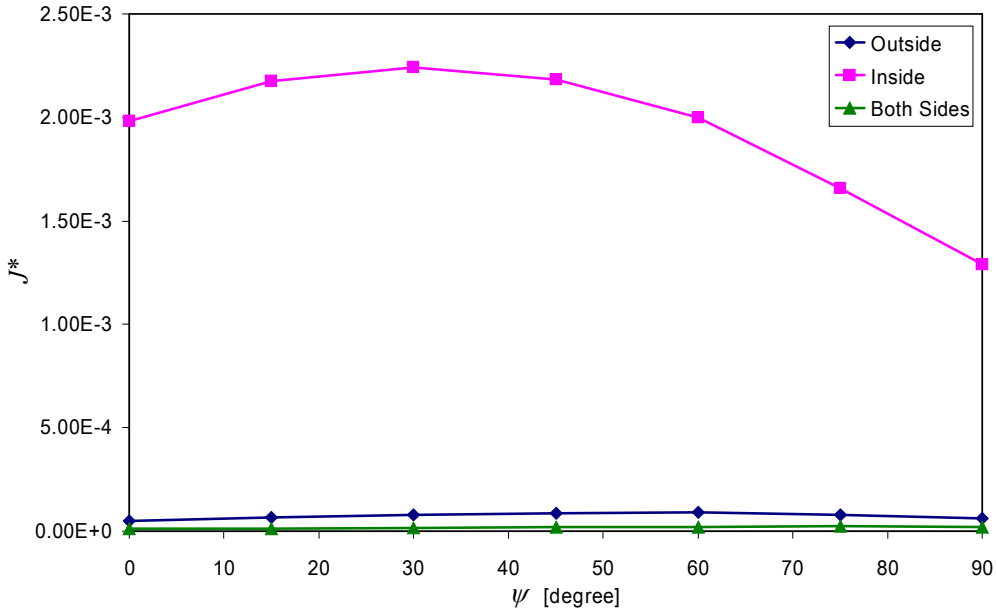


Figure 5.61 Normalized J-integral versus Inclination Angle ($\psi$)
(Crack at Weld Toe 2, Lateral Force is **not** Included, $\beta$=63$^0$)

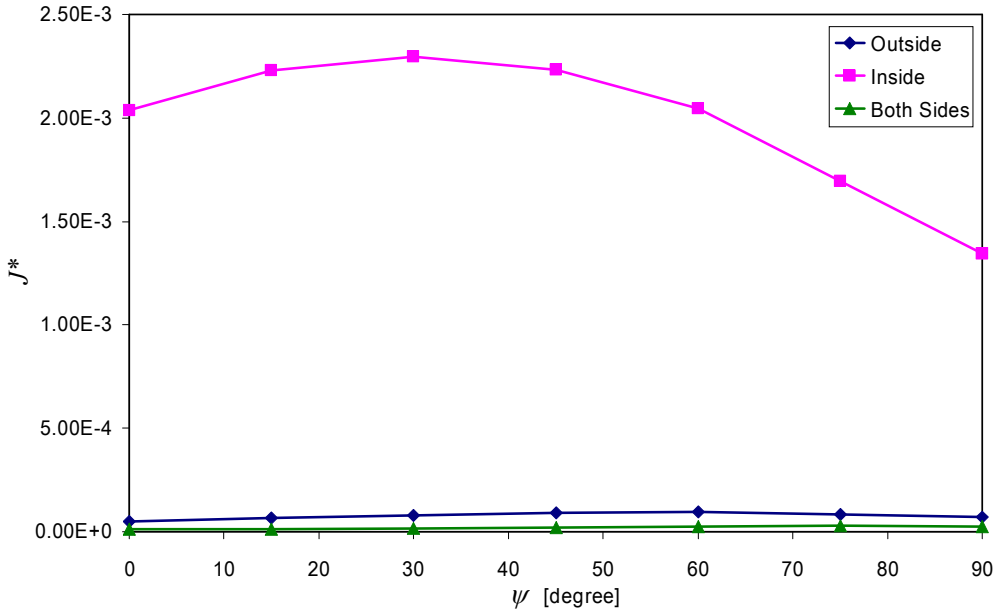


Figure 5.62 Normalized J-integral versus Inclination Angle ($\psi$)
(Crack at Weld Toe 2, Lateral Force is **not** Included, $\beta$=90$^0$)

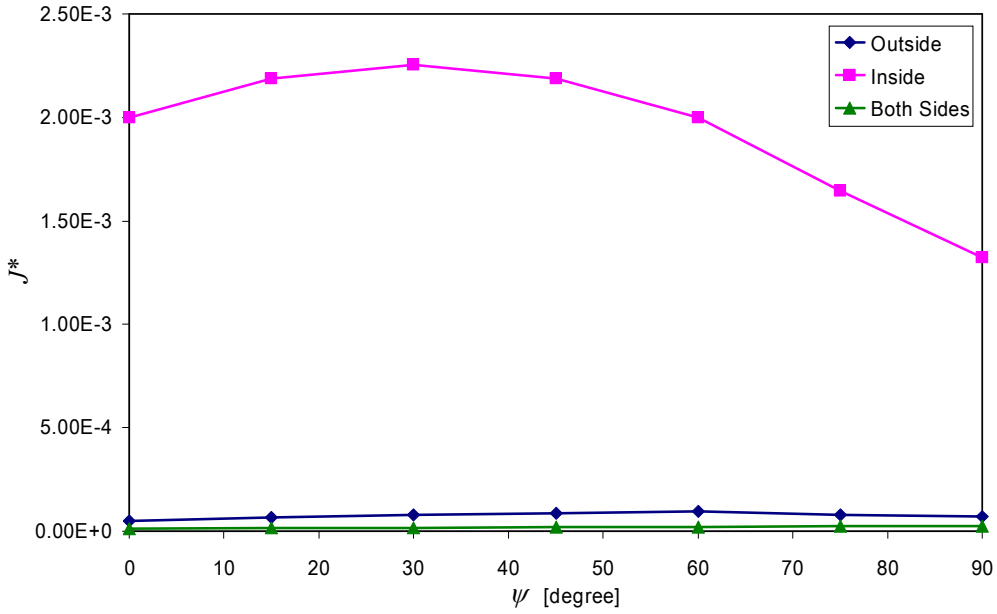


Figure 5.63 Normalized J-integral versus Inclination Angle ($\psi$)
(Crack at Weld Toe 2, Lateral Force is **not** Included, $\beta$=117$^0$)

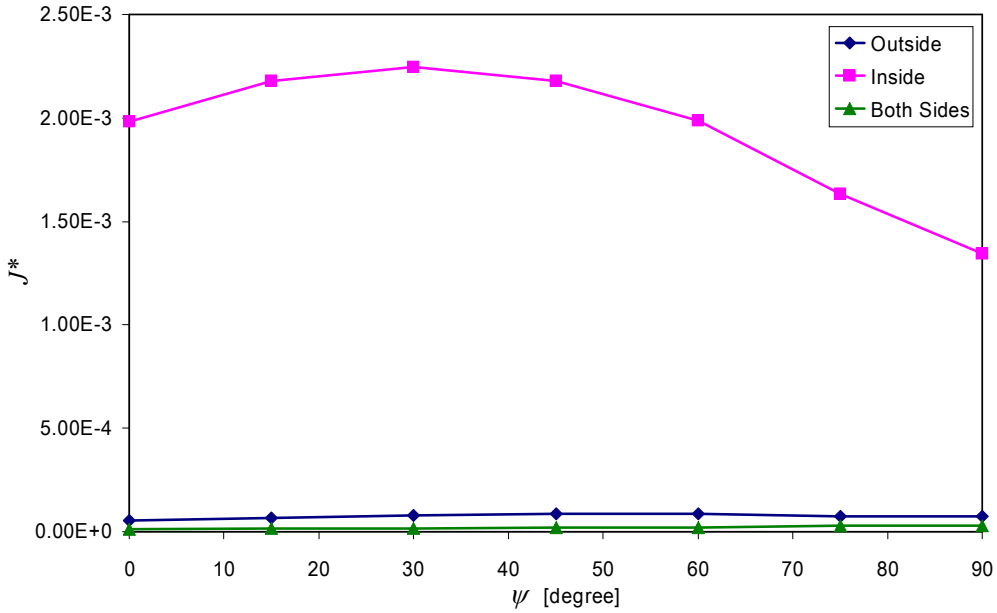


Figure 5.64 Normalized J-integral versus Inclination Angle ($\psi$)
(Crack at Weld Toe 2, Lateral Force is **not** Included, $\beta$=149$^0$)

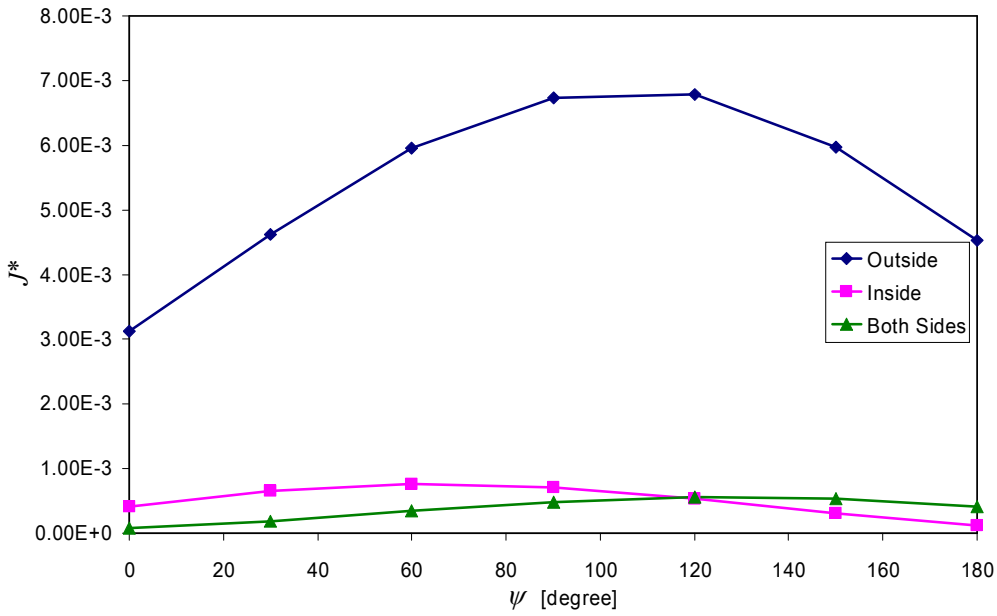


Figure 5.65 Normalized J-integral versus Inclination Angle ($\psi$)
(Crack at Weld Root, Lateral Force is **not** Included, $\beta$=31$^0$)

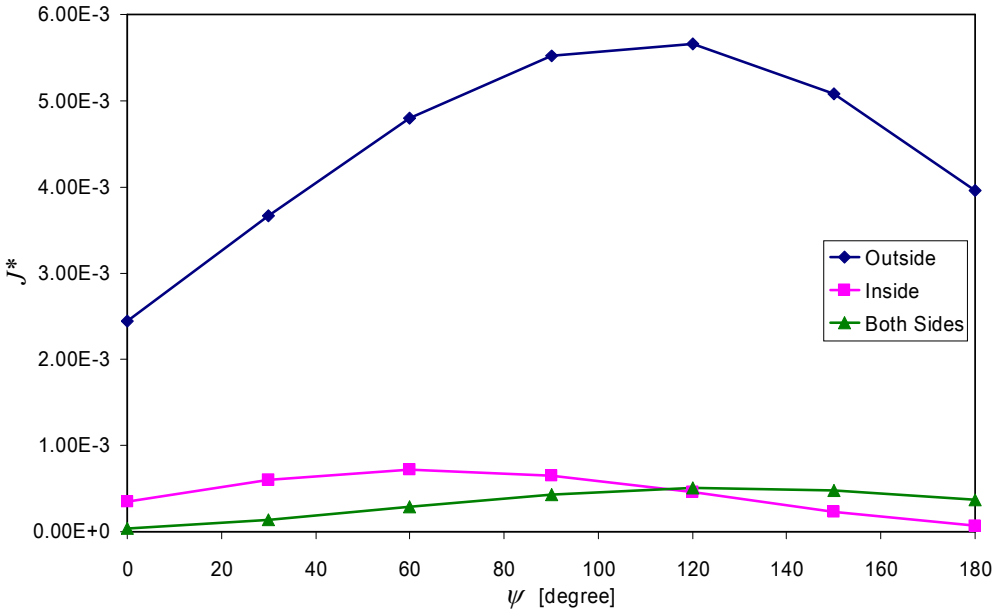


Figure 5.66 Normalized J-integral versus Inclination Angle ($\psi$)
(Crack at Weld Root, Lateral Force is **not** Included, $\beta$=63$^0$)

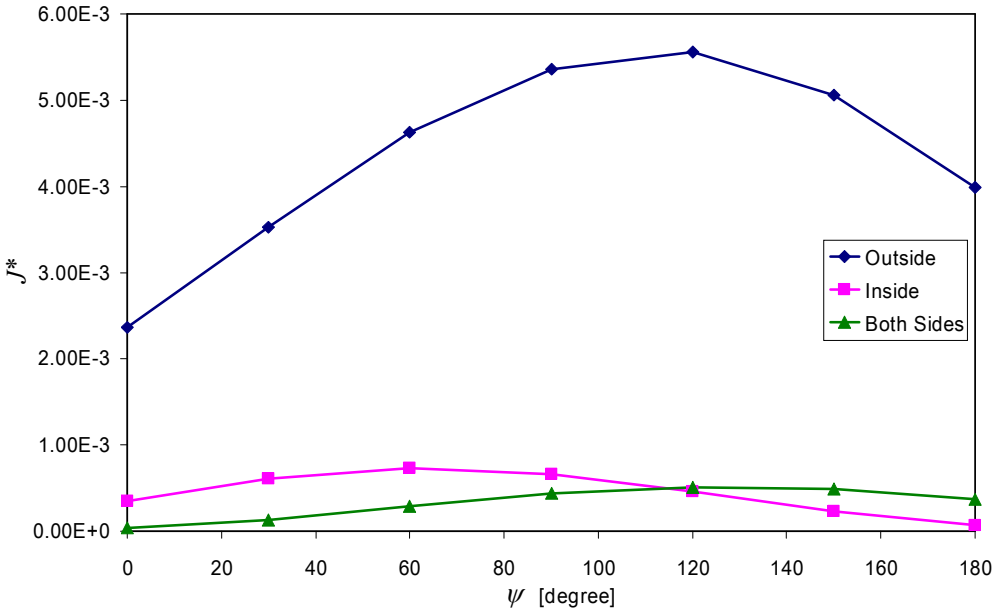


Figure 5.67 Normalized J-integral versus Inclination Angle ($\psi$)
(Crack at Weld Root, Lateral Force is **not** Included, $\beta$=90$^0$)

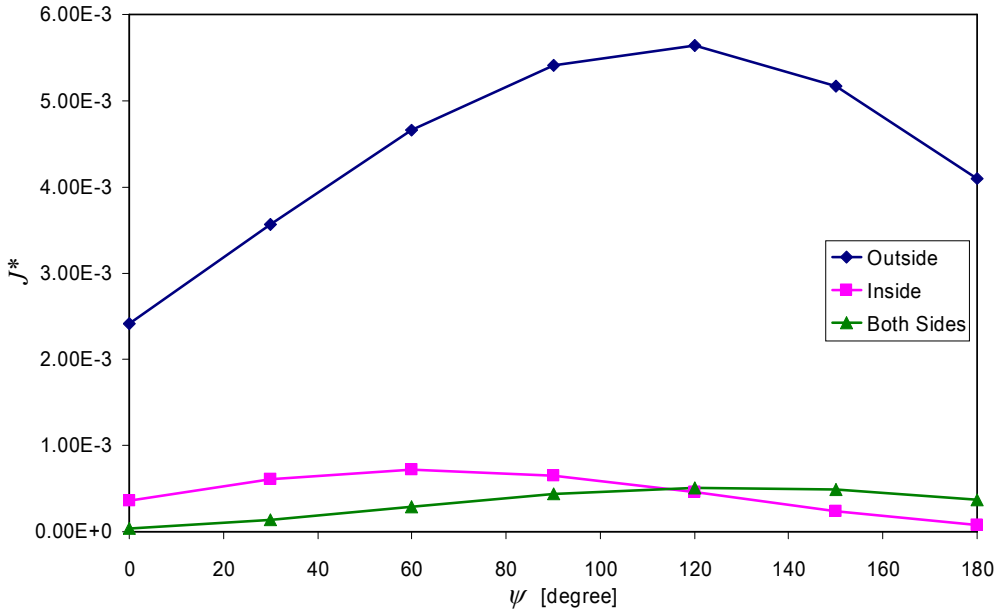


Figure 5.68 Normalized J-integral versus Inclination Angle ($\psi$)
(Crack at Weld Root, Lateral Force is **not** Included, $\beta$=117$^0$)

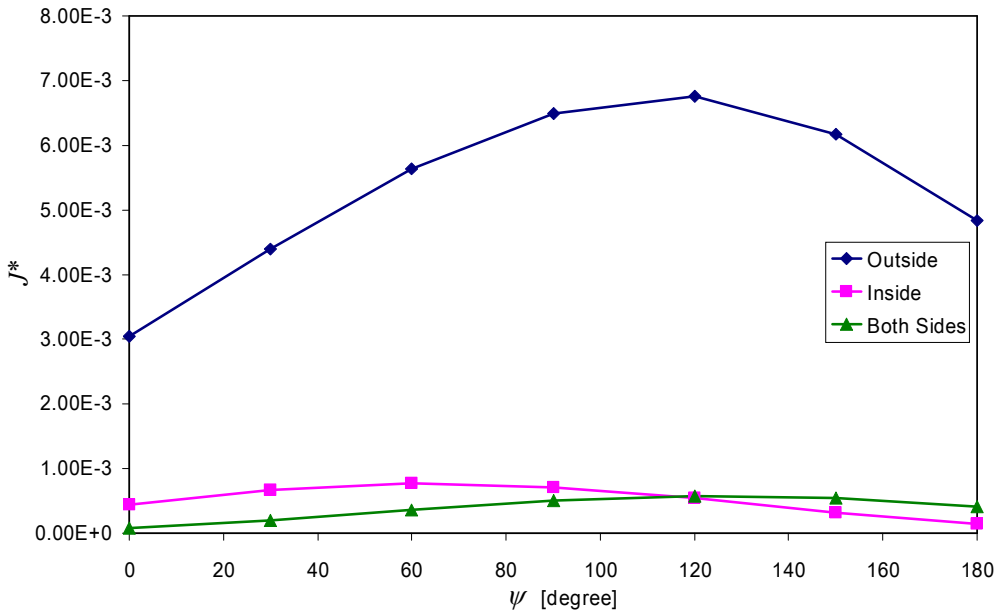


Figure 5.69 Normalized J-integral versus Inclination Angle ($\psi$)
(Crack at Weld Root, Lateral Force is **not** Included, $\beta$=149$^0$)

## 5.3 Numerical Results

The obtained results give useful knowledge about the welding location (one-sided, two-sided) and geometry and probable failure locations of boom and arm welded connections. Since the performed analyses are divided into two groups as boom and arm analysis, it will be reasonable to examine the results group by group.

Boom and arm analyses can be investigated in two groups: analyses including lateral force in boundary conditions and analyses not including lateral force in boundary conditions. A vital result attained in the analyses is the effect of lateral force on J-integral. It can easily be seen that the corresponding J-integral values in Figures 5.5-5.19 are much more higher than the values in Figures 5.20-5.34, which means that the lateral force has an important increasing effect on J-integral. Thus, if a machine is exposed to lateral force too much, the expected life of the digging mechanism may decrease dramatically. Therefore, if the total life of the digging mechanism is going to be estimated, the fraction of the lateral force in loading spectrum is very important and must be carefully taken into consideration.

If boom analyses are examined (Figures 5.5-5.34), it is seen that if the welding is made from outside the probable failure location is the root of the weld, if the welding is made from inside the probable failure location is toe 2 of the weld and if the welding is made from both sides the probable failure location is toe 1 of the weld. The tendency of toe 1 weld failure of both sides welded connections shifts to the root failures if the lateral force is excluded from boundary conditions. If the three welding locations (outside, inside and both sides) are compared to each other, in all boom analyses both sides weld gives the best and outside weld gives the worst J-integral values. Therefore, both sides weld is more suitable than the other two alternatives at the specified assumptions, made in previous chapters.

Arm analyses (Figures 5.40-5.69) show also similar trend with boom analyses. The probable failure locations for the three weld locations and the shift to root failures for both sides weld applications are the same. The ordering of the weld location is also the same. Thus, the results indicate that the weld from both sides is the best and the weld from outside is the worst alternative among them.

A significant result is that the risk of failure on the selected region of the boom is higher than the selected region of the arm in spite of the high stresses on the latter case.

# CHAPTER 6

## CONCLUDING REMARKS

In the present study, three-dimensional semi-elliptic surface crack problem in T-welded joints are examined using a three-dimensional finite element sub-modeling technique. An interface, which lets the user define the related weld and crack parameters, has been developed during the study. The developed interface enables the creation of three dimensional finite element solid model of a selected region by using a shell-to-solid conversion method. The prepared models are analyzed by using commercial finite element analysis software MSC.Mentat-Marc. The linear analyses results give the energy release rate for mixed mode loading type. In the analyses J-integral approach is used and the local solid models are prepared in this manner. The local solid models consist of 20-node and collapsed 20-node isoparametric three dimensional brick elements. The failure locations of a typical weld are assumed be the two weld toes and the weld root. It is also assumed that these locations have semi elliptical surface cracks, which are inclined for a range of inclination angles ($\psi$).

The accuracy of the adopted method is analyzed in two steps: global model verification and local model verification. Since this study is a sub-modeling study, which takes the kinematic boundary conditions directly from the global model, the global model analysis must be verified first. The performed experiments in Hidromek Ltd. Sti. show that the global model analyses results and experiment results fit in well. Therefore, the global model is

assumed to be sufficiently precise for the local model analyses. To verify the local models, the solutions of Sneddon [50], Irwin [51], Noda et al [52]. and Isida et al. [53] are compared with the results found by J-integral method. According to the obtained results, the J-integral method is sufficiently reliable unless the inclination angle is above $45^o$ or the interested node is at free surface.

In case study analyses, two different regions one is on boom and the other is on arm of HMK 300 LC excavator are analyzed in terms of fracture mechanics. Each region is investigated either including the lateral force or not including the lateral force in boundary conditions. In all groups, three weld location cases namely welding from outside, welding from inside and welding from both side are studied for different inclination angles ($\psi$). In toe regions the range of inclination angle is $0^o$ - $90^o$ and in root region the range of inclination angle is $0^o$ - $180^o$. Thus, the resulting graphs are formed in that way.

The computations show that welding from both side is the best and welding from outside is the worst alternative among the three welding location cases for the indicated global model and for the specified assumptions, which are made in previous chapters.

Fatigue failure of welded connections is the main criteria determining the total life of the construction machinery. This study aims to analyze the different weldments in construction machineries in terms of fracture mechanics. The method used in this study is applicable to linearly varying box cross section corners. By improving the method, curvilinear parts of the box cross sections and sheet metal thickness transition regions can also be examined. Thus, any region on any parts can be investigated by fracture mechanics point of view. The study can also be improved by including the total life assessments of the weldments. In this manner, a crack map for all parts of the construction machinery can be defined for the given loading spectrum. In addition to

these, the effect of heat treatment and the weld material can also be taken into consideration in subsequent studies. After completing all studies, the models must be verified by controlled experiments as future work.

## REFERENCES


[1] E. A. Avallone, T. Baumaister iii, Marks' Standard Handbook for Mechanical Engineers 10th edition, McGRAW-HILL International editions, pp 10.25

[2] "Wikipedia The Free Encyclopedia" http://en.wikipedia.org/wiki/Excavator, Last accessed 13.05.2007.

[3] "SAE J1057 SEP88: Identification Terminology of Earthmoving Machines"

[4] Taylor D., Barrett N., Lucano G., "Some New Methods for Predicting Fatigue in Welded Joints", International Journal of Fatigue, Vol.24, 509-518, 2002.

[5] Singh P. J., Guha B., Achar D. R. G., "Fatigue Life Prediction Using Two Stage Model for AISI 304L Cruciform Joints, with Different Fillet Geometry, Failing at Toe", Science and Technology of Welding and Joining, Vol.8, 69-75, 2003.

[6] Kainuma S., Mori T., "A Fatigue Strength Evaluation Method for Load-Carrying Fillet Welded Cruciform Joints", International Journal of Fatigue, Vol.28, 864-872, 2006.

[7] Darcis P., Santarosa D., Recho N., Lassen T., “A Fracture Mechanics Approach for the Crack Growth in Welded Joints with Reference to BS 7910”, The 15th European Conference of Fracture, 2004.

[8] Sidhom N., Laamouri A., Fathallah R., Braham C., Lieurade H. P., “Fatigue Strength Improvement of 5083 H11 Al-alloy T-welded Joints by Shot Peening: Experimental Characterization and Predictive Approach”, International Journal of Fatigue, Vol.27, 729-745, 2005.

[9] Ferreira J., Castiglioni C. A., Calado L., Agatino M. R., “Low Cycle Fatigue Strength Assessment of Cruciform Welded Joints”, Journal of Construction Steel Research, Vol.47, 223-244, 1998.

[10] Haagensen P. J., Statnikov E. S., Martinez L. L., “Introductory Fatigue Tests on Welded Joints in High Strength Steel and Aliminium Improved by Various Methods Including Ultrasonic Impact Treatment (UIT)”, International Institute of Welding, IIW Doc. XIII- 1748-98, 1998.

[11] Singh P. J., Guha B., Achar D. R. G., “Fatigue Life Prediction of GTA Welded AISI 304L Cruciform Joints with Lack of Penetration Using Local-Stress Approach”, Engineering Failure Analysis, Vol.10, 25-36, 2003.

[12] Ranestad Q., Zhang Z. L., Thaulow C., “An Engineering Method for Constraint Based Fracture Assessment of Welded Structural Components with Surface Cracks”, Engineering Fracture Mechanics, Vol.63, 653-674, 1999.

[13] Baumjohann F., Kröning J., “A Practical Method for Computation of Ductile Crack Growth by Means of Finite Elements and Parametric 3D-modelling”, Nuclear Engineering and Design, Vol.190, 197-206, 1999.

[14] Nykänen T., Marquis G., Björk T., “Fatigue Analysis of Non-load-carrying Fillet Welded Cruciform Joints”, Engineering Fracture Mechanics, Vol.74, 399-415, 2007.

[15] Lin X.B., Smith R.A., “Finite Element Modelling of Fatigue Crack Growth of Surface Cracked Plates Part I: The Numerical Technique”, Engineering Fracture Mechanics, Vol.63, 503-522, 1999.

[16] Courtin S., Gardin C., Bezine G., Hamouda H. B. H., “Advantages of the J-integral Approach for Calculating stress Intensity Factors When Using the Commercial Finite Element Software ABAQUS”, Engineering Fracture Mechanics, Vol.72, 2174-2185, 2005.

[17] Ficici F., “Three Dimensional Fracture Analysis of Fillet Welds”, Ms. Thesis Submitted to Middle East Technical University, Turkey, 2007.

[18] Inan O., “Three Dimensional Fracture Analysis of FGM Coatings”, Ms. Thesis Submitted to Middle East Technical University, Turkey, 2004.

[19] Ayhan A. O., “Mixed Mode Stress Intensity Factors for Deflected and Inclined Surface Cracks in Finite-Thickness Plates”, Engineering Fracture Mechanics, Vol.71, 1059-1079, 2004.

[20] dell’Erba D. N., Aliabadi M. H., “BEM Analysis of Fracture Probşems in Three-dimensional Thermoelasticity Using J-integral”, International Journal of Solids and Structures, Vol.38, 4609-4630, 2001.

[21] Rigby R. H., Aliabadi M. H., “Decomposition of the Mixed-Mode J-integral- Revisited”, International Journal of Solids and Structures, Vol.35, 2073-2099, 1998.

[22] Statnikov E. S., Muktepavel V. O., Trufyakov V. I., Mikheev P. P., Kuzmenko A. Z., Blomqvist A., “Efficiency Evaluation of Ultrasonic Impact Treatment (UIT) of Welded Joints in Weldox 420 Steel in accordance with the IIW Program”, IIW Doc. XIII-1817-00, 2000.

[23] Lahti K. E., Hanninen H., Niemi E., “Nominal Stress Range Fatigue of Stainless Steel Fillet Welds — the Effect of Weld Size”, Journal of Constructional Steel Research, Vol.54, 161-172, 2000.

[24] Fricke W., Doerk O., “Simplified Approach to Fatigue Strength Assessment of Fillet-Welded Attachment Ends”, International Journal of Fatigue, Vol.28, 141-150, 2006.

[25] “ISO/DIS 14345: Fatigue testing of welded components”, 2001

[26] Gray L. J., Phan A. V., Paulino G. H., Kaplan T., “Improved Quarter-Point Crack Tip Element”, Engineering Fracture Mechanics, Vol.70, 269-283, 2003.

[27] Sabuncuoglu B., “Fatigue Crack Growth Analysis Models for FGM’s”, Ms. Thesis Submitted to Middle East Technical University, Turkey, 2006.

[28] Kadioglu S., Dag S., Yahsi S., “Crack Problem for a Functionally Graded Layer on an Elastic Foundation”, International Journal of Fracture, Vol.47, 533-545, 1991.

[29] Guo L.C., Wu L.Z., Zeng T., Ma L., “Mode I Crack Problem for a Functionally Graded Orthotropic Strip”, European Journal of Mechanics A/Solids, Vol. 23, 219-234, 2004.

[30] Guo K., Bell R., Wang X., “The Stress Intensity Factor Solutions for Edge Cracks in a Padded Plate Geometry under General Loading Conditions”, International Journal of Fatigue, Vol.29, 481-488, 2007.

[31] Hou J., Goldstraw M., Maan S., Knop M., “An Evaluation of 3D Crack Growth Using ZENCRACK”, DSTO-TR-1158, 1-28, 2001.

[32] Gerstle W., “Structural Zooming Research and Development of an Interactive Computer Graphical Interface for Stress Analysis of Cracks", NASA/American Society for Engineering Education (ASEE) Summer Faculty Fellowship Program 1989, Tiwari, S. N. (Compiler), NASA Contractor Report 181894, pp. 67-68, Sept., 1989.

[33] Gerstle, W., Martha, L., Ingraffea, A., "Finite and Boundary Element Modeling of Crack Propagation in Two and Three Dimensions," Engineering with Computers, Vol. 2, pp. 167-183, 1987.

[34] Giglio M., “FEM Submodelling Fatigue Analysis of a Complex Helicopter Component”, International Journal of Fatigue, Vol.21, 445-455, 1999.

[35] Kitamura M., Ohtsubo H., Akiyama A., Bandoh H., “Submodeling Analysis of Ship Structure with Superconvergent Patch Recovery Method”, International Journal of Offshore and Polar Engineering, Vol.13, 2003.

[36] Larson M. G., “Adaptive Submodeling”, Computational Mathematics, Chalmers

[37] MSC.MARC Volume A: Theory and User Information Version 2005, Vol.A, Chapter 5, 123-127.

[38] ABAQUS Analysis User's Manual v6.5-1: Part III Analysis: Section 7.3

[39] ANSYS Advanced Analysis Techniques Guide Release 11.0, Chapter 9, 229-239.

[40] “Lecture 12.10: Basics of Fracture Mechanics”, ESDEB WG12, http://www.kuleuven.ac.be/bwk/materials/Teaching/master/wg12/l1000.htm#SEC_1, Last accessed 18.05.2007.

[41] Lee Y., Pan J., Hathaway R. B., Barkey M. E., “Fatigue Testing and Analysis (Theory and Practice)”, Elsevier, 2005.

[42] “ME 583 Engineering Fracture Mechanics” http://www.me.metu.edu.tr/me583, Last accessed 21.05.2007.

[43] Yildirim B., Dag S., Erdogan F., “Three Dimensional Fracture Analysis of FGM Coatings Under Thermo-mechanical Loading”, International Journal of Fracture, Vol.132, 369-395, 2005.

[44] Sharma A. K., “Kinematics and Finite Element Analysis of Excavator Attachments”, Ms. Thesis Submitted to Nirma University of Science & Technology, Ahmedabad, 2005.

[45] Cook R. D., “Finite Element Modeling for Stress Analysis”, John Wiley & Sons, Inc., 1995.

[46] Eriksson A., Lignell A. M., Olsson C., Spennare H., “Weld Evaluation Using FEM”, Industrilitteratur AB., 2003.

[47] Yener M., “Design of a Computer Interface for Automatic Finite Element Analysis of an Excavator Boom”, Ms. Thesis Submitted to Middle East Technical University, Turkey, 2005.

[48] Makinen H., “Global and Local FE Models in the Fatigue Analysis of Ships”, Ms. Thesis Submitted to VTT Technical Research Centre of Finland, Finland, 2005.

[49] SAE J1179, “Hydraulic Excavator and Backhoe Digging Forces”, SAE Handbook, Vol.3, 40.355, 1995.

[50] Broek D., “Elementary Engineering Fracture Mechanics”, Martinus Nijhoff Publishers, 1984

[51] Sanford R.J., “Principles of Fracture Mechanics”, Prentice Hall, 2003

[52] Noda N., Kobayashi K., Yagishita M., “Variation of mixed modes stress intensity factors of an inclined semi-elliptical surface crack”, International Journal of Fracture, Vol.100, 207-225, 1999

[53] Isida M., Tokumoto A., Noguchi H., “Oblique Semi-elliptical Surface Crack in Semi-infinite Solid Subjected to Tension”, Engineering Fracture Mechanics, Vol.36, 889-892, 1990.

[54] Cherepanov G.P., “The Propagation of Cracks in a Continuous Medium”, Journal of Applied Mathematics and Mechanics, Vol. 31, 503-512, 1967

[55] Rice J.R., “A Path Independent Integral and the Approximate Analysis of Strain Concentration by Notches and Cracks”, Journal of Applied Mechanics Transactions of the ASME, Vol. 35, 379-386, 1968

[56] Newman J.C., Raju I.S., “An Empirical Stress Intensity Factor Equation for the Surface Crack”, Engineering Fracture Mechanics, Vol. 15, 185-192, 1981